AD-A082 059 NATIONAL RESEARCH COUNCIL OF CANADA OTTAWA (ONTARIO) --ETC F/G 13/6
QUARTERLY BULLETIN OF THE DIVISION OF MECHANICAL ENGINEERING AN--ETC(U)
SEP 79
UNCLASSIFIED DME/NAE-1979(3) NL

1 OF 2
AD A082059

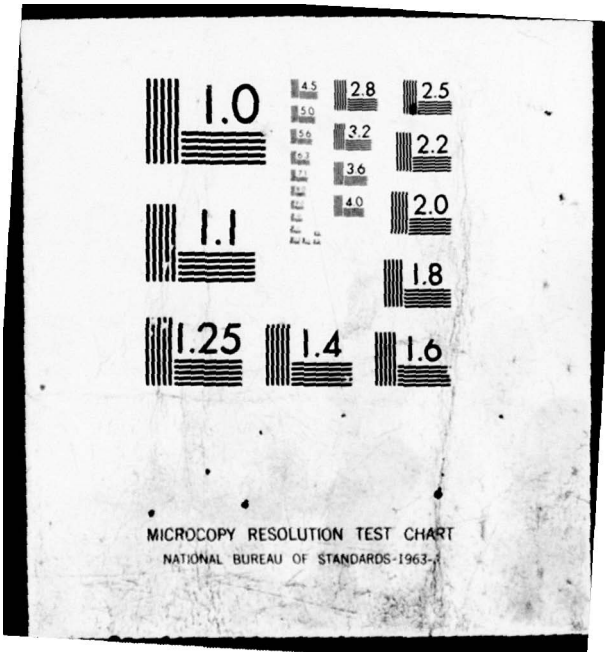
1.0
1.1
1.25
1.4
1.6
1.8
2.0
2.2
2.5
2.8
3.2
3.6
4.0
4.5
5.0
5.6
MICROCOPY RESOLUTION TEST CHART
NATIONAL BUREAU OF STANDARDS-1963-A

REPORT NO. DME/NAE 1979(3)

National Research Council Canada

Conseil national de recherches Canada

QUARTERLY BULLETIN OF THE DIVISION OF MECHANICAL ENGINEERING AND THE NATIONAL AERONAUTICAL ESTABLISHMENT

OTTAWA

1 JULY TO 30 SEPTEMBER 1979

ISSN 0047-9055

FOREWORD

The Quarterly Bulletin is designed primarily for the information of Canadian industry, universities, and government departments and agencies. It provides a regular review of the interests and current activities of two Divisions of the National Research Council Canada:

Division of Mechanical Engineering
National Aeronautical Establishment

Some of the work of the two Divisions comprises classified projects that may not be freely reported and contractual projects of limited general interest. Other work, not generally reported herein, includes calibrations, routine analyses and the testing of proprietary products.

Comments or enquiries relating to any matter published in this Bulletin should be addressed to: *DME/NAE Bulletin, National Research Council Canada, Ottawa, Ontario, K1A 0R6*, mentioning the number of the Bulletin.

AVANT-PROPOS

Le Bulletin trimestriel est conçu en premier lieu pour l'information de l'industrie Canadienne, des universités, des agences et des départements gouvernementaux. Il fournit une revue régulière des intérêts et des activités actuelles auxquels se consacrent deux Divisions du Conseil national de recherches Canada:

Division de génie mécanique
Établissement aéronautique national

Quelques uns des travaux des deux Divisions comprennent des projets classifiés qu'on ne peut pas rapporter librement et des projets contractuels d'un intérêt général limité. D'autres travaux, non rapportés ci-après dans l'ensemble, incluent des étalonnages, des analyses de routine, et l'essai de produits de spécialité.

Veuillez adresser tout commentaire et toute question ayant rapport à un sujet quelconque publié dans ce Bulletin à: *DME/NAE Bulletin, Conseil national de recherches Canada, Ottawa, Ontario, K1A 0R6*, en faisant mention du numéro du Bulletin.

CONTENTS

CONTENTS (Cont'd)

ILLUSTRATIONS

CONTENTS (Cont'd)

ILLUSTRATIONS (Cont'd)

CONTENTS (Cont'd)

ILLUSTRATIONS (Cont'd)

SEDIMENT LOAD UNDER WAVES AND CURRENTS

D.H. Willis

Hydraulics Laboratory

Division of Mechanical Engineering

ABSTRACT

A technique is proposed for calculating sediment load, the mass concentration of sediment in motion, under combinations of waves and currents. The technique is based on the unidirectional flow method of Ackers and White, Reference 1. The technique is being calibrated against measurements of sediment load under waves made in the Hydraulics Laboratory beach flume.

SEDIMENT LOAD

Sediment load is not sediment transport. It is an essential part of sediment transport, the concentration by mass of sediment in motion, but it requires the presence of a current to transport it from one place to another.

Although this paper will primarily deal with sediment load under waves, or waves and currents, the concept is best grasped for the case of currents alone. In this case there is, of course, always a current and therefore always a sediment transport. Sediment load is then the mass rate of sediment transport divided by the mass rate of current discharge.

The sediment load concept is however most useful when there are only very small currents, for example the mass transport associated with water waves. Here the sediment load due to the oscillatory wave motion may be quite high, but because of the very small currents involved, sediment transport calculations frequently fail. It is still handy to know how much sediment is available to fill in a navigation channel, even if the rate at which infilling takes place remains uncertain.

We, at the Hydraulics Laboratory of the National Research Council of Canada, have therefore undertaken a program to develop a technique for calculating sediment loads under combinations of waves and currents, covering the range from currents only to waves only. We are initially aiming for a technique applicable seaward of the breaker line, but will not be at all disappointed if it turns out to be useful in the surf zone as well.

Like Swart in Reference 19, we chose as a basis the method of Ackers and White, Reference 1, for calculating sediment load in currents only. Their method has proved to be very successful in predicting sediment loads in rivers, see for example Fleming and Hunt, Reference 5. The theoretical modification of the Ackers and White method for the presence of waves is virtually complete. But in making that modification, we added a new empirical coefficient, the calibration of which is being carried out at present. Sediment load under waves only is being measured in the Laboratory's beach flume, and this together with published data, is used to calibrate the coefficient. This then is a report on work in progress.

ACKERS AND WHITE METHOD

The technique of Ackers and White, Reference 1, was developed for calculating the sediment load in unidirectional flow over an alluvial bed. Ackers and White take a transporting power approach: the work done in moving sediment is the product of the power available to move the sediment and the efficiency of the system.

Despite its being a total load concept, their derivation does make a distinction between bed load and suspended load. But the distinction is made, not on the basis of position in the water column, but rather on dimensionless grain size,

$$D_{gr} = D\left(\frac{g\,(s-1)}{\upsilon^2}\right)^{1/3} \tag{1}$$

Coarse material, $D_{gr} \geqslant 60$, is considered to be moved as bed load. Grains are rolled along the surface of the bed by the component of bed shear parallel to the local bed surface,

$$\tau_{cg} = \rho\,\frac{V^2}{C_{h^2_{cg}}} \tag{2}$$

where

$$C_{h_{cg}} = 5.75 \log \frac{11d}{D} \tag{3}$$

Fine material, $D_{gr} \leqslant 1$, is moved as suspended load. The turbulence which keeps the grains in suspension is a function of the total shear on the bed,

$$\tau_{fg} = \rho\,\frac{V^2}{C_{h^2_{cg}}} \tag{4}$$

where

$$C_{h_{fg}} = 5.75 \log \frac{11d}{r} \tag{5}$$

The total shear includes components both parallel and normal to the local bed surface.

The power per unit area available to move sediment then becomes

$$P_{cg} = \tau_{cg} V \tag{6}$$

and

$$P_{fg} = \tau_{fg} V$$

It is not the purpose of this paper to repeat the derivation by Ackers and White. The reader is instead referred to Reference 1. It will suffice to say that they develop two sets of relationships, one for coarse grains and one for fine grains. Transition sizes, $1 < D_{gr} < 60$, are handled by mixing the relationships using an exponent, n. This is illustrated by the Ackers and White mobility number,

$$F_{gr} = \frac{u_{*fg}^{n}\, u_{*cg}^{1-n}}{\sqrt{gD\,(s-1)}} \tag{7}$$

where the shear velocity is as usual,

$$u_* = \sqrt{\frac{\tau}{\rho}} \tag{8}$$

An important feature of the method, and one which makes it almost unique, is the inclusion of a criterion for the beginning of sediment motion, the threshold of movement. This is expressed as a critical value of the mobility number, F_{gr_c}, below which no sediment motion takes place. They then derive the following expression for sediment load:

$$X = C\left(\frac{F_{gr}}{F_{gr_c}} - 1\right)^m \frac{sD}{d}\left(\frac{\rho^{1/2} P_{fg}}{\tau_{fg}^{3/2}}\right)^n \left(\frac{P_{cg}}{\tau_{cg} V}\right)^{1-n} \tag{9}$$

In the currents only case of Ackers and White, this reduces to

$$X = C\left(\frac{F_{gr}}{F_{gr_c}} - 1\right)^m \frac{sD}{d} C_{h_{fg}}^n \tag{9a}$$

At this point, the values of C, F_{gr_c}, m and n are still undefined. Ackers and White considered them to be empirical coefficients and calibrated them against over 1000 field and laboratory measurements of sediment load, obtaining

$$\log C = 2.86 \log D_{gr} - (\log D_{gr})^2 - 3.53, \; 2.95 \times 10^{-4} \leqslant C \leqslant 0.025 \tag{10}$$

$$F_{gr_c} = \frac{0.23}{\sqrt{D_{gr}}} + 0.14, \; 0.17 \leqslant F_{gr_c} \leqslant 0.37 \tag{11}$$

$$m = \frac{9.66}{D_{gr}} + 1.34, \; 1.5 \leqslant m \leqslant 11.0 \tag{12}$$

$$n = 1 - 0.56 \log D_{gr}, \; 0 \leqslant n \leqslant 1 \tag{13}$$

MODIFICATION FOR WAVES

The principal criterion in modifying the Ackers and White method for the presence of both waves and currents, was that the basic method should remain intact when no waves were present. Ackers and White have, after all, calibrated their method against more than 1000 measurements, and such a wealth of data can not be lightly tossed aside.

Vector addition of wave and current velocities produces a shear relationship which meets that criterion. Shear is proportional to the instantaneous velocity squared:

$$V_{TOT}^2 = \left(V + u_o \sin \frac{2\pi t}{T} \cos \alpha\right)^2 + \left(u_o \sin \frac{2\pi t}{T} \sin \alpha\right)^2 \tag{14}$$

Averaging V_{TOT}^2 over a wave period,

$$\overline{V_{TOT}^2} = V^2 + \frac{{u_o}^2}{2} \tag{15}$$

which is independent of direction.

If we assume that the unidirectional Chézy friction factor can be applied to the unidirectional term only, the Jonsson wave friction factor, $f_w/2$ see Reference 11, to the oscillatory term only, and that f_w is independent of wave phase, we obtain for the combined bed shear

$$\tau = \rho\left(\frac{V^2}{{C_h}^2} + \frac{f_w}{4} {u_o}^2\right) \tag{16}$$

Power is a scalar, and therefore we only need obtain an expression for the wave power available to move sediment and add that to the unidirectional term, Equation (6). The wave power per unit area, available to move sediment is

$$P_w = E \frac{dC_g}{dx} + C_g \frac{dE}{dx} \tag{17}$$

Since a locally horizontal bed is assumed in the Ackers and White Method, C_g does not vary with distance and

$$P_w = C_g \frac{dE}{dx} \tag{17a}$$

There are a number of factors affecting the wave energy attenuation, dE/dx: bottom friction, bottom percolation, surface contamination, to name a few. But we are only interested in that part of dE/dx available to move sediment, the part due to bottom friction or bed shear. Therefore

$$P_w = C_g \rho \frac{f_w}{4} u_o^2 \tag{17b}$$

The total power per unit bed area under waves and currents then becomes

$$P_w = \rho \left(\frac{V^2}{C_h^2} V + C_g \frac{f_w}{4} u_o^2 \right) \tag{18}$$

Subscripts have been dropped from Equations (16) and (18) but there are fine grain and coarse grain versions, analogous to Equations (2), (4) and (6). In both Equations (16) and (18), the first term is that for currents only, as in the Ackers and White method, with the second term adding the wave effect.

It is quite clear that when no currents are present, Equation (9) would "blow up" unless a minimum velocity is specified. This minimum is the mass transport velocity of the waves, the net velocity at which waves transport water in the direction of propagation. The mass transport velocity was studied by Dalrymple in Reference 4. He concluded that the Levi-Civita equation for Airy Waves,

$$V_m = \frac{g H^2 T}{8 d L} \tag{19}$$

overestimated the velocity by an average factor of about 1.25. Therefore, for the minimum velocity in Equation (9), we have used

$$V_m = \frac{0.1 g H^2 T}{d L} \tag{19a}$$

One further modification is necessary to compensate for the fact that the threshold of sediment motion is different under waves than under unidirectional flow. If the expression for F_{gr_c}, Equation (11), is modified, as Swart has done in Reference 18, then it ceases to be a function of D_{gr} alone; it also becomes a function of the flow conditions. However, the flow conditions are already contained in the mobility number, F_{gr} Equation (7), by way of the modified shear stress of Equation (16). We therefore decided to leave the threshold of movement criterion alone, and further modify the shear stress to compensate for differences in wave and current thresholds. A new empirical coefficient, W_c, was added to the wave terms of Equation (16) and (18), which become respectively:

$$\tau = \rho\left(\frac{V^2}{C_h{}^2} + W_c{}^2\,\frac{f_w}{4}\,u_o{}^2\right) \tag{20}$$

$$P = \rho\left(\frac{V^2}{C_h{}^2}\,V + W_c{}^2\,C_g\,\frac{f_w}{4}\,u_o{}^2\right) \tag{21}$$

LABORATORY EXPERIMENTS

Equations (20) and (21) not only reduce to their unidirectional flow forms when no waves are present, but when no currents are present they also reduce to their wave terms. It should therefore be possible to calibrate W_c against measurements of sediment load under waves alone.

Such measurements are presently being made in the Laboratory's beach flume, see Figures 1 and 2. The working section of the flume is 31 m long, 1.27 m wide and 0.8 m deep. Waves are generated by a hydraulically actuated paddle, in piston mode, controlled by an electronic sinusoidal signal generator. A 50 mm deep depression in the floor 5.80 m long, is located 13.72 m from the paddle. This is the test section, and is filled with uniform silica sand, in the present tests having a grain size of 250 μm. The 3 m long test section has glass walls on both sides.

The test procedure is as follows:

1. Fill flume to desired depth of water.
2. Screed sand bed level.
3. Run uniform, monofrequency waves until a stable ripple pattern has formed on the sand bed. Depending on wave conditions, this can take hours or days.
4. Measure sediment load at 10 phases within the wave period over the ripple crest and ripple trough. Average the 20 measurements to obtain the temporal and spatial mean sediment load.
5. Simultaneously measure wave height and period and water temperature at the test section.

MEASUREMENT OF SEDIMENT LOAD

The laboratory is developing a unique system for measuring sediment load, based on counting the number of particles within a very small measuring volume at any instant. As shown schematically in Figure 2, the measuring volume is defined by the beam from a Spectraphysics 6.5 mw helium-neon laser, shining vertically to illuminate a water column 1 mm in diameter. A particle within the measuring volume scatters light out through the flume windows where it can be focussed on photographic film using a Hasselblad 500 EL/M camera with 80 mm lens. The camera is triggered by the signal generator controlling the wave paddle. Using High Speed Ektachrome colour film (ASA 400), an exposure time of 1/500 s is possible at f2.8 aperture. Particles in the photographs are then manually counted to determine sediment load.

An electronic camera is under development, see Reference 22, substituting a linear array of photosensitive cells for the film. Particle counting will then be done by dedicated computer. This should allow faster sampling and shorter exposure times as well as the use of irregular waves.

EXPERIMENTAL RESULTS

Table I summarizes the measured and computed results for the 17 tests performed to date. Ripple height and length are not measured, because for the case of waves only, the design curves of Mogridge, Reference 15, have been found to be sufficiently accurate to allow the calculation of bed roughness. The last two columns of Table I give the value of W_c and the Shields Parameter, θ, needed to make the computed sediment load agree with the measured.

ADDITIONAL DATA

In addition to our own measurements, 63 suitable measurements of sediment load under waves were found in the literature: 4 field measurements of which one included a current velocity; and 59 laboratory measurements, 13 with currents. "Suitable" simply means that enough data were presented to allow an Ackers and White calculation of sediment load to be made and a value of W_c to be determined. Even for such "suitable" measurements, it was usually necessary to make one or more of the following assumptions:

1. Mass density of sea water, 1020 kg/m^3, or of fresh water, 1000 kg/m^3.
2. Mass density of sand, 2650 kg/m^3.
3. Kinematic viscosity of laboratory water, 1×10^{-6} m^2/s (20°C), or of sea water 1.3×10^{-6} m^2/s (10°C).
4. Ripple dimensions given by the design curves of Mogridge, Reference 15.

In most cases, sediment load was presented as a plot of concentration vs. depth. We integrated these plots, either analytically or numerically, from water surface to bed to obtain the total load, X. We then calculated the values of W_c or θ necessary to make the computed load match the measured one, as with our own data.

THRESHOLD OF MOVEMENT

All the computed thresholds are plotted on Figure 3 as Shields parameter, θ, against dimensionless grain size, D_{gr}. The Shields parameter is simply the square of the Ackers and White mobility numbers, F_{gr} or F_{gr_c}. The following are also plotted on Figure 3.

1. The Shields curve, Reference 16, for threshold of movement under unidirectional flow over a plane bed. Threshold was determined by observation and is somewhat subjective.
2. The Ackers and White threshold of movement criterion, Equation (11), for unidirectional flow over a rippled bed. This criterion has been inferred from measured rates of sediment transport, and may therefore be more objective than the Shields curve.
3. Thirty-five points presented by Komar and Miller, Reference 13, for threshold of movement under oscillatory flow. These points come from a variety of sources, but in general are the results of observation of the initiation of motion on a plane bed.

Regression analysis was performed on the sediment load data, i.e. not the Komar and Miller pure threshold data, of Figure 3. This showed the primary correlation to be between W_c^2, (and thus θ) and D_{gr}. A secondary, but very much weaker correlation was found between W_c and the wave height to water depth ratio. The best fit is given by

$$W_c^2 = 0.04141\, D_{gr} + 0.20354 \tag{22}$$

This too can be converted to a threshold of movement criterion for waves only, using Equation (11)

$$\theta_{c_w} = \frac{F_{gr_c}^2}{W_c^2} = \frac{\left(\frac{0.23}{\sqrt{D_{gr}}} + 0.14\right)^2}{0.04141\, D_{gr} + 0.20354} \tag{23}$$

Equation (23) is plotted on Figure 3 as "'Best fit' waves only".

The data of Bliven, Huang and Janowitz, Reference 3, clearly do not fit on this "best fit" line, lying considerably below it. This indicates a measured sediment load larger than that predicted by the modified Ackers and White technique. This is one of the few data sets which includes the effects of currents, in addition to waves, but the sediment transports, measured using a dyed sand tracer technique, are two orders of magnitude larger than the similar data of Inman and Bowen, Reference 9, who used sediment traps. It therefore seems that Bliven et. al. may have made an erroneous assumption in converting their measured dispersion of dyed sand into transport rates. Their data was therefore not used in calculating the "best fit" line. The correlation coefficient of W_c against D_{gr} is 0.8 without this data.

The data of Sleath, Reference 17, also lies below the two currents-only threshold curves and the oscillatory flow thresholds reported by Komar and Miller. It does, however, conform to the "best fit" line of the finer-grained sediments. This may mean that there are factors other than threshold of movement involved in W_c, for example flow through the bed, for coarse-grained sediments. This must be checked with more measurements of sediment load at the coarse-grained end of the range.

For the present, therefore, we are using Equation (22) for the prediction of W_c, but limiting the technique to the calculation of sediment loads for values of D_{gr} less than 10.

SUMMARY OF METHOD

1. Calculate D_{gr} from Equation (1).

2. Calculate empirical coefficients, C, F_{gr_c} m and n from Equations (10), (11), (12) and (13).

3. If waves predominate and bedform dimensions are unknown, use Mogridge curves, Reference 15, to calculate ripple height Δ and wavelength λ.

4. Calculate bed roughness, r

$$r = 25\frac{\Delta^2}{\lambda} \tag{24}$$

from Reference 19.

5. Calculate the dimensionless Chézy coefficients $C_{h\,cg}$ and $C_{h\,fg}$ using Equations (3) and (5).

6. Calculate the Jonsson wave friction factors,

$$\left.\begin{aligned} f_{w\,cg} &= \exp\left(-5.98 + 5.21\left(\frac{d_o}{2D}\right)^{-0.19}\right) \qquad (25)\\ f_{w\,fg} &= \exp\left(-5.98 + 5.21\left(\frac{d_o}{2r}\right)^{-0.19}\right) \qquad (26)\end{aligned}\right\} \quad f_w \leqslant 0.30$$

These approximate formulae are from Swart, Reference 19.

7. Calculate threshold factor, W_c^2, from Equation (22).

8. Calculate bed shears, τ_{cg} and τ_{fg}, using Equation (20) and convert to shear velocities, u_{*cg} and u_{*fg}, with Equation (8).

9. Calculate powers, P_{cg} and P_{fg}, using Equation (21).

10. Calculate the mobility number, F_{gr}, using Equation (7).

11. Calculate the mass transport velocity, V_m, using Equation (19a).

12. Calculate sediment load by Equation (9). If the current velocity, V, is less than the mass transport velocity, V_m, V_m should be used instead of V in Equation (9).

ACKNOWLEDGEMENTS

I am indebted to many people for their help and advice in the formulation of the technique reported here. In particular, thanks are due to Dr. C.A. Fleming, Ir. J. Moes, Dr. G.R. Mogridge and Dr. D.H. Swart. I am especially grateful to Dr. Swart for making his vast collection of sediment concentration data available to me.

Ms. M.A. Palmer, a summer student at NRC, presently in the Department of Civil Engineering at the University of New Brunswick, made the sediment load measurements reported in Table I. Her care in collecting and analyzing the data is greatly appreciated.

REFERENCES

1. Ackers, P.; White, W.R. *Sediment Transport: New Approach and Analysis.* Proceedings of the American Society of Civil Engineers, Vol. 99, No. HY11, November 1973, pp. 2041-2060.

2. Bhattacharya, P.K. *Sediment Suspension in Shoaling Waves.* Ph.D. Thesis, University of Iowa, 1971.

3. Bliven, L.; Huang, N.E.; Janowitz, G.S. *An Experimental Investigation of Some Combined Flow Sediment Transport Phenomena.* University of North Carolina, Center for Marine and Coastal Studies, Report No. 77-3, 1977.

4. Dalrymple, R.A. *Wave-Induced Mass Transport in Water Waves.* Proceedings of the American Society of Civil Engineers, Vol. 102, No. WW2, May 1976, pp. 255-264.

5. Fleming, C.A.; Hunt, J.N. *A Mathematical Sediment Transport Model for Unidirectional Flow.* Proceedings of the Institution of Civil Engineers, Great Britain, Part 2, Vol. 61, 1976, pp. 297-310.

6. Hom-ma, M.; Horikawa, K. *Suspended Sediment Due to Wave Action.* Proceedings of the 8th Conference on Coastal Engineering, 1962, Vol. I, pp. 168-191.

7. Hom-ma, M.; Horikawa, K.; Kajima, R. *A Study on Suspended Sediment Due to Wave Action.* Coastal Engineering in Japan, Vol. 8, 1965, pp. 85-103.

8. Horikawa, K.; Watanabe, A. *Turbulence and Sediment Concentration Due to Waves.* Proceedings of the 12th Conference on Coastal Engineering, 1970, Vol. II, pp. 751-766.

9. Inman, D.L.; Bowen, A.J. *Flume Experiments on Sand Transport by Waves and Currents.* Proceedings of the 8th Conference on Coastal Engineering, 1962, pp. 137-150.

10. Jensen, J.K.
Sorensen, T.
Measurement of Sediment Suspension in Combinations of Waves and Currents.
Proceedings of the 13th Conference on Coastal Engineering, 1972, Vol. II, pp. 1097-1104.

11. Jonsson, I.G.
Wave Boundary Layers and Friction Factors.
Proceedings of the 10th Conference on Coastal Engineering, 1966, Vol. I, pp. 127-148.

12. Kennedy, J.F.
Locher, F.A.
Sediment Suspension in Water Waves.
IN Waves on Beaches and Resulting Sediment Transport, R.E. Meyer (ed.), Academic Press, New York, 1972, pp. 249-295.

13. Komar, P.D.
Miller, M.C.
Sediment Threshold Under Oscillatory Waves.
Proceedings of the 14th Conference on Coastal Engineering, 1974, Vol. II, pp. 756-775.

14. Madsen, O.S.
Grant, W.D.
The Threshold of Sediment Movement Under Oscillatory Waves: A Discussion.
Journal of Sedimentary Petrology, Vol. 45, No. 1, March 1975, pp. 360-361.

15. Mogridge, G.R.
Bedforms Generated by Wave Action.
National Research Council of Canada, Quarterly Bulletin of the Division of Mechanical Engineering and the National Aeronautical Establishment, April-June 1973, Report No. DME/NAE 1973(2), pp. 21-41.

16. Shields, A.
Anwendung der Aehnlichkeitsmechanik und der Turbulenzforschung auf die Geschiebewegung.
Mitteilungen der Preuszischen Versuchsanstalt füw Wasserbau und Schiffbau, Heft 26, Berlin 1936.

17. Sleath, J.F.A.
Sediment Transport by Waves.
University of Cambridge, Department of Engineering, Report No. CUED/A-Hydraulics/TR1, January, 1977.

18. Swart, D.H.
Weighted Value of Depth of Initiation of Movement.
Stellenbosch, South Africa, August 1977.

19. Swart, D.H.
Coastal Sediment Transport, Computation of Longshore Transport.
Delft Hydraulics Laboratory, Report No. R968, Part 1, 1976.

20. Wang, H.
Liang, S.S.
Mechanics of Suspended Sediment in Random Waves.
Journal of Geophysical Research, Vol. 80, 1975, No. 24, pp. 3488-3494.

21. Willis, D.H.
Sediment Load Under Waves and Currents.
Proceedings of the 16th Conference on Coastal Engineering, 1978, Vol. II, pp. 1626-1637.

22. Willis, D.H.
Wiegert, A.W.
Measurement of Sparse Sand Concentrations in a Laboratory Wave Flume.
Proceedings of the Workshop on Instrumentation for Currents and Sediments in the Nearshore Zone, NRC Associate Committee for Research on Shoreline Erosion and Sedimentation, October 1979, in preparation.

APPENDIX I

GENERAL NOTATION

C	coefficient in sediment load function (Equation 10)
C_g	wave group velocity $\left(\frac{L}{T}\right)$
C_h	dimensionless Chézy coefficient (Equations 3 and 5)
D	typical grain diameter $[L]$
D_{gr}	dimensionless grain size (Equation 1)
d	water depth $[L]$
d_o	maximum water particle excursion at the bed $[L]$
E	wave energy $\left(\frac{M}{T^2}\right)$
F_{gr}	sediment mobility number (Equation 7)
f_w	Jonsson wave friction factor, Reference 11, (Equations 25 and 26)
g	acceleration due to gravity $\left(\frac{L}{T^2}\right)$
H	wave height, trough to crest $[L]$
m	exponent in sediment load function (Equation 12)
n	transition exponent (Equation 13)
P	power per unit bed area (Equation 21) $\left(\frac{M}{T^3}\right)$
r	ripple roughness, a function of ripple geometry (Equation 24) $[L]$
s	ratio of mass density of sediment to that of the fluid
u_o	maximum wave orbital velocity at the bed $\left(\frac{L}{T}\right)$
u_*	shear velocity (Equation 8) $\left(\frac{L}{T}\right)$
V	mean unidirectional flow velocity $\left(\frac{L}{T}\right)$
V_m	mass transport velocity of the waves (Equation 19a) $\left(\frac{L}{T}\right)$
W_c	empirical wave shear coefficient (Equation 22)
X	sediment load (Equation 9)
x	horizontal co-ordinate $[L]$
α	horizontal angle between wave orbital velocity and mean current velocity
Δ	ripple height, trough to crest $[L]$

GENERAL NOTATION (Cont'd)

θ	Shields parameter, see Figure 3
λ	ripple wavelength $[L]$
υ	kinematic viscosity of the fluid $\left(\frac{L^2}{T}\right)$
ρ	mass density of the fluid $\left(\frac{M}{L^3}\right)$
τ	shear stress at the bed (Equation 20) $\left(\frac{M}{LT^2}\right)$

Subscripts

c	critical for initiation of sediment motion
cg	coarse grain
fg	fine grain
TOT	total
w	due to waves

TABLE I

EXPERIMENTAL RESULTS

Data Set	Measured Quantities					Computed Quantities				
	Depth	Wave Height	Wave Period	Water Temperature	Sediment Load	Ripple Height	Ripple Length	D_{gr}	W_c	θ
	m	m	s	°C	—	m	m	—	—	—
Roll 4546	0.252	0.063	1.54	19.2	6.8×10^{-5}	0.008	0.052	6.21	0.768	0.088
Roll 4748	0.250	0.078	1.54	20.1	3.3×10^{-5}	0.010	0.064	6.30	0.602	0.143
Roll 4950	0.249	0.088	1.33	19.2	4.7×10^{-6}	0.009	0.059	6.21	0.508	0.202
Roll 5354	0.244	0.098	1.25	19.9	4.8×10^{-5}	0.009	0.061	6.28	0.543	0.176
Roll 5556	0.244	0.064	1.43	20.0	2.4×10^{-5}	0.008	0.049	6.30	0.701	0.105
Roll 5758	0.244	0.051	1.43	20.3	2.1×10^{-5}	0.006	0.039	6.32	0.845	0.072
Roll 6162	0.252	0.069	1.43	23.0	9.2×10^{-6}	0.008	0.051	6.59	0.635	0.126
Roll 6364	0.250	0.051	1.33	22.1	6.2×10^{-6}	0.005	0.035	6.50	0.829	0.075
Roll 6566	0.248	0.068	1.33	22.8	1.7×10^{-5}	0.007	0.046	6.57	0.673	0.113
Roll 6768	0.248	0.061	1.25	23.6	3.1×10^{-6}	0.006	0.038	6.65	0.705	0.102
Roll 6970	0.246	0.057	1.43	22.9	0	0.007	0.043	6.58	0.651	0.120
Roll 7172	0.246	0.079	1.25	23.1	3.5×10^{-5}	0.008	0.049	6.60	0.634	0.127
Roll 7374	0.245	0.067	1.54	23.2	9.7×10^{-6}	0.009	0.056	6.61	0.629	0.129
Roll 7576	0.245	0.075	1.43	22.8	1.2×10^{-4}	0.009	0.056	6.57	0.701	0.104
Roll 7778	0.243	0.068	1.46	21.7	3.2×10^{-5}	0.008	0.053	6.46	0.671	0.114
Roll 7980	0.242	0.067	1.20	21.4	9.6×10^{-6}	0.006	0.040	6.43	0.681	0.111
Roll 8182	0.239	0.058	1.37	20.0	1.3×10^{-5}	0.007	0.043	6.28	0.737	0.096

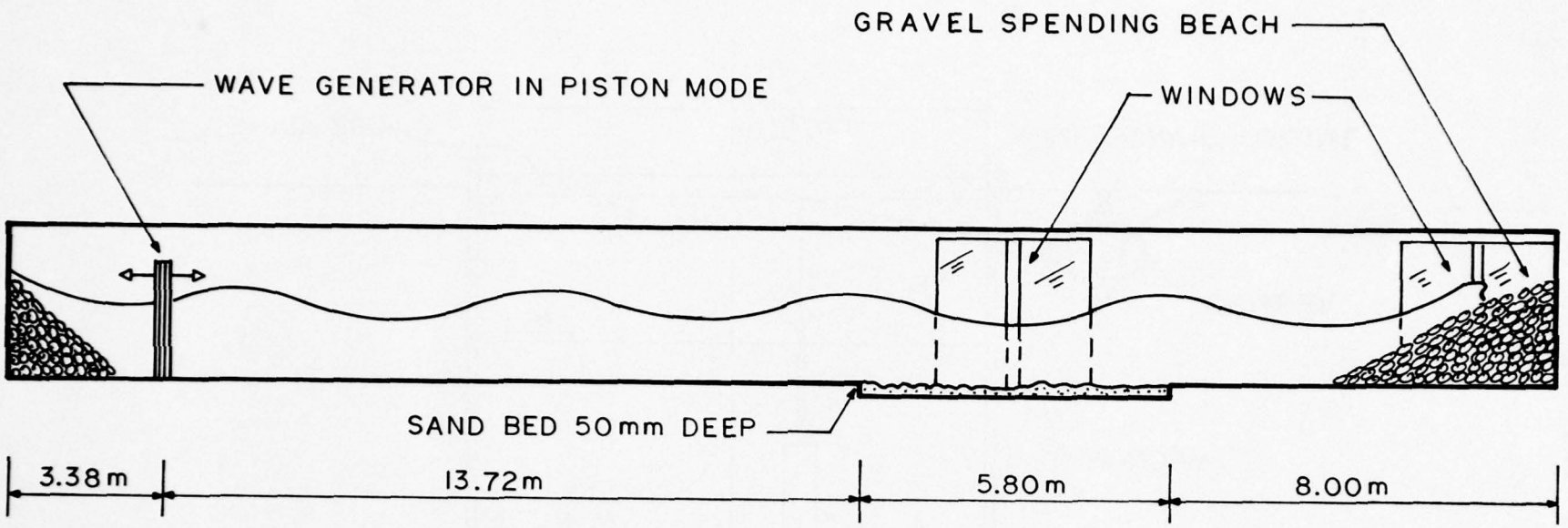

FIG. 1: LONGITUDINAL SECTION OF BEACH FLUME

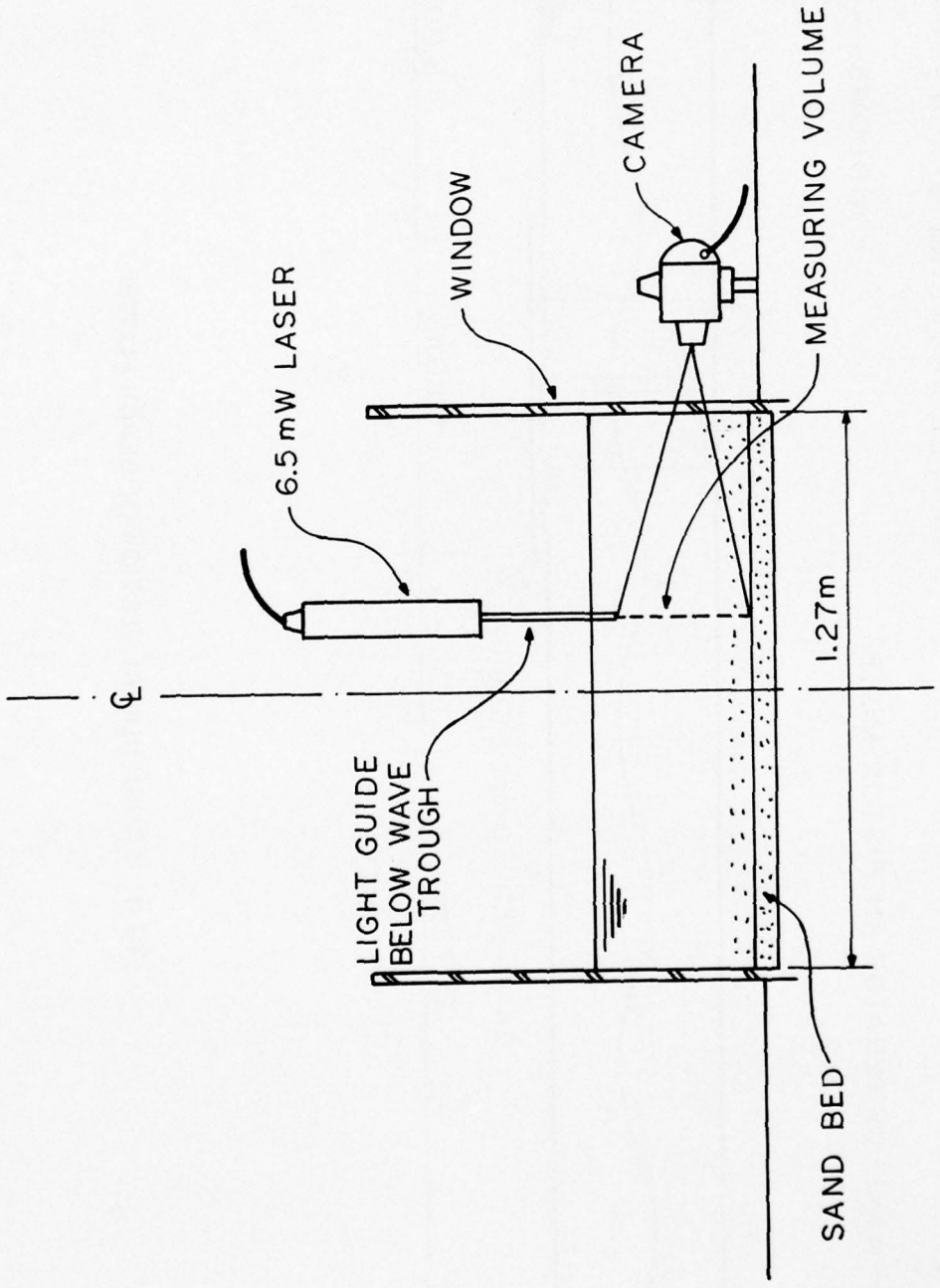

FIG. 2: FLUME CROSS-SECTION

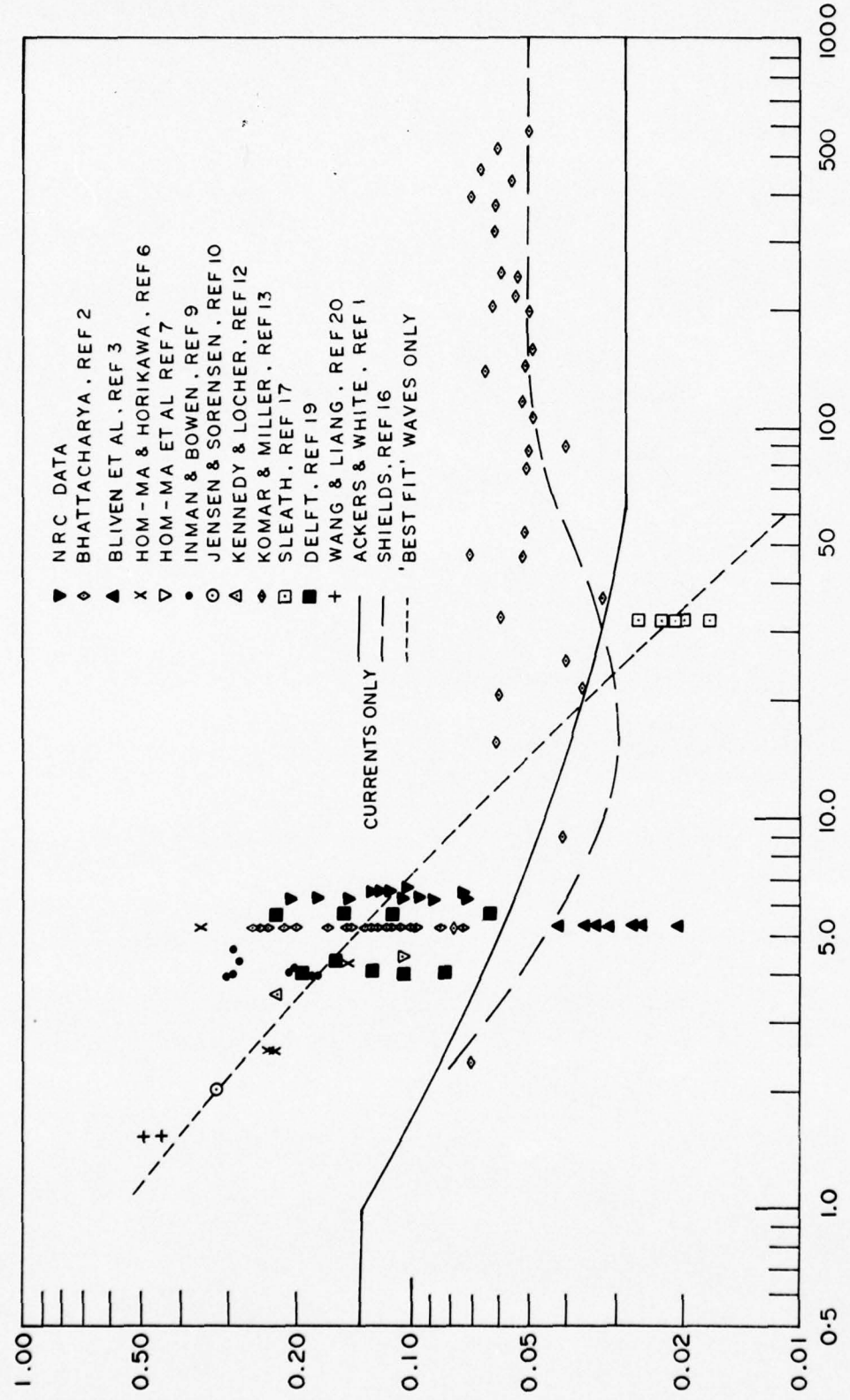

FIG. 3: THRESHOLD OF MOVEMENT

A WIND TUNNEL INVESTIGATION OF A RETRACTABLE FABRIC ROOF FOR THE MONTREAL OLYMPIC STADIUM†

H.P.A.H. Irwin and R.L. Wardlaw

Low Speed Aerodynamics Laboratory

National Aeronautical Establishment

ABSTRACT

The Stadium playing field is to be covered by a retractable fabric roof that is attached to the fixed part of the roof covering the stands. The fabric is tensioned by cables rising up to a tower above the Stadium. The purpose of the investigation has been to determine the effect of wind on the forces imparted to the fixed roof structure by the deployed fabric roof. A 1:100 scale model has been studied in the National Research Council 9m × 9m (30 ft. × 30 ft.) Low Speed Wind Tunnel. The fabric roof and supporting cables have been modelled elastically.

NOTATION

A	area of roof
A_c	cross-sectional area of a cable
b	typical length of roof (e.g. its major axis)
c	speed of sound
D	aerodynamic drag of cable per unit length
E	Young's modulus
g	gravitational acceleration
K_T	slope of tension versus strain curve for warp or weft direction
K_S	slope of shear loading versus shear strain curve for warp or weft direction
L	integral scale of the turbulence
M_A	added mass
M_c	mass of cable per unit length
M_F	mass of roof fabric per unit area
M_v	virtual mass
n	frequency
P_I	absolute internal pressure

† A paper presented at the Fifth International Conference on Wind Engineering, July 8 - 14th, 1979, Fort Collins, Colorado.

Δp	excess of internal over external pressure in zero wind
q_{60}	$\frac{1}{2}\rho U_{60}^2$
S(n)	power spectrum of longitudinal velocity fluctuations
U	mean wind speed
U_e	velocity above boundary layer
U_{60}	value of U at representative height of roof, 60m (200 ft.)
u'	root-mean-square of longitudinal velocity fluctuations
V_I	internal volume covered by roof
X,Y	horizontal forces at perimeter attachment point, respectively parallel to and normal to the console axis (Fig. 3)
Z	vertical force at perimeter attachment point
$\overline{\Delta X}, \overline{\Delta Y}, \overline{\Delta Z}$	mean change in X, Y and Z due to wind
γ	ratio of specific heats for air
ζ	damping ratio in vacuo (mechanical damping)
ζ_a	*damping ratio due to acoustic damping*
μ	viscosity of air
ρ	density of air
ϕ	wind angle, see Figure 3

INTRODUCTION

An unusual feature of this investigation is that it focusses on the dynamic behaviour under wind action of a membrane-like structure — a retractable roof that will be installed over the playing field of the 70,000 seat Montreal Olumpic Stadium (Fig. 1). While there have been some analyses of wind action on such structures (Ref. 1), the only other similar wind tunnel investigations, to the authors' knowledge, are References 2, 3 and 4. Interesting scaling requirements, acoustic considerations and virtual mass effects have been encountered in the course of the present study.

The 168m (552 ft.) high tower that will support the roof is, itself, a major structure and will visually dominate the Stadium as can be seen in Figure 2, a photograph of the 1:100 scale model that has been studied in the National Research Council 9m × 9m (30 ft. × 30 ft.) Low Speed Wind Tunnel. The base of the tower already houses the Olympic swimming pools and when completed, the tower will accommodate extensive additional athletic facilities, administrative offices and a high level restaurant.

The retractable fabric roof is attached to the fixed roof that covers the stands and is tensioned upwards by cables leading into the tower as illustrated in Figure 3. The roof is retracted by the paying out of cables at the rigid roof while drawing it upwards and into the tower where the collapsed roof is stored. The open elliptical area to be covered is about 180m (600 ft.) × 120m (400 ft.) and the fabric has an area of 18,000m^2 (190,000 ft.^{2}).

FIG. 1: AERIAL VIEW OF THE OLYMPIC SITE

The purpose of the investigation has been to determine the effect of wind on the forces imparted to the attachment points on the fixed roof structure by the retractable roof while in the deployed position. These forces create bending moments in the long, curved cantilever beams (subsequently referred to as consoles) that support the shell of the fixed structure and there had been some concern that the effect of wind on the forces was not known with adequate precision. A secondary purpose, that will not be discussed in this paper, was the measurement of surface pressures on the tower for cladding design. In 1973, at a much earlier stage in the design of the Stadium, wind tunnel investigations were undertaken by Romani (Ref. 5) at the Laboratoire Eiffel, Paris, France. Measurements were made of the wind pressure on the roof using a 1:150 scale rigid model. These data were then used by the French roof designers, Technique Avancée de l'Architecture et de l'Aménagement (TAAA), of Paris to compute the roof loading using quasi-static assumptions. In the present investigation, the removable roof was modelled elastically and tested in a simulated turbulent wind layer so that the forces, including dynamic behaviour, could be measured directly using three-component strain gauge balances at each of the seventeen attachment points on the fixed roof. In addition, deflections were measured at six points. It was not considered necessary to model the tower or the fixed shell of the Stadium elastically. Two configurations were tested — one for winter usage where the gap between the fabric roof and the fixed roof is sealed and the other for summer usage during rainstorms where the gap is left open.

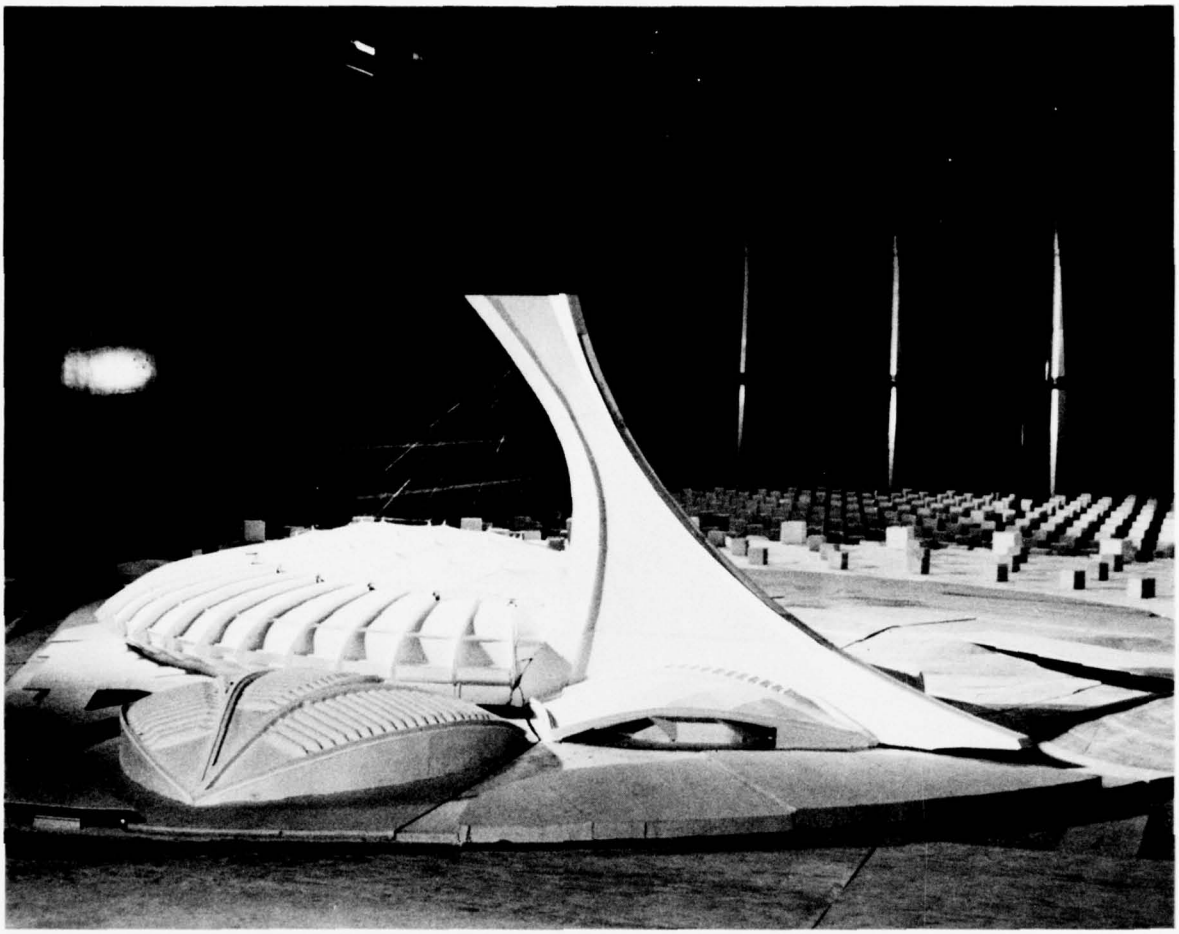

FIG. 2: 1:100 SCALE MODEL IN 9m X 9m (30 ft. X 30 ft.) LOW SPEED WIND TUNNEL

A novel feature of the model design has been the fabrication of a model scale material having the appropriate mass and elastic properties to simulate the full-scale material which is a woven Kevlar mat coated on both sides with plasticized polyvinylchloride. The development of a satisfactory technique for fabricating the material in the laboratory lagged behind the rest of the program. As a result, a preliminary investigation (Ref. 6) was done using Dacron sailcloth weighing 0.83 N/m^2 (0.017 $lb/ft.^2$), about four times the correctly scaled weight of 0.21 N/m^2 (0.0045 $lb/ft.^2$). Subsequently, when the lighter roof material was available, a final test was done that is reported here. Some disparity was found between the measured forces and the earlier TAAA force predictions used in the Stadium design but it has been concluded that under wind action, the forces will remain within acceptable limits. Response peaks suggestive of wind-induced instability were observed but it has been determined that they were excited by the characteristic acoustic frequencies of the wind tunnel and no purely aerodynamic instability was detected. Mean deflections of the roof occurred which would have an effect on the measured forces, thus supporting the use of an aeroelastic as opposed to a rigid model.

As well as describing the investigation, the paper considers novel scaling requirements, added mass effects, acoustic damping and the importance of the elastic and mass properties of the roof material.

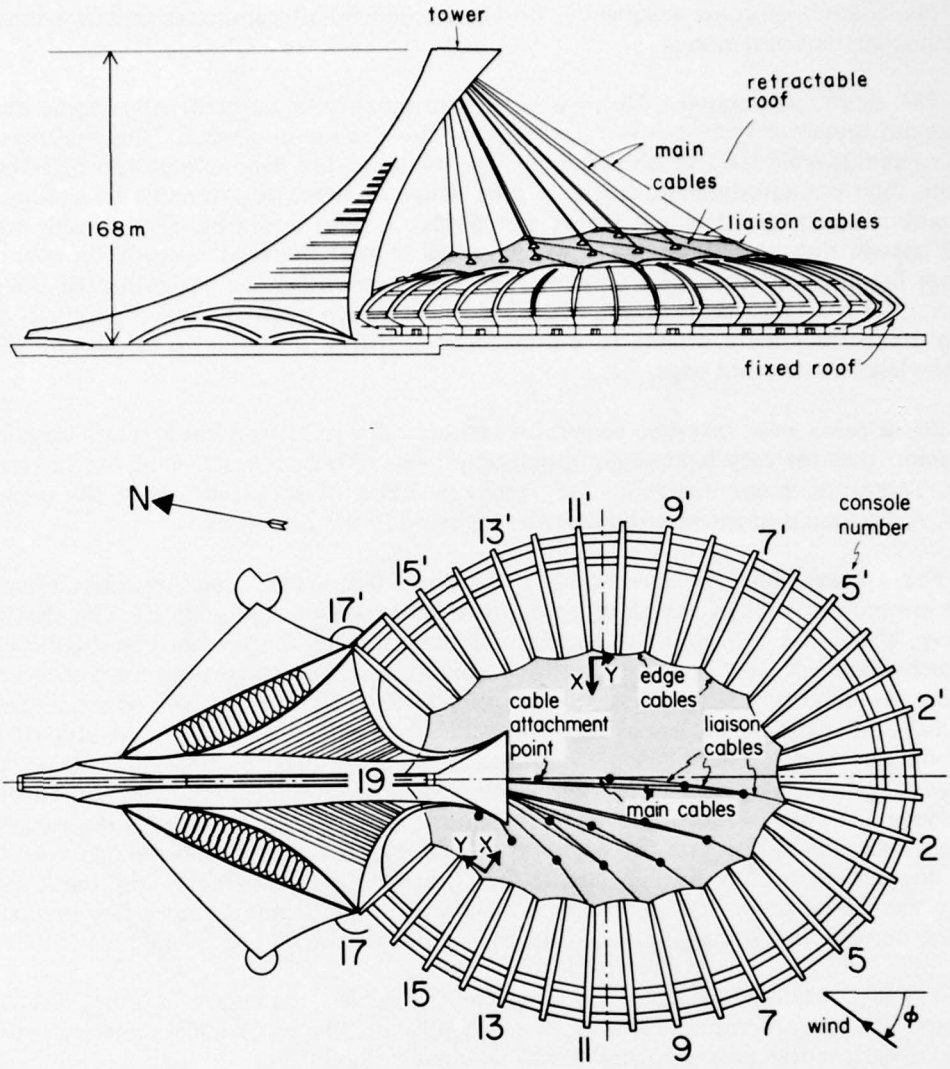

FIG. 3: STADIUM DETAILS

SIMILARITY REQUIREMENTS

For a cable-supported membrane roof system that is attached to a rigid structure, the following physical quantities have potential roles in determining its behaviour under wind action: M_F, M_c, ρ, b, K_T, K_S, U, μ, EA_c, D, g, Δp, ζ, V_I, γ, P_I.

Since woven fabric membranes have non-linear stress-strain relationships, the stiffnesses K_T and K_S were taken to be representative values in the range of stress of most importance. There are a total of sixteen physical quantities in the preceding list and they are made up from three fundamental units. Thus, by the Pi Theorem, a minimum of thirteen non-dimensional parameters are required to describe the behaviour of the complete roof system. An appropriate set is:

$$\frac{\rho Ub}{\mu}, \frac{U^2}{bg}, \frac{M_F}{\rho b}, \frac{K_T}{\rho U^2 b}, \frac{K_S}{K_T}, \frac{M_c}{\rho b^2}, \frac{EA_c}{\rho U^2 b^2}, \frac{D}{\rho U^2 b}, \zeta, \frac{\Delta p}{\rho U^2}, \gamma, \frac{P_I b^3}{\rho U^2 V_I}, \frac{\gamma P_I}{\rho U^2}$$

The non-dimensional frequency, nb/U, is a dependent parameter that is a function of the preceding independent parameters.

The Reynolds number, $\rho Ub/\mu$, was, as with most tests, ignored. After some analysis it was also considered unnecessary to achieve similarity of the Froude number, U^2/bg, because the gravitational forces at full scale tend to be much smaller, owing to the light weight and high tension of the roof system, than the aerodynamic forces in high winds or those due to cable tensioning. An exceptional situation, where gravitational forces would play a role, would be when a cable went slack at high wind speeds due to the tendency of the wind to pull the roof upwards in some areas. The gravitational force would then be of importance for determining the excitation of the slack cable itself but not for the loads at the perimeter of the roof which were under study here. If a cable were sufficiently slack for gravity effects to influence its stiffness, it would no longer contribute significantly to the loads at the roof edge.

Some pains were taken to obtain the correct value of $M_F/\rho b$ but at a late stage in the work, it was realized that for very lightweight membranes, the added mass effect of the surrounding air is important. Therefore, there was room for some relaxation of the accuracy of the membrane mass simulation. A discussion of the added mass effect is given in the Appendix.

For a completely flat membrane, the natural frequencies and the small deflections under static load are independent of the elastic properties of the membrane material. The elastic properties do, however, affect the behaviour of curved membranes so in the present investigation it was considered worthwhile that they be simulated. Accordingly, the velocity scaling for the experiments was derived from the condition that the stiffness parameter $K_T/\rho U^2 b$ be the same at model and full scale. Since the full-scale fabric had, essentially, negligible shear stiffness, a very low value of K_S/K_T was aimed for on the model. There is some evidence (Refs. 2, 3) that the behaviour of tensioned membranes in wind is not very sensitive to their elastic properties, the membrane deflections being such as to require very little strain, but more work is required in this area to establish the range of applicability of such an assumption and the degree to which elastic similarity can be relaxed. When a cable supported membrane roof is initially tensioned, the resulting movement and the final shape are affected by the elastic properties and this must be borne in mind, and the necessary precautions taken to obtain the correct final shape, if elastic similarity conditions would be relaxed.

It was considered desirable to simulate the cable parameters $M_c/\rho b^2$, $EA_c/\rho U^2 b^2$ and $D/\rho U^2 b$ and this was accomplished using steel piano wire. The mechanical damping ratio, ζ, of the full-scale roof system was unknown but it was thought unlikely that the model mechanical damping ratio would be higher than at full scale because the model cables were mono-filaments compared with the full-scale stranded cables, which have high damping.

The parameter $\Delta p/\rho U^2$ is of importance for air-supported structures but for the present cable-supported roof, the only form of internal pressurization came from the air-conditioning and heating systems and it was estimated to have only a minor effect compared with the wind pressure at high speeds. For a sealed structure, the internal volume contributes a pneumatic stiffness if the membrane roof deflections produce a net change of internal volume. To model this effect correctly, Tryggvason and Isyumov (Ref. 2) assumed isothermal conditions in the internal volume and deduced that $P_I b^3/\rho U^2 V_I$ should be the same at model and full scale. A better approximation, at least for rapid movements of the roof, would appear to be that the volume change takes place adiabatically but the result is still that $P_I b^3/\rho U^2 V_I$ is the relevant parameter. Since P_I is essentially atmospheric pressure (in practice $\Delta p \ll P_I$ even for air-supported structures), it transpires that correct scaling of pneumatic stiffness requires exaggeration or diminution of the model internal volume, compared with scaling according to b^3, unless the ratio of model velocity to full-scale velocity is 1:1. The Olympic Stadium internal volume could not be considered completely sealed, even with the roof-edge gap sealed, because underground passageways lead to large air vents and because the structure has many points where leakage would take place thus preventing the full pneumatic stiffness from being realized. On the model V_I was many times greater than the parameter $P_I b^3/\rho U^2 V_I$ would dictate since the underside of the model opened into a large volume under the turntable and the velocity scaling was close to 1:1. No attempts were made to seal the interior. Thus, the pneumatic

stiffness effect was certainly less than at full scale, resulting in a conservative model behaviour. In fact, from an order of magnitude analysis given in the Appendix, it appears unlikely that modes of membrane vibration that result in a net volume change would ever be excited to large amplitude. This is because they radiate low frequency acoustic waves into the external air resulting in a damping of the membrane motion. The term acoustic is used for convenience, although at full scale the wavelength would be much larger than those normally associated with acoustics. To simulate the acoustic damping effect correctly at model scale, similarity of the parameter $\gamma P_I/\rho U^2$, which is equivalent to $(U/c)^{-2}$ where c = speed of sound, is required. Thus Mach number scaling is required and implies that strictly the velocity scaling should be 1:1, assuming c is unalterable. However, having the model Mach number less than at full scale can be regarded as conservative (see Appendix). Aerodynamic damping also contributes to the overall damping but the size of this effect has not been estimated. No additional similarity parameters, over and above those already considered, need be introduced in order to correctly simulate aerodynamic damping.

Similarity of the wind was provided by the spire/roughness technique and a 3.7m (12 ft.) thick boundary layer was produced. Figures 4 and 5 show the mean velocity profile, turbulence intensity and power spectrum. The integral scale, L, of the turbulence, defined as the area under the autocorrelation curve for the longitudinal turbulence, was 1.2m (4 ft.) at the roof height.

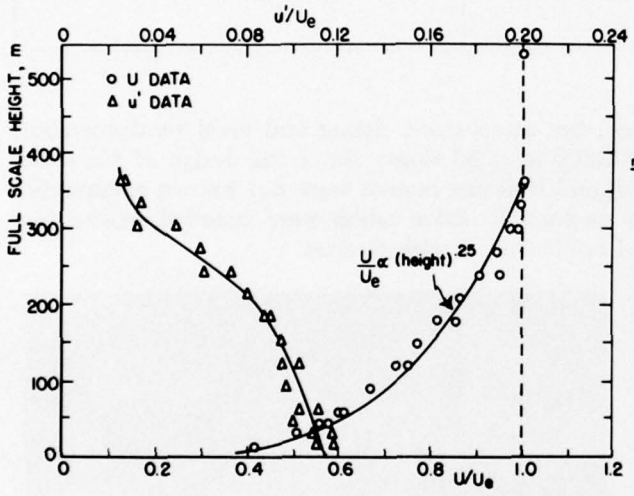

FIG. 4: MEAN VELOCITY AND TURBULENCE INTENSITY IN WIND SIMULATION

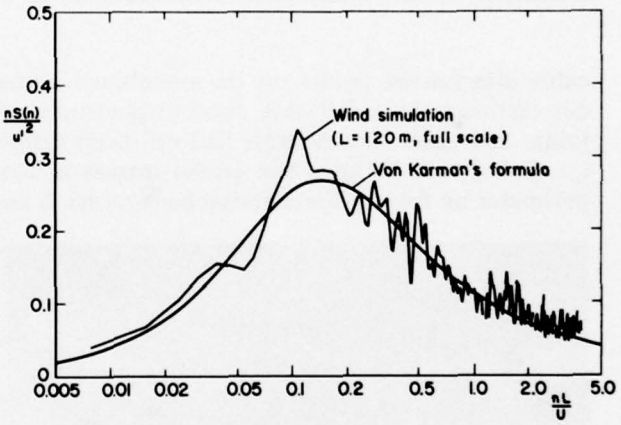

FIG. 5: POWER SPECTRUM OF VELOCITY AT ROOF HEIGHT

MODEL FABRICATION

The details of the full scale and model roof materials are summarized in Table 1 while Figure 6 shows the model roof. The values of K_T and K_S in the table were measured in the laboratory on some samples of the full scale and model fabric.

The Kevlar net, from which the model roof was made, was specially woven as a 32cm (12.6 in.) wide strip with a mesh size of 0.5cm X 0.5cm (0.2 in. X 0.2 in.). Segments of the Kevlar net were stretched over a rectangular frame to maintain stability and the polyethylene sheet was bonded to the Kevlar using diluted contact cement that had been sprayed onto the polyethylene. The roof was then assembled on a mould from the segments of composite material. Joints in the material were made using reinforcing strips of Dacron fabric and epoxy resin, the total weight added from all joints being equivalent to approximately 15% of the membrane weight. The joints in the full-scale roof are also made in a manner that results in significant added weight. At each of the 25

TABLE 1

ROOF MATERIAL

	Full Scale	Model
Fabric	1420 denier Kevlar 49 closely woven	100 denier Kevlar 29 woven as an open net
Airtight Coating	PVC on both sides	High density polyethylene sheet on underside
Mass	Kevlar 1.1 kg/m^2 Coating 1.1 kg/m^2 Total 2.2 kg/m^2	Kevlar 0.009 kg/m^2 Coating 0.006 kg/m^2 Adhesive 0.005 kg/m^2 Total 0.020 kg/m^2
Approximate K_T	16 MN/m	0.14 MN/m
Approximate $\frac{K_S}{K_T}$	6.2×10^{-4}	20×10^{-4}

cable attachment points on the membrane surface, the attachment fitting and local reinforcement corresponded to a full-scale concentrated mass of 3300 kg (230 slugs). Since the design of full-scale joints and cable attachments had not been settled, and thus the masses were not known accurately, the policy was to keep the model masses as low as possible. Edge cables were installed around the perimeter by folding the material back on itself and reinforcing it with Dacron.

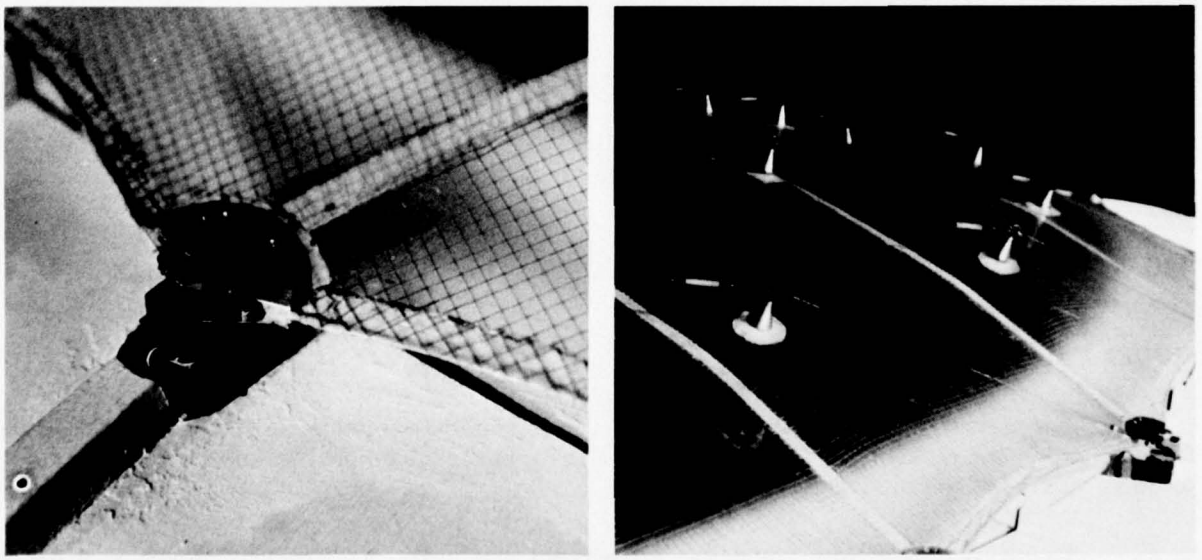

FIG. 6: MODEL ROOF

The external shape of the fixed Stadium structure was modelled in wood but inside was a rigid steel frame upon which the seventeen, three-component strain-gauge balances were mounted in order to measure the forces at the perimeter attachment points of the roof. After attaching the roof to the balances, the tension was applied to the main cables from the tower by a system of weights

and pulleys. This system circumvented some of the iterative process that would have been required to obtain the correct distribution of cable tensions. However, a considerable time was still spent in obtaining the desired distribution of tension amongst 'liaison' cables (see Fig. 3) and edge cables by means of screw adjustments. The target distribution of tensions had been computed by the roof designers and the tensions on the model were either measured directly using a strain-gauge tension meter or indirectly by measuring the fundamental frequency of vibration with the aid of a microphone. The edge-cable tensions were adjusted by monitoring the force balance readings and comparing them with the computed forces.

Attempts were made to excite the roof in zero wind and measure its natural frequencies which had not been previously computed. Figure 7 gives an example of a signal from a proximeter close to the centre of the roof, after the roof had been tapped at the far end from the tower. This figure also snows the motion power spectrum in which several modes of vibration are evident in the full-scale frequency range 0.1 to 0.3 Hz. No attempts were made to determine mode shapes since this would have been an elaborate experiment in itself because of the complexity of the structure.

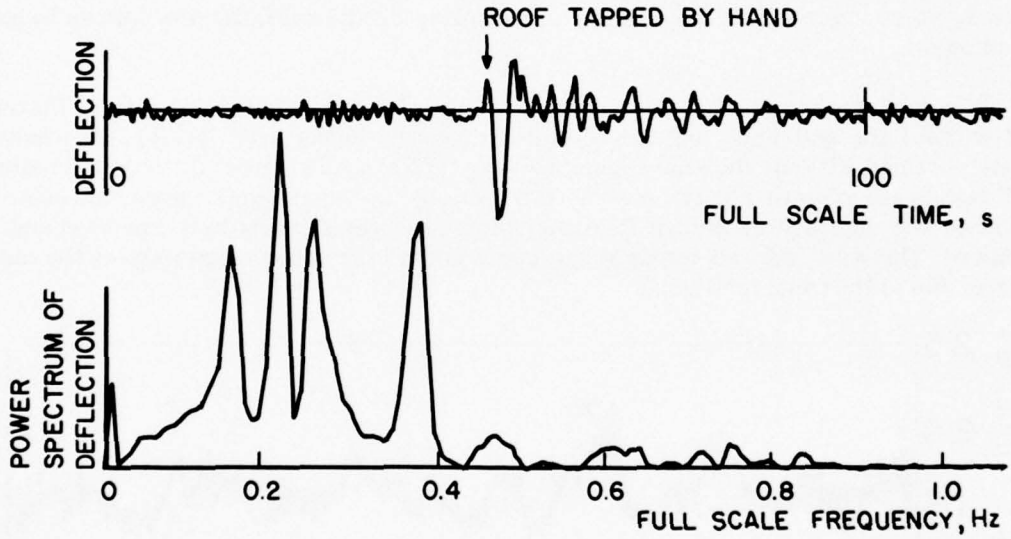

FIG. 7: EXAMPLE OF DAMPING TRACE AND POWER SPECTRUM OF DEFLECTION IN ZERO WIND

The roof vibration can be seen to be very highly damped. It is worth noting that on membrane structures the natural frequencies will in general depend on the mean wind speed because the wind changes the mean membrane tension which in turn affects the frequency. On the Stadium, the roof tension was increased by the wind so the natural frequencies would have increased to values above those measured in zero wind.

TESTING METHODS

The strain gauge balances were connected to the tunnel data system which was used to digitally analyze the balance signals. Up to six channels were sampled simultaneously. For some conditions, complete time histories were obtained and for others only statistical quantities such as mean, root-mean-square and peak forces were measured. The averaging period for the statistical quantities was equivalent to ½ hour and in some cases 1 hour at full scale and the sample rate on each channel was 200 points per second at model scale. Six proximeters were used to measure the membrane deflections, again the data being acquired and analyzed on the tunnel data system.

Tunnel noise and vibration were monitored using a microphone, mounted on the tunnel wall above the simulated boundary layer, and accelerometers mounted on the model structure and tunnel structure. A digital Fourier Analyzer was used to compute power spectra.

DISCUSSION OF RESULTS

One of the main reasons for conducting tests of this kind is to bring to light any unforeseen aerodynamic instabilities. Thus, large amplitude vibrations are looked for. It was found that the model roof, being a taut membrane, was sensitive to wind tunnel noise and it was important not to mistake the resulting large amplitude vibration for an aerodynamic excitation. Wind tunnel noise takes three principal forms, fan noise, standing waves and noise originating from vibration of the tunnel structure. In the present experiments, standing waves, whose frequency is independent of fan speed, caused considerable roof excitation at certain resonant speeds and significant contributions from the other two sources were also evident. Therefore, the discrete frequencies of the tunnel noise and vibration were measured over a range of speeds with the roof absent and the results were then used to remove the worst of the acoustic contamination from the force and deflection measurements. After this had been done, no significant aerodynamic instability could be detected over the mean wind speed range tested, equivalent to 0 to 30 m/s (0 to 67 mph) at full scale. The vibratory forces reported in Reference 6, which describes the preliminary investigation on the roof, are now known to have been acoustic in origin.

The roof was tested with and without the edge of the roof sealed but most of the data were obtained without the seal since this last condition produced higher wind loading. All results in this paper were obtained without the seal. Figure 8 shows typical time histories of force at an attachment point (all results are expressed at full scale in this section). In the example shown, the acoustic contamination of the data, visible as high frequency vibration, was at a relatively low level and has not been removed. The wind induced forces at the upper end of the speed range were of the same order as the forces due to the cable tensioning.

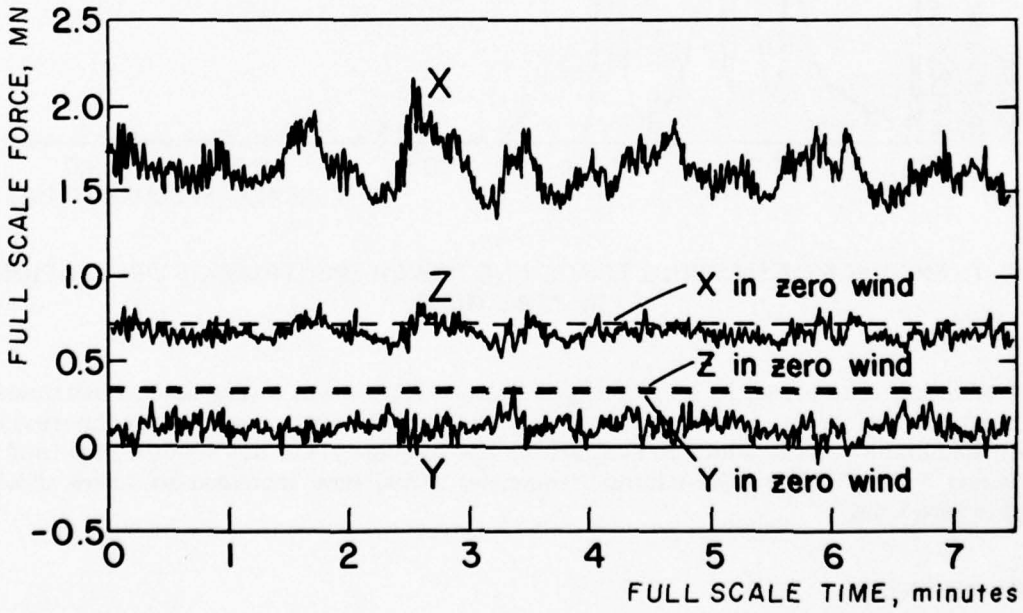

FIG. 8: TIME HISTORY OF FORCES ON CONSOLE 9, U_{60} = 26.7 m/s, ϕ = 90°

Figure 9 gives examples of the variation with wind angle of the mean and peak X-component forces. The angles ϕ = 90° and ϕ = 270° produced the greatest wind forces, which may be explained in terms of these being the directions where the highest flow curvature was generated over the roof. It was expected that at ϕ = 180°, at which angle the tower was upwind of the roof,

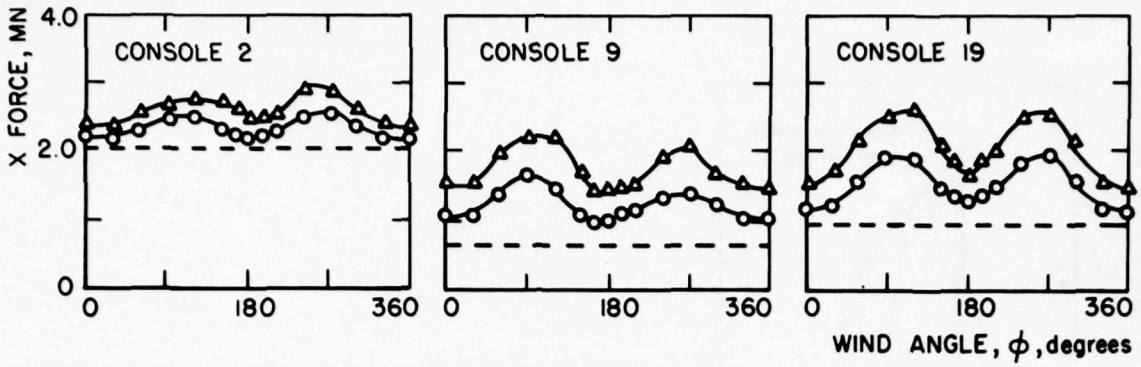

FIG. 9: VARIATION WITH WIND ANGLE OF MEAN AND PEAK X-COMPONENT FORCES ON THREE CONSOLES, U_{60} = 26.7 m/s
○-MEAN, △-PEAK, – – – ZERO WIND FORCE DUE TO INITIAL ROOF TENSION

there might be some excitation due to the tower wake but none was observed. Figure 10 shows the variation with wind speed of the root-mean-square (rms) of fluctuations in the X-component force on console 9 after being corrected for noise. The corrected rms forces varied smoothly with wind speed indicating no aerodynamic instability.

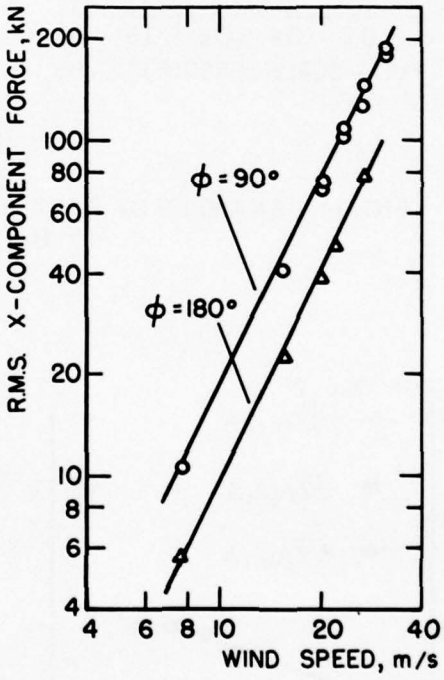

FIG. 10: RMS X-COMPONENT FORCE CONSOLE 9

The rms forces measured in the preliminary tests (see Introduction), where the roof mass was too high by a factor of approximately four, were very similar to the present values, thus verifying that the membrane mass need not be accurately simulated because of the large added mass effect. Figures 11(a),(b) show one of the worst cases of noise contamination and illustrate the degree to which wind-tunnel noise affected some of the measurements. Figure 12 shows examples of the mean force coefficients $\overline{\Delta X}/q_{60}A$, $\overline{\Delta Y}/q_{60}A$, $\overline{\Delta Z}/q_{60}A$ as functions of wind speed. It can be seen that significant changes occurred in some of the force coefficients as the wind speed increased. These changes are attributed mainly to deflections of the roof altering the mean pressure distribution and to the non-linear stiffness of the roof. Examples of mean deflections, some of which exceeded 10% of the local roof depth are given in Figure 13. In view of these results, the use of rigid pressure-tapped models for membrane-like structures should be approached with caution because of the neglect of deflection effects and the consequent danger of underestimating wind forces.

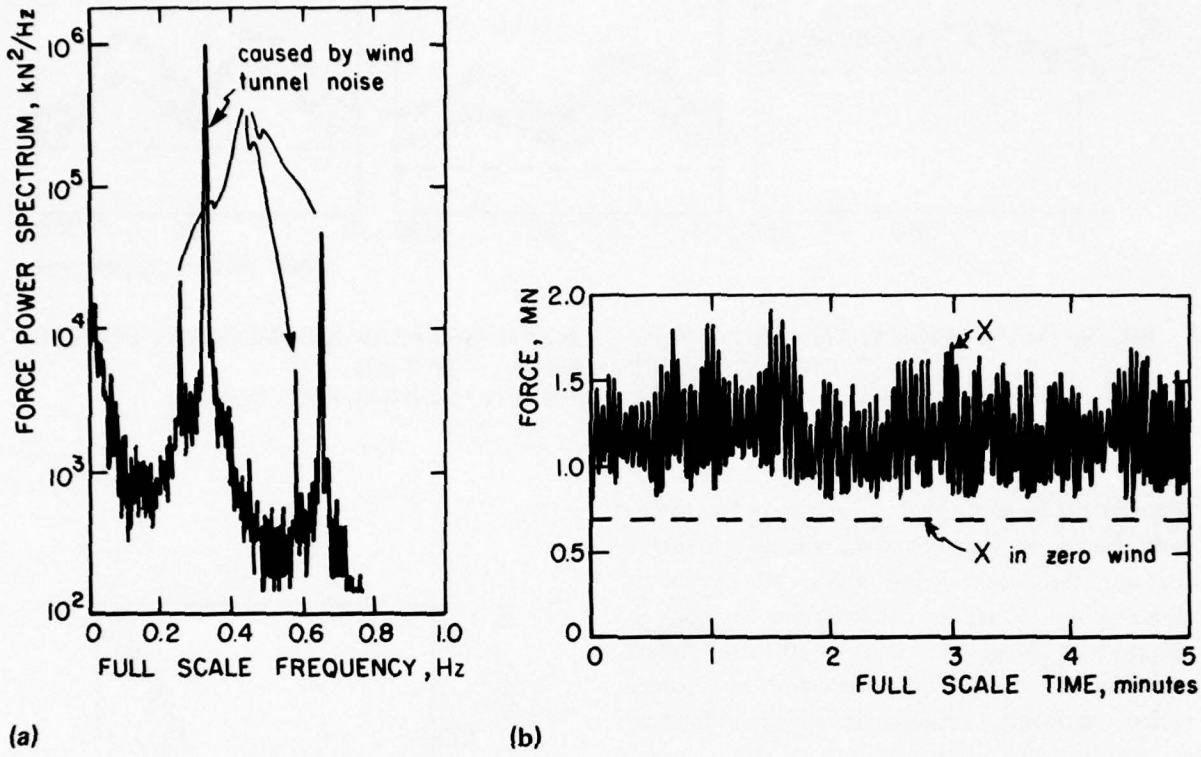

FIG. 11: EXAMPLE OF DATA BADLY AFFECTED BY WIND TUNNEL NOISE, U_{60} = 30 m/s, ϕ = 90°

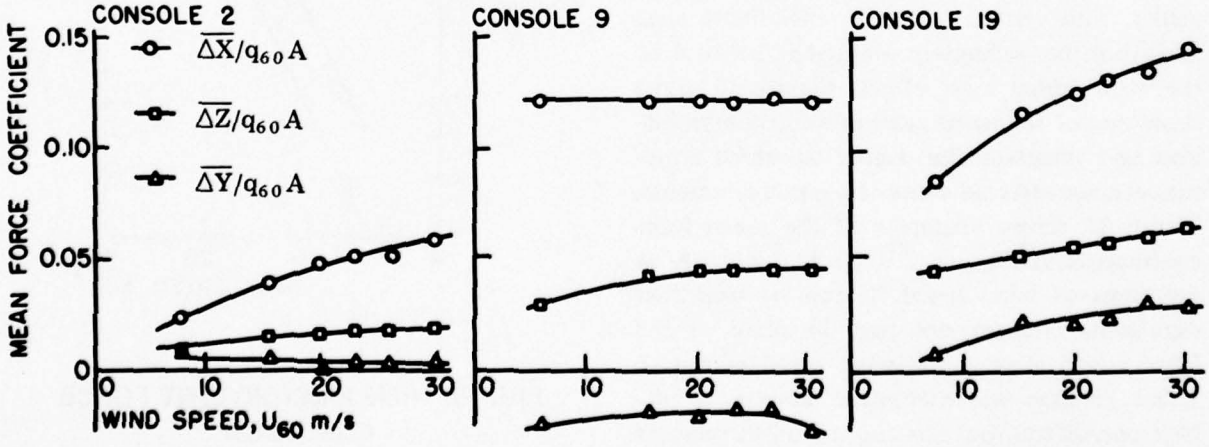

FIG. 12: MEAN FORCE COEFFICIENTS, ϕ = 90°

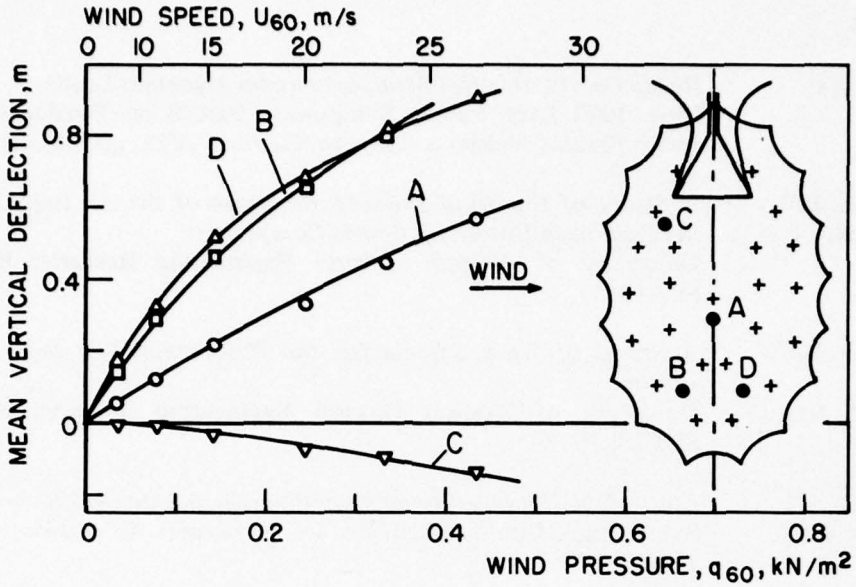

FIG. 13: MEAN DEFLECTIONS AT $\phi = 90°$

CONCLUSIONS

From this particular investigation, the following conclusions can be drawn which bear on wind effects on membrane-like structures in general:

(i) Added mass effects are significant and may in some instances be dominant for light-weight membranes. Thus, great precision is not always required in modelling the membrane mass.

(ii) Acoustic damping is likely to prevent volume displacing modes of vibration from being excited. To model this effect correctly requires Mach number scaling, i.e. a velocity scaling of 1:1 in normal wind tunnels, but velocity scaling of less than 1:1 is conservative. A velocity scaling of 1:1 has an additional advantage for sealed models in that no distortion of the internal volume is then required when modelling pneumatic stiffness.

(iii) Membranes are sensitive to wind tunnel noise and a thorough knowledge of the acoustic environment in the wind tunnel is essential in interpreting the data.

(iv) On the present roof the deflections due to wind were significant. It is felt inadvisable to estimate wind forces on membrane-like structures on the basis of pressure measurements on rigid models.

(v) No signs of aerodynamic instability were observed on the present model. References 2, 3 and 4 report the same absence of serious instabilities on other tensioned membrane structures.

REFERENCES

(1) Knudsen, W.C. — *Response of Cable-Net Structures under Dynamic Loads.* Proc. 1971 IASS Pacific Symposium Part II on Tension Structures and Space Frames, Tokyo and Kyoto, October 1971, pp. 365-376.

(2) Tryggvason, B.V. Isyumov, N. — *A Study of the Wind Induced Response of the Air Supported Roof for the Dalhousie University Sports Complex.* University of Western Ontario Engineering Research Report BLWT-SS7-1977.

(3) Tryggvason, B.V. Surry, D. Davenport, A.G. — *A Study of Wind Effects for the Haj Terminal at Jedda International Airport.* University of Western Ontario Engineering Research Report BLWT-SS9-78, 1978.

(4) Grillaud, G. Gandemer, J. — *Étude de la Réponse Dynamique d'une Structure Gonflable.* Symposium International sur les Structures Gonfables, C.I.B. Venise, June 1977.

(5) Romani, L. — *Stade Olympique de Montréal: Études Aérodynamiques sur Maquette.* Report to Architect Roger Taillibert from Laboratoire Eiffel, July 16, 1973.

(6) Irwin, H.P.A.H. Proulx, J. — *A Wind Tunnel Investigation of the Montreal Olympic Stadium.* Proceedings of the Second Canadian Workshop on Wind Engineering, Varennes, Quebec, September 1978.

(7) Campbell, W.F. — *Additional Mass and Inertia Effects.* NRC/NAE Lab. Tech. Report LTR-LA-223, National Research Council of Canada, Ottawa, 1979.

(8) Irwin, H.P.A.H. Wardlaw, R.L. Wood, K. Bateman, K. — *A Wind Tunnel Investigation of the Montreal Olympic Stadium Roof.* NRC/NAE Lab. Tech. Report LTR-LA-228, National Research Council of Canada, Ottawa, 1979.

APPENDIX

ADDED MASS AND ACOUSTIC DAMPING

To estimate the order of magnitude of the added mass, consider a sphere, of surface area A, whose surface is somehow made to pulsate with a radial velocity uniform over the surface. Neglecting compressibility, the added mass of the air external to the sphere, per unit surface area, is

$$M_A = \rho\sqrt{\frac{A}{4\pi}} = 0.282\,\rho\,\sqrt{A}$$

Thus, if the surface is a fabric membrane of mass per unit area, M_F, the virtual mass per unit area, M_V, is

$$M_V = M_F + M_A = M_F + 0.282\,\rho\,\sqrt{A}$$

Now suppose A is 18,000 m^2, equal to the toal area of the Stadium roof, $M_F = 2.2$ kg/m^2 and $\rho = 1.23$ kg/m^3. Then $M_V = 2.2 + 46.6 = 48.8$ kg/m^2. Thus, the added mass is concluded to be large, an order of magnitude greater than the membrane mass. Campbell (Ref. 7) and Irwin (Ref. 8) have computed results of similar magnitude for flat membranes resembling the roof. Clearly, from the preceding analysis, the size of the effect depends on the membrane area and its mass.

In Reference 8 it is shown that for volume displacing modes of vibration of a nearly flat roof covering a sealed volume the radiated acoustic energy gives rise to an increment, ζ_A, in the damping ratio given by

$$\zeta_A = \frac{k}{2}\,\frac{\rho n A}{c M_v}$$

where c = speed of sound and k is a constant of order unity depending on the mode shape. In arriving at this expression, it was assumed that for typical frequencies of roof motion the wavelength of sound was much larger than the roof. Thus, for a sealed roof, with the same size and mass as the Stadium roof, and with frequencies in the range 0.1 to 1.0 Hz, it is deduced that the order of magnitude of ζ_A is in the range 0.06 to 0.6. This is a very large contribution to the damping. For an unsealed roof, the value of ζ_A would be reduced. The expression for ζ_A can be rearranged into the form

$$\zeta_A = \frac{k}{2}\left(\frac{M_v}{\rho b}\right)^{-1}\left(\frac{nb}{U}\right)\left(\frac{A}{b^2}\right)\left(\frac{U}{c}\right)$$

from which it is seen that for correct simulation of ζ_A it is necessary for the Mach number, U/c, to be the same on the model as at full scale. In many wind tunnels, the full-scale Mach number cannot be achieved but if the model Mach number is less than the full-scale value ζ_A will be less on the model than at full scale, and this is conservative.

CONCEPTUAL DESIGN STUDY OF A HIGH SPEED MAGLEV GUIDED GROUND TRANSPORTATION SYSTEM

W.F. Hayes

Control Systems and Human Engineering Laboratory

Division of Mechanical Engineering

1.0 INTRODUCTORY BACKGROUND

Non-contacting guided ground transportation systems have been seriously advocated since the early 60's as an extension to the available spectrum of passenger ground transport modes in offering potential for operational speeds which are limited only by energy consumption considerations, for minimal guideway maintenance, for a high utilization rate of the guideway, and for system operation without direct reliance on petrochemical fuels.

Early worldwide R&D activity was concerned largely with air cushion suspension and guidance concepts combined with either aerodynamic (i.e. ducted fan) or linear electrical motor propulsion. Investigations were pursued to the extent of building full-scale test vehicles and guideways in France (Société-Bertin et Cie), England (Tracked Hovercraft Ltd.) and U.S.A. (U.S. Dept. of Transport).

The relatively high power requirements of the tracked air cushion vehicle concept (typically 30-50 kw to statically support one metric ton) coupled with its requirement for relatively wide close-toleranced guideway surfaces and its high exterior noise level as generated by escape of the cushion air prompted investigation into alternative non-contacting magnetic suspension or "Maglev" concepts which typically require substantially less power, do not generate noise, and generally do not require as high a standard of guideway construction. Practical magnetic suspensions may be classified into two distinctly differing types as considered below. The conceptual engineering design for a Canadian high speed intercity Maglev guided ground transportation system as based on one of the two practical magnetic suspension types is summarized herein.

1.1 Electromagnetic Suspension System

1.1.1 Electromagnetic Suspension Characteristics

The electromagnetic suspension concept is based on the feedback control of the air gap between conventional dc electromagnets on the vehicle and ferromagnetic guideway rails towards which the magnets are attracted as shown in Figure 1. This suspension system must operate with small air gaps between the magnet pole faces and the steel guideway rails in order to realize its performance potential in terms of low suspension power and weight requirements. For example, a suspension electromagnet input power of only about 3-5 kw will statically levitate a metric ton at a nominal air gap of 15 mm with a magnet having a lift-to-weight ratio of about eight. This is about 1/10 the static suspension power per metric ton required for the air cushion concept. These suspension power requirements both increase quite substantially (i.e. up to the order of ten times the static suspension power requirement for velocities in the order of 400-500 km/hr) and at something like the same rate with increasing vehicle velocity. Such suspension power degradation is due to the adverse effects of eddy currents which are dynamically generated in the guideway rails in the case of electromagnetic suspension and of air curtain leakage in the case of air cushion suspensions. The relatively stiff electromagnetic suspension operating at small air gaps results in the magnets closely "tracking" the guideway irregularities. This necessitates relatively closely aligned steel rails mounted on a fairly stiff guideway structure to prevent magnet face contact with the rails at high vehicle speeds. Small air gap operation also necessitates a secondary suspension spring-damper between the magnets and the vehicle cabin to isolate passengers from guideway roughness induced vibration.

The small operational gap of the electromagnetic suspension has tended to favour the use of an electrical Linear Induction Motor (LIM) for propulsion. Such a LIM is typically comprised of electrically energized iron-core windings mounted on the vehicle which induce eddy currents in a closely adjacent aluminium sheet "reaction plate" mounted on the guideway so as to generate propulsion thrust. Such a linear induction motor requires vehicle electrical power pick-up from guideway mounted conductors and on-board power conversion to variable frequency and/or voltage in order to attain tolerable motor efficiency over an extended velocity range.

More recently there has been the increasing tendency to favour an iron-core Linear Synchronous Motor (LSM) concept for the propulsion of electromagnetically suspended vehicles. Such an iron-core LSM may be comprised of variable frequency electrically energized iron-core windings mounted on the guideway which magnetically couple with iron-core d.c. field windings distributed lengthwise along the vehicle. There are also other configurations of this general linear motor type as based on the reluctance motor principle which do not require active guideway windings but require only passive ferromagnetic material distributed along the guideway. The small air gap of the iron-core LSM is compatible with that of the suspension system while its requirement for substantial quantity of ferromagnetic material to be installed along the guideway tends to be offset by its improved operational efficiency and/or reduced vehicle-on-board weight relative to the linear induction motor. There is also the possibility of simultaneously generating both lift and thrust force by means of appropriate iron-core LSM phase control whereby the propulsion motor would become an integral part of the electromagnetic suspension.

1.1.2 Electromagnetic Suspension R&D Status

The electromagnetic suspension and linear induction motor propulsion concept for high speed applications is being very extensively hardware developed in West Germany for high speed application by the industrial consortium of Messerschmitt-Bolkow-Blohm and Krauss-Maffei under the sponsorship of the German Federal Ministry of Research and Technology. Extensive electromagnetic system test facilities have been constructed and successfully operated by this consortium. Such facilities include three linear induction motor propelled test vehicles and a magnetically suspended steam rocket propelled test sled with their associated test tracks. A linear induction motor propelled full scale 16.5 metric ton passenger-carrying prototype vehicle has successfully attained its design speed of 250 km/hr. The rocket sled test vehicle has successfully demonstrated near full-scale operation of the suspension concept at speeds of up to 400 km/hr.

The active guideway concept, which combines the functions of electromagnetic suspension plus iron-core linear synchronous motor propulsion, is also being extensively developed in West Germany by Thyssen-Henschel. Full scale test rigs have been successfully operated and a 1-km demonstration track constructed and operated using a 36 metric ton, 70-passenger vehicle at the International Traffic Fair in Hamburg in June 1979.

Currently, a consortium of seven West German companies including the above three referenced organizations are constructing a 31.5 km test track at Emsland for a 400 km/hr prototype 200-passenger revenue vehicle as based on the Thyssen-Henschel electromagnetic combined suspension-propulsion concept.

Japan Airlines (JAL) have also demonstrated the feasibility of the electromagnetic suspension concept at speeds in excess of 300 km/hr using a rocket sled test vehicle at their Kawasaki test track site. JAL have also constructed and successfully operated a six-passenger low speed LIM propelled demonstration vehicle.

Other organizations such as British Rail, Japanese Ministry of Transport, Rohr Industries Inc., as well as a number of University teams are also actively investigating the electromagnetic suspension concept but primarily for low speed urban mass transit rather than high speed intercity link vehicle application.

1.2 Electrodynamic Suspension System

1.2.1 Electrodynamic Suspension Characteristics

The electrodynamic suspension concept is based on the repulsion forces generated between vehicle-mounted superconducting magnets moving at velocity over electrical conductor sheets or coils mounted on the guideway as shown in Figure 1. Such levitation superconducting magnets have winding conductor comprised of a stabilizing copper matrix interspersed with a multitude of very fine filaments of superconducting alloy such as niobium-titanium. Such conductors exhibit zero electrical resistance when maintained at temperatures very near to absolute zero by means of immersion in liquid helium plus containment within a very low heat leak cryostat and are capable of carrying a very large current per unit cross section area.

The electrodynamic suspension system is inherently stable and may operate with a relatively large gap between the vehicle magnets and the guideway conductor while realizing cruise velocity levitation power requirements which are comparable with those for the electromagnetic suspension concept. For example, that portion of the vehicle propulsion power associated with the magnetic drag required to induce the electrodynamic levitation of one metric ton is about 40-60 kw for a typical operating gap of 20 cm at a vehicle cruise velocity of 500 km/hr. This magnetic drag, which is directly associated with the electrodynamic generation of lift, characteristically increases rapidly from zero vehicle velocity to a large drag peak at a low vehicle velocity (i.e. typically in the range 40-80 km/hr). Above this magnetic drag peak velocity, the magnetic drag continuously decreases with increasing vehicle velocity. This magnetic drag characteristic of the electrodynamic suspension limits this concept to high cruise speed applications.

The relatively soft electrodynamic suspension operating at substantial magnet-to-guideway gaps allows for vehicle operation on relatively loose toleranced guideways as may be readily realized with standard reinforced concrete construction practice. The relatively large operating gap also improves the tolerance of the system to climatic conditions relative to both the electromagnetic and the air cushion suspensions in locations where snow and ice accumulation are potential operational hazards.

The substantial operational gap of the electrodynamic suspension (i.e. typically 20-30 cm) favours the use of an air-core Linear Synchronous Motor (LSM) for propulsion wherein highly competitive motor operational efficiency can be realized even at the relatively large motor air gap required to be compatible with the suspension system clearances. Such an LSM is typically comprised of an array of superconducting magnets distributed lengthwise along the vehicle so as to magnetically couple with a travelling magnetic wave as generated by conventional conductor cable windings which are surface mounted on the guideway. An air-core LSM does not incorporate ferromagnetic material to concentrate the magnetic fields either in association with the vehicle magnet or the guideway windings in marked contrast with the iron-core LSM concept as is being used for the propulsion of electromagnetically suspended vehicles. The elimination of iron in association with the LSM guideway windings is made feasible by the use of superconducting vehicle magnet windings to maintain very intense magnetic fields with negligible expenditure of energy and with very low weight and volume penalty. Such an air-core linear synchronous motor may be powered entirely from guideway wayside variable frequency converter stations which activate selected block lengths of the motor guideway windings. Typically, high linear synchronous motor efficiency may be realized over the full vehicle velocity range without the need for vehicle power pick-up or heavy on-board power conversion equipment.

1.2.2 Electrodynamic Suspension R&D Status

The electrodynamic magnetic suspension and linear electrical motor propulsion concept is being extensively investigated specifically for high speed intercity transportation application by the Japanese National Railways (JNR) with extensive support from a number of Japanese heavy electrical industries as well as many Universities, and by the West German industrial consortium of Siemens, Brown-Boveri, and A.E.G. Telefunken under the sponsorship of the German Federal Ministry for Research and Technology. Extensive test facilities continue to be constructed and/or utilized in both countries in support of their respective electrodynamic R&D programs.

In West Germany, such test facilities include a linear motor propelled 18 metric ton, 200 km/hr Maglev test vehicle operating on a 280-m diameter circular test track located at Erlangen including appropriate track wayside cryogenic support equipment as well as additional extensive system component test facilities for the superconducting magnets, linear electrical motors, cryogenic sub-systems, etc. The experimental test vehicle, as was originally propelled by a small air gap linear induction motor which was continuously servo-positioned relative to the guideway motor reaction plate, is currently being used to experimentally evaluate the superconducting air-core linear synchronous motor design concept. Prototype superconducting magnets for electrodynamic suspension and for LSM propulsion have been designed, constructed and extensively evaluated on both specialized test beds and on the experimental test vehicle. Governmental funding of further West German R&D activity as applicable to the electrodynamic Maglev concept is understood to be unlikely in view of increased emphasis on the development of the electromagnetic Maglev system option. This latter electromagnetic Maglev system option is fundamentally more suited to operation over a wide range of cruise speeds rather than only at a very high speed and is perceived to be less demanding than the electrodynamic Maglev system option with respect to advancing the technical state-of-the-art for its practical implementation. Hence, the electromagnetic Maglev system may be considered to be closer in terms of technical development and accordingly in terms of potential commercial exploitation as is consistent with the schedule requirements understood to be advocated for a high speed European Maglev system network. However, this system should not necessarily be superior to the electrodynamic system option for high speed intercity application in terms of either the eventual revenue system performance or the capital investment effectiveness, at least to the extent that such factors may be currently assessed.

In Japan, such test facilities include an evolutionary family of four Maglev test vehicles, the first three of which operated at modest velocities on short linear test tracks and the most recent being a 10 metric ton air-core linear synchronous motor propelled test vehicle based on full scale superconducting magnet components. This current test vehicle has completed over 2,200 test runs to date in order to extensively investigate both component operational performance and vehicle dynamic response at speeds of up to 350 km/hr over 4.7 km of substantially straight test track located at Miyazaki. The test track is currently being extended to 7.0 km and the wayside power conditioning station modified to allow for vehicle electrodynamic component testing up to 500 km/hr. A substantial number of alternative design configuration prototype superconducting magnets and magnet winding combinations for electrodynamic suspension and LSM propulsion have been designed, constructed, and experimentally evaluated by various Japanese electrical engineering companies using specialized component test bed facilities and in some cases the high speed test vehicle. The development of higher performance and lighter weight superconducting magnets for Maglev application is continuing. A relatively lightweight helium refrigerator for on-board cryogenic cooling of the superconducting magnets has been recently developed and will soon be operationally evaluated in the test vehicle. It is understood that there are tentative plans to eventually build a revenue system test line for the operational evaluation of multiple vehicle passenger carrying trains depending upon the outcome of the Miyazaki test track technical activities over the next 3-2 years as they affect the economic viability of the JNR advocated Maglev transportation system concept.

The R&D investment in the electrodynamic system concept on the part of the Japanese National Railways with some financial support from their Ministry of Transportation is understood to be currently in the order of tens of millions of dollars per year.

In Canada, the electrodynamic suspension and electrical linear motor propulsion concept has been investigated, under the financial sponsorship of Transport Canada, by an interdisciplinary University research team under the direction of CIGGT* and complimented by extensive NRC engineering design support. Basic analytical investigations of the electrodynamic suspension plus air-core linear synchronous motor propulsion have been conducted and experimentally verified by the CIGGT research team using a 7.6 meter diameter test wheel and a liquid helium bath type stationary superconducting test magnet located at Queen's University in Kingston. The conceptual engineering design study of a revenue passenger high speed guided ground transportation system, as based on the results of the CIGGT research team fundamental investigations over some six years, was carried out by the Control Systems and Human Engineering Laboratory of the Division of Mechanical Engineering (DME). A summary of the results of the CIGGT research team which are directly relevant to the Maglev system conceptual design are:

---

* Canadian Institute of Guided Ground Transport, Kingston, Ontario.

- the derivation and test wheel experimental evaluation of analysis for the prediction of superconducting magnet forces as induced by movement of the magnet above an electrically conducting sheet (i.e. by electrodynamic interaction).
- derivation and near full-scale test wheel experimental verification of analysis for air-core linear synchronous motors.
- investigation of electrodynamic interactions associated with vehicle levitation, guidance, and propulsion using impedance modelling techniques.
- definition of the electrodynamic elements and linear motor operational characteristics for a "baseline" Maglev transportation system in terms of the vehicle superconducting magnet design requirements, the guide-conductor sheet geometry, the guideway linear motor winding specifications, and the guidance null flux loop geometry.

2.0 SUMMARY DESCRIPTION OF PROPOSED CANADIAN BASELINE MAGLEV SYSTEM

The proposed baseline Maglev intercity guided ground transportation system is comprised of single 100-passenger vehicles magnetically levitated and guided on a flat topped pier supported reinforced concrete elevated guideway having 25-meter beam spans and propelled by an air-core linear synchronous motor at a cruise velocity of 483 km/hr (i.e. based on a selected nominal 300 mph vehicle velocity). The system route profile is the 592-km long Canadian Toronto-Ottawa-Montreal corridor with elective intermediate stops at Ottawa and Mirabel Airport. Separate elevated guideways are provided for travel in each direction over the entire route length and the intermediate station stops are accessible via sidings off the high-speed through-traffic guideway.

A cut-away pictorial view of the proposed Maglev vehicle design configuration is shown in Figure 2. This configuration was evolved directly from the NRC detailed design studies of the following:

- the vehicle body shell structure for both static and dynamic loading conditions.
- the superconducting magnet cryostats with emphasis on their heat leak performance.
- the vertical and lateral suspension systems as required to realize acceptable vehicle ride quality with practical guideway construction standards.
- cryogenic helium refrigeration system requirements for two alternative system concept options.
- the vehicle aerodynamics including its influence upon propulsion motor requirements, vehicle lateral stability, and vehicle lateral ride quality.
- the mechanical low speed vertical support and lateral guidance means.
- the on-board auxiliary power system with emphasis on vehicle cabin environmental control and on-board cryogenic refrigeration system requirements.

The design layout of the proposed Maglev vehicle is shown in Figure 3, while a typical vehicle cross-section is shown in Figure 4. A 1/32 scale "cut-away" model of the proposed Maglev vehicle and guideway beam was built by DME technicians for purposes of more realistically illustrating the engineering design concept to non-specialists. Exterior views of this scale model are shown in Photographs A and B.

The proposed vehicle design as illustrated in Figures 2 to 4 accommodates 100 passengers in 25 rows of 2 by 2 seating on each side of a centre aisle. The seat width and pitch is equivalent to aircraft first-class seating comfort standards. The proposed vehicle passenger cabin could be converted

to accommodate 145 passengers in 29 rows of 2 by 3 seating having aircraft economy seating comfort standards. The 3.2 meter width and the 36.5 meter length of the Maglev vehicle were established by optimizing for minimal vehicle propulsion power required per passenger seat as based on vehicle aerodynamic drag dependency upon frontal area plus exterior surface wetted area and on vehicle magnetic drag dependency upon gross weight. This parametric investigation of drag dependency upon overall vehicle dimensions indicated a substantial but progressively decreasing reduction in propulsion power required per passenger seat with increasing vehicle overall length for any given vehicle cross-section. This trend demonstrates the power consumption improvement which can be realized by using multi-vehicle trains rather than single vehicles in situations where the route traffic density is sufficiently high to retain acceptable frequency of service. Accordingly, DME has extensively investigated the design implications, particularly with regard to the linear motor guideway winding requirements and body shell vibrational resonance, of using multiple car trains rather than single vehicles for purposes of possibly eventual increasing the passenger capacity of the system should this become required in the long term.

Among modern commercial passenger aircraft, the proposed Maglev vehicle design most closely resembles the fuselage of a McDonnell Douglas DC-9 as will be evident from Figure 5. A tabulation of comparative design layout parameters are listed in Table I to provide a basis of reference for the proposed Maglev vehicle design relative to the DC-9 aircraft with which there is fairly wide familiarity. Notable in this Table is the very high percentage of the Maglev vehicle gross weight which is passenger plus baggage payload in comparison with a high performance commercial jet aircraft such as the DC-9. This results directly from the bulk of the vehicle electrical propulsion system including all of the power conditioning equipment as well as the source power generating station being situated off of the vehicle while aircraft must carry on-board its complete propulsion system as well as all of the required petrochemical fuel. An estimated breakdown of the net and gross weight for the proposed Maglev vehicle design as per Figures 2, 3 and 4 is given in Table II.

Auxiliary power for the vehicle on-board hydraulic and electrical equipment requirements, as well as air-cycle cabin cooling and hot air cabin heating is provided by a small commercial gas turbine (less than 250 hp) located at the rear of the vehicle. Such gas turbines are widely used as aircraft auxiliary power units (APU's) and are accordingly highly developed. The extensively heat insulated vehicle cabin enclosure is slightly pressurized by the APU compressor bleed air to ensure passenger cabin comfort when passing near buildings, etc. at high speed. There is also provision on-board for an aircraft type galley, three washrooms, and a forward two-seat crew cabin as shown in Figure 3. Vehicle cabin access is via both forward and rear doors having built-in stairs as per Photograph B.

The vehicle volume below the cabin floor is used to accommodate the superconducting levitation and linear motor magnet assemblies plus their associated mechanical suspensions, the retractable low speed wheel-sets, the baggage bays, the APU fuel tanks, and the vehicle cabin air ducting as shown in Figures 2, 3 and 4.

At low velocities, where the generated electrodynamic lift and guidance forces are inadequate (i.e. below 50 km/hr), the vehicle is supported on the guideway by hydraulically retractable pneumatic tired wheel-sets similar in design to aircraft undercarriages and is guided by small hydraulically retractable pneumatic tired "outrigger" wheels running on vertical side surfaces of the guideway beam. The guidance wheels are shown stowed in Figure 2 and deployed in Photographs A and B.

The basic vehicle body shell structure utilizes riveted aluminium sheet-stringer-frame construction as per conventional aircraft fuselage design practice with local reinforcement at the major load application points. The body shell is designed to be sufficiently stiff to minimize any structural resonant vibration which might be excited by elevated guideway beam flexure. Allowance is made for body shell material fatigue as per standard aircraft structural design practice. The cabin floor is located at sufficient height (i.e. 1.0 m) above the plane of the superconducting magnet windings to generally maintain the d.c. magnetic field intensity within the cabin enclosure at relatively low levels (i.e. about 50 gauss at seat level and 20 gauss at passenger head level). Magnetic field peaks over the ends of linear motor superconducting magnet array and over the levitation superconducting magnets are passively shielded by 1.6 metric tons of variable thickness iron sheets. Such iron sheets, which form a part of the cabin floor, eliminate local regions of higher magnetic field intensity within the cabin enclosure.

2.1 Vehicle Electrodynamic Levitation

Vehicle high speed electrodynamic levitation is provided by ten liquid helium cooled superconducting magnets having surrounding heat-insulating lightweight dewars. The magnets are distributed in pairs lengthwise along the vehicle as shown in Figure 3 so as to minimize the applied vehicle structure bending load moments as well as to largely filter out the dominant vehicle periodic input disturbance due to guideway beam flexing. The levitation magnet fields interact with 1 cm thick and 60 cm wide guideway-mounted aluminium sheet strips to generate the required levitation force at a nominal magnet coil to guideway conductor height of 22 cm. Each levitation magnet has a race-track shaped coil nominally 1.0 m long by 0.3 m wide which is wound from commercial available superconducting wire. The specified current loading of the superconducting magnet winding is relatively conservative in comparison with current superconducting magnet design state-of-the-art.

The DME proposed levitation magnet preliminary design as per Figures 6, 7 and 8 is based on a lightweight magnet cryostat structure incorporating a stainless steel tubular inner pressure vessel which surrounds and supports the superconducting windings. There is provision for two helium reservoir tanks for supplying heat absorption capacity while operating the magnet independent of a cryogenic refrigeration source, the tanks being contained within the single magnet assembly cryostat as illustrated. The cryostat design incorporates low heat leak folded column load transfer members, a liquid nitrogen cooled intermediate heat shield, and superinsulation within the vacuum cavities of the cryostat to realize a computed heat leak to the helium of less than 2 watts per magnet winding. A structurally stiff support frame is provided for the superconducting windings and has cross-tie members as shown in Figure 6 to resist the large internal electromagnetic forces which tend to stress the superconductor wire by repelling the winding outwards. Such magnet winding stressing is known to rapidly diminish the current carrying capacity of the superconducting wire and accordingly eliminate the magnet's electrodynamic levitating capability. The conceptual study identified this proposed light weight superconducting magnet design as requiring substantial development to realize practical operational hardware implementation, particularly if a high performance type of advanced superconductor should be required to realize system performance.

The possible failure to realize in practice the proposed design of the levitation magnets with respect to light weight while retaining a very low heat leak in comparison with the substantially more conservative designs of the full scale superconducting magnets currently operating in Maglev experimental test vehicles in West Germany and in Japan, is not anticipated to introduce a significant vehicle weight penalty in that the proposed levitation magnets and their associated on-board cooling system represent only about 3.6% and 2.4% of the vehicle gross weight respectively as per Table II.

2.2 Vehicle Electrical Motor Propulsion

Vehicle propulsion is provided over the full speed range by an electrical linear air-core synchronous motor. The proposed linear motor is comprised of an array of forty-nine superconducting d.c. magnet windings located along substantially the full length of the bottom of the vehicle and stranded aluminium cable windings fixed along the full length of the guideway top surface as per Figure 9. In operation, the linear motor is powered from a variable frequency and regulated current source as supplied to 5 km block lengths of the guideway windings by wayside converter stations located at 10 km intervals along the guideway. The travelling magnetic wave, as generated when the guideway windings are powered from the adjacent converter station, couples with the magnetic field of the vehicle superconducting magnet array so as to "pull" the vehicle along the guideway at a velocity which is directly proportional to the converter output frequency. The vehicle is maintained "locked into" or synchronized with the travelling magnetic wave by means of feedback control of the electrical current output from the wayside converter stations. This linear motor feedback control derives its input information directly from the guideway winding electrical input to each block length whereby the velocity of a vehicle within any activated block length may be fully controlled upon demand from an overall system computer control centre without the necessity of depending upon a vehicle telemetry link.

The system components, which together comprise the linear propulsion motor, are divided between being located on the vehicle and being fixed to or located beside the guideway. The vehicle-mounted superconducting motor magnets, which are analogous to the iron-core field windings of a conventional rotary synchronous electric motor, are relatively lightweight and do not require any significant on-board power. Accordingly, neither the linear motor guideway-mounted conductor cable windings, which are analogous to the iron-core armature windings of a conventional rotary synchronous electric motor, nor their associated power converters contribute to the vehicle weight. As previously noted, this "off-vehicle" location of major weight contributing elements of the proposed system linear propulsion motor is largely responsible for realizing the very high Maglev vehicle payload-to-gross weight (see Table I) as compared with other types of high performance transportation vehicles.

Each of the vehicle's linear motor superconducting magnets has a racetrack shaped coil nominally 1.70 meters across the vehicle width and 0.53 meters along the vehicle length and which is wound from the same commercially available superconducting wire as the levitation magnets coils. Seven full-size motor magnet windings and one reduced length "mini-magnet" as shown schematically in Figure 9 were initially proposed to be contained within and supported by each of seven large flat lightweight tubular heat-insulating magnet dewar pods. The mini-magnet serves to effectively eliminate electromagnetic forces between adjacent magnet pods. The design for the proposed vehicle motor magnet pod dewar would have to be substantially more complex than that proposed for the levitation magnets as per Figures 6, 7 and 8 in order to realize adequate mechanical stiffness to avoid strain induced winding superconductor degradation.

Practical hardware and performance realization of the proposed lightweight linear motor superconducting magnet pod design is anticipated to require substantial further development additional to that required for the levitation magnets as a result of the very formidable design complexities associated with the flexure and the differential thermal expansion of the large flat pod dewar components. The possible failure to realize in practice the proposed design of the linear motor magnet pods with respect to light weight while retaining a very low heat leak in comparison with the substantially more conservative designs of the full-scale linear motor superconducting magnets currently under evaluation in test vehicles in West Germany and Japan would be anticipated to introduce a significant vehicle weight penalty in that the proposed motor magnets and their associated on-board cooling system are estimated to represent about 17.6% and 2.4% of the vehicle gross weight respectively as per Table II. Such a vehicle weight penalty could be offset by reducing the number of vehicle linear motor magnets but at the expense of larger diameter guideway cable conductor windings with the attendant increase in the system capital costs.

Subsequent to the initially proposed large flat pod cryostats for the LSM magnet winding array as reflected by the details of the vehicle configuration shown in Figures 2, 4 and 9, a preferred alternative cryostat design concept was evolved. This newer design concept incorporates much smaller individual cryostats for each of an array twenty-eight superconducting magnet windings which are located one full motor wavelength apart as per Figure 10 and which have twice the ampere-turn rating of each of the originally proposed forty-nine back-to-back magnet windings which were located one-half motor wavelength apart. Such individual LSM magnet winding cryostats would be quite similar in construction to the proposed levitation magnet cryostats as per Figures 6, 7 and 8. This alternatively proposed LSM vehicle magnet array of twenty-eight windings would not be anticipated to result in any significant performance degradation of either the linear propulsion motor or the electrodynamic lateral guidance system, both of which are directly dependent upon the design of this magnet array as the result of its interaction with the guideway mounted motor windings and null flux loops respectively as explained in Section 2.3. Sets of four individual magnet winding cryostats, including one end winding which incorporates an auxiliary "mini-magnet" winding, are attached to the bottom of an aluminium carrier frame truss structure as shown diagrammatically in Figure 10 so as to form seven identical magnet array assembly pods, each of which are coupled to the vehicle frame via an appropriate lateral secondary suspension system. The mini-magnet winding serves to effectively eliminate electromagnetic forces between each of the adjacent magnet winding assembly pods. The four magnet cryostats of each assembly pod are coupled together cryogenically by means of flexible helium transfer pipes so as to present a single cryogenic cooling system heat load for each pod.

The provision for separate individual magnet winding cryostats allows for a much more rigid individual cryostat structure as compared with the large flat pod cryostat of the initially proposed design and accordingly for much reduced susceptibility to magnet winding superconductor strain induced degradation associated with cryostat loading induced deflections.

2.3 Vehicle Electrodynamic Lateral Guidance

Vehicle high-speed electrodynamic lateral guidance is provided by the magnetic fields of the linear motor superconducting magnet array interacting with guideway surface-mounted figure-of-eight shaped "null flux" loops as shown in Figure 9 so as to generate vehicle lateral restraint forces which progressively increase with vehicle lateral displacement. This configuration of the loops ensures that current is induced in the loops only when the vehicle LSM magnets are laterally displaced relative to the loops and accordingly that the magnetic drag associated with the generation of lateral guidance forces reduces to zero when the vehicle is laterally centered over the loops. The guidance loops as shown schematically in Figure 9 are comprised of stranded aluminium cabling which are fixed to the guideway surface overlying the "meandering" linear motor windings.

Additional back-up guidance is provided by electromagnetic interaction between the linear motor superconducting magnet array and the edges of the lift-inducing guideway conductor strips should the vehicle lateral displacement become excessive.

2.4 Magnet Cryogenic Cooling Support System

Two different vehicle superconducting magnet cryogenic cooling system options were considered and compared as part of the conceptual design study:

- an on-board closed-cycle refrigeration system, which is referred to as the isothermal or constant temperature system option, and which consists of a single helium compressor coupled either to a number of individual helium liquefiers mounted on each superconducting magnet cryostat assembly or to a single centrally located helium liquefier whose output is coupled to each of the magnet cryostat assemblies by means of a low heat leak cryogenic piping distribution system. It is proposed that small cryogenic fluid reservoir tanks also be located on top of each magnet dewar to provide short duration emergency magnet cryogenic cooling in the event of a refrigeration system component failure.

- an on-board sealed cryostat helium heat absorption system, which is referred to as the isochoric or constant volume system, and which is comprised of a heat insulated reservoir tank(s) located on top of and directly connecting with each superconducting magnet dewar. Heat absorption by the initially largely liquid phase helium results in its vapourization and then in the progressive increase in the gas phase temperature and pressure at a rate which is directly dependent upon the dewar heat leak. The on-board reservoir tanks are on a daily basis discharged by release of the helium gas into and refilled with liquid helium from a large capacity wayside cryogenic refrigeration plant via quick-disconnect type flexible transfer lines.

The former isothermal cooling system is anticipated to require relatively complicated and perhaps heavy on-board cryogenic refrigeration hardware which has yet to be adequately demonstrated to have a level of reliability considered acceptable for the proposed transportation system application. Herein, the very high reliability potential of helium liquefiers which are based on helium gas bearing supported high speed turbine expanders is beginning to be realized in practice (i.e. up to 30,000 hours maintenance free between major overhauls) but such liquefiers tend to become quite inefficient in the small capacity sizes anticipated to be required for individual magnet cryostat refrigerators due to practical turbine manufacturing tolerance constraints. A vehicle centrally located single helium liquefier would require sufficient refrigeration capacity to facilitate the efficient use of a high reliability turbine expansion type unit but the associated overall refrigeration system reliability turbine expansion type unit would tend to be compromised by the relatively complicated on-board liquid helium piping distribution system which would be required between the liquefier and

the numbers of magnet cryostats. A centrifugal type of rotary helium compressor incorporating helium gas bearings should have much the same high reliability potential as the turbine expander based helium liquefier but does not appear to be practical due to the inherently very low pressure ratio per stage requiring an unreasonably large number of stages for an operational helium refrigeration compressor. In contrast, oil-flooded rotary screw type gas compressors which have been modified for helium service by the addition of high reliability oil separation devices in the output line have recently begun to demonstrate operation reliability approaching that for turbo-expander type helium liquefiers while efficiently generating high pressure ratios within a single stage. However, such rotary screw compressors are still relatively heavy and bulky in their commercial versions.

The latter isochoric cooling system requires advanced high performance superconducting cubic structured A15 type alloys as are still under extensive commercial development for the magnet windings. Such alloys are known to be highly susceptible to rapid reduction of the windings' current carrying capacity when only slightly mechanically strained. The latter system also requires daily vehicle liquid helium refill servicing which is anticipated to require procedures similar to those developed for the space program rocket liquid hydrogen refueling. There is a further anticipated problem associated with the economics of the wayside helium reliquefication of the very substantial quantity of low temperature helium gas which would be released to a wayside plant from a fleet of Maglev vehicles during the few night hours when the transportation system would be inoperative. Either the helium would have to be reliquefied on-line as it is released to the plant from the vehicles as would require a very large and accordingly expensive refrigeration capacity or the released helium gas would have to be held in storage at cryogenic temperature and be slowly reliquefied on a substantially continuous basis as would require large capacity and accordingly expensive pressurized cryogenic storage tanks.

There is probably as yet insufficient cryogenic refrigeration system hardware development data available to objectively assess the relative practicality of the two vehicle superconducting magnet cryogenic cooling system options considered. However, current high speed Maglev test vehicle experimental evaluation by the Japanese National Railways of a lightweight on-board liquefier for an isothermal helium refrigeration system is anticipated to improve this situation in providing practical operational experience with at least one of the cooling system options.

2.5 Vehicle Passenger Ride Quality

Vehicle ride quality at least as good as that typical for a full-size North American automobile travelling at speed on a good quality express highway has been predicted by extensive computer modelling to be attainable using secondary suspensions between the vehicle frame structure and the superconducting magnet assemblies. In particular, an active hydraulic force actuator with a paralleled emergency back-up mechanical spring is provided between each of the ten levitation magnet cryostats and the vehicle structure as shown in Figure 11. Herein, the hydraulic actuator provides for both the spring and the damper functions of the secondary vertical suspension. Torsion bar springs and oil dash-pot type dampers are provided between each of the LSM magnet pod assemblies and the vehicle structure as shown in Figure 12 so as to form the secondary lateral suspension. The proposed secondary suspensions combined with the primary electrodynamic suspensions largely eliminate vehicle vibration as induced by guideway running surface roughness, elevated guideway beam deflection, and side wind gusting.

The active hydraulic vertical suspension is responsive to feedback of magnet-to-vehicle displacement as well as to the magnet acceleration and the vehicle body acceleration. The feedback is designed so that the active suspension will function the same as a simple mechanical spring plus damper as is common for automobile suspensions. A vehicle-to-guideway gap sensor, as would be anticipated to exhibit questionable reliability under all weather operational conditions, is not required to implement the proposed active vertical secondary suspension. An active rather than a passive vertical suspension is proposed to allow for "retraction" of the levitation magnets in order to minimize the magnetic drag peak at low vehicle speeds, to regulate the vehicle/guideway averaged operating gap in order to prevent any degradation of the linear propulsion motor design performance and, if deemed desirable, to tilt the vehicle body through curves. Vehicle fore and aft surge motion is damped by means of the linear motor feedback control system.

2.6 System Guideway

The baseline system proposed guideway as shown in Figure 13, is comprised of 25-meter long elevated box sectioned flat topped beams simply supported by nominally 7-meter high piers standing on foundation slabs which are supported by heavy sectioned piles or caissons, driven down to the local bedrock or its equivalent to prevent frost heave pier misalignment. The foundation slabs, piers, and beams are fabricated from conventional steel reinforced concrete. The reinforcing rods in the beam top slab are unconnected at the cross-points and probably would be made from high manganese alloy steel having much reduced magnetic permeability so as to minimize rod eddy current induced vehicle magnetic drag. The flat top of the elevated wind-swept guideway beam will minimize snow accumulation as has been conclusively demonstrated by winter tests of various full scale track section configurations conducted by the Low Temperature Laboratory of DME.

The proposed elevated guideway design represents a compromise between the practical limitations of low cost mass production fabrication techniques, the flexibility of the guideway as it affects vehicle ride quality, and overall guideway capital cost considerations.

A guideway switching concept which does not require mechanical moving parts has been proposed by the CIGGT research team. This passive electrodynamic switch design concept is shown in Figure 14 and incorporates the replacement of the guideway conductor sheet strips by conductor loops through the switch section and the overlay on the guideway surface of such levitation loops plus the null-flux guidance loops and the linear motor windings so as to provide electrodynamic guidance and levitation for both the straight through and for the turn-out branches of the switch. The desired branch route is selected, in response to a wayside command signal, by setting an electrical switch in each of the guidance and levitation loops so as to short circuit the loops which together define the unwanted branch route while the appropriate guideway switch LSM winding branch is activated. Provision is also made for low speed switching as shown in Figure 14 by means of the selected deployment of appropriate vehicle outrigger guidance wheel sets.

The reliance of such a switch design solely upon vehicle electrodynamic guidance at the higher speeds without provision for an in-place mechanical safety back-up guidance system in the event of a vehicle LSM magnet array failure prompted the design investigation of alternative guideway switch concepts by DME. Such a concept is the active "inclined ramp type" switch shown in Figure 15. This switch is comprised of a 180-meter length of especially designed relatively flexible aluminium guideway beam which is vertically deflected as shown in Figure 15 by hydraulic actuator sets between its unbent condition which corresponds to the high speed through traffic switch setting and its smooth transition curve condition which corresponds to the reduced speed branch-off switch setting is proposed. Detailed design analysis of the flexible beam member for such an active vertical switch concept indicated that the beam would not be particularly expensive to fabricate, would exhibit acceptable fatigue life, and would not require excessive hydraulic power to deflect within an acceptable short time duration. Back-up emergency mechanical guidance would be continuously provided over both the switch length as well as along regular elevated guideway beams by means of vehicle attached external skid pods which straddle the guideway sides.

A "lateral traversing type" of active switch as shown in Figure 16 was proposed for the handling of Maglev vehicles in the terminal stations and in the maintenance yard areas. This alternative switch concept is based on stopping a Maglev vehicle on the guideway such that the vehicle undercarriage wheel sets are located on a pair of short carriage platforms as shown in Figure 16. The vehicle is then laterally traversed on the carriage platforms which are displaced by hydraulic actuators while air cushion supported so as to clear the guideway for following vehicle traffic. An additional set of carriage platforms are moved into place on the guideway by the lateral transfer carriage assemblies as shown in Figure 16 so as to provide a substantially continuous in-place guideway running surface when the switch traversing operation has been completed. Such a switch concept would be substantially less costly and less bulky than the alternative "inclined ramp" type switch but would not be considered appropriate for application where high speed mainline through traffic is carried by the guideway due to the necessity to fully stop a vehicle precisely on the guideway carriage platforms prior to clearing the mainline by lateral transfer switching.

2.7 System Passenger Capacity

The passenger capacity of the proposed system is based on a selected vehicle cruise velocity of 483 km/hr (300 mph) in common with the baseline performance requirements set for other electrodynamic Maglev system conceptual design studies (i.e., for example the U.S. Dept. of Transport sponsored Philco-Ford conceptual design study, the Japanese National Railways Miyazaki test vehicle design velocity, and the West German consortium's revenue system conceptual design). This selected vehicle cruise velocity provides for terminal-to-terminal travelling times directly comparable with that for current aircraft schedules within the Canadian Toronto-Montreal corridor while exhibiting vehicle propulsion power requirements as determined by aerodynamic drag considerations which compare quite favourably with the scheduled competitive air transportation mode at least over stage length distances typical of the central Canadian corridor (i.e. about 500-700 km).

An economic study of the proposed Maglev system which is currently being conducted by the Canadian Institute of Guided Ground Transport is understood to include the optimization of the vehicle cruise velocity on the basis of a judgment trade-off between system capital costs, vehicle operational costs, and acceptable trip durations. It is anticipated that such an optimum cruise velocity would be somewhat less than the 483 km/hr selected for this initial conceptual design study in view of the anticipated continually increasing costs of energy over the long term. The averaged velocity and estimated travelling time for the proposed Maglev transportation system as based on the selected vehicle cruise velocity of 483 km/hr and a maximum vehicle acceleration/deceleration of 0.1 g is tabulated below with the comparative data for current scheduled aircraft operation between the city airports:

Route	Proposed Maglev System (483 km/hr Cruise Velocity)			Commercial Jet Aircraft Schedules (930 km/hr Averaged Cruise Velocity)		
	Estimated Route Distance (km)	Travel Time (min)[1]	Average Velocity (km/hr)	Approximate Route Distance (km)	Scheduled Travel Time (min)[2]	Average Velocity (km/hr)
Toronto-Montreal (non-stop)	592 (via Ottawa)	76	467	500 (direct)	60	500
Toronto-Ottawa	355	47	453	338	50	406
Ottawa-Montreal (via Mirabel)	237	32	444	177 (direct)	30	354

[1] Urban centre-to-urban centre.
[2] Airport-to-airport.

It is estimated that a fleet of about sixteen Maglev vehicles having 100 1st class passenger seats and operating bi-directionally on the system's dedicated dual guideway routing on a 16-hour/day basis so as to provide on the average about six departures per hour in each direction would satisfy the total capacity of about 20,000-passenger seats per day estimated to be currently provided in both directions by all of the conventional intercity public transportation modes of scheduled aircraft, railway passenger train, and highway bus directly between Toronto and Montreal as well as between Toronto and Ottawa. This requirement to satisfy all of the current intercity public transportation capacity in this Canadian corridor would be reduced to a fleet of only eleven Maglev vehicles if economy rather than 1st class seating was to be provided.

The overall bi-directional passenger seat capacity of the proposed Maglev system could be increased to about 64,000 available passenger seats/day to satisfy possible long term traffic loading (i.e. slightly over three times the available seat capacity currently provided by all of the conventional public transportation modes) by reducing the headway between Maglev vehicles to the minimum of about three minutes as dictated by vehicle collision avoidance considerations.

The passenger capacity of the proposed system could be much further expanded to such levels as might be eventually required in the very long term within this Canadian corridor without significant further capital investment in the basic guideway structure by using trains of two or more vehicles coupled together. Such a higher traffic density system would also exhibit a somewhat lower operational energy intensity per passenger seat due to the reduced aerodynamic drag per vehicle.

2.8 Vehicle Comparative Energy Intensity

The baseline system conceptual design is based on practical restraints imposed by anticipated operation within this relatively low traffic density Canadian corridor wherein the capital costs of the system guideway is expected to very strongly dominate the system economic considerations. Accordingly, the optimization of the electromagnetic elements of the system by the CIGGT research team was necessarily biased towards reducing the required guideway conductor material (i.e. aluminium sheet levitation strips and stranded aluminium wire guidance loops plus linear motor windings) at the expense of somewhat compromising the vehicle operational performance with respect to propulsion energy requirements.

The estimated power required to propel the proposed baseline 100-passenger vehicle at the selected cruise velocity of 483 km/hr over the porposed guideway designed to reduce guideway capital costs rather than minimize propulsion power requirements, is shown in Figure 17 as a function of head-wind velocity and guideway grade. This propulsion power estimate is based on a relatively conservative theoretical prediction of vehicle aerodynamic drag in the absence of experimental wind tunnel data specifically for the proposed vehicle design body shape.

The overall energy intensity per vehicle for the proposed Maglev system (i.e. the equivalent fuel consumption per passenger) is estimated on the basis of the heating value of hydrocarbon fuel which would be required to produce, in a large conventional thermal generating station, the electrical power to propel the vehicle at cruise velocity by means of its linear motor. Accordingly, such a Maglev vehicle energy intensity estimation includes the energy conversion efficiencies of the central electrical power thermal generating station plus the power distribution transmission line losses (assumed 30% efficient), the guideway wayside converters (assumed 85% efficient), and the proposed linear synchronous propulsion motor (predicted to be 75% efficient). This allows for the direct comparison of the equivalent fuel consumption energy intensity for the proposed Maglev vehicle with the actual fuel consumption of "conventional" transportation vehicles such as aircraft, diesel-electric trains, buses, etc. as shown in Figure 18. In Figure 18 the energy intensity is expressed in terms of liters of fuel consumed per passenger-kilometer as based on the approximate heating value of gasoline and kerosene. Herein, it will be appreciated that the electrical energy required to propel a Maglev vehicle could very well be generated by hydro or nuclear power rather than an increasingly expensive petrochemical fuel. Accordingly, a Maglev transportation system has the potential for being significantly more energy cost effective than transportation modes having equivalent propulsion energy intensity performance but being solely dependent upon on-board petrochemical fuels.

All of the fuel consumption data shown in Figure 18, except that for the automobile, is based on a passenger load factor of 60% which closely approximates the current load factor performance of domestic North American commercial airlines. The jet aircraft fuel consumption shown in Figure 18 is based on recent operational statistical data for U.S. airlines which lists the fuel efficiency realized over the average of the flight stage lengths for each aircraft make. In Figure 18, the aircraft fuel consumption data has been compensated for the relatively short Toronto-Montreal 500-km stage length in accordance with an air transport industry advocated "haul factor" which accounts for the fuel requirements associated with take-off and landing procedures plus the ascend

to cruise altitude. The significance of this air transportation mode "haul factor" is evident in the escalating energy intensity associated with aircraft operation over increasingly diminishing route stage lengths as exemplified by the fuel consumption data for representative aircraft types as shown in Figure 19 with the comparative fuel consumption performance predicted for the proposed Maglev system.

Figures 18 and 19 indicate that the proposed conceptual design of Maglev transportation system would be considerably more energy efficient than existing commercial aircraft having equivalent seating comfort standards and roughly comparable travelling time performance over the Toronto-Ottawa-Montreal 592-km stage length. Figure 19 further indicates that the proposed Maglev transportation system would be competitive in energy efficiency with commercial aircraft having economy class seating for up to about a 1,000-km stage length when offering the equivalent of 1st class seating and more than energy efficiency competitive for any stage length when offering the equivalent of economy class seating. Some further improvement in this predicted Maglev system energy intensity performance would be expected if the system design was to be biased towards reducing the vehicle direct operating costs rather than towards reducing the initial system capital investment costs. Figure 18 also indicates that a Maglev system offering economy class seating and operating at only a 60% load factor would be very close in overall energy requirements even when including the inefficiencies of generating the required electrical power from a thermal fuel energy source, with the typical full-size North American automobile when carrying two passengers. However, the Maglev system could offer Toronto-to-Montreal service in less than 1½ hours as compared with about 5 hours for the automobile.

2.9 Environmental Impact of Proposed System

There is no air pollution directly associated with operation of the proposed Maglev transportation system other than that due to the exhaust of the small on-board auxiliary power gas turbine. The only significant potential air pollution source which might be indirectly attributed to the system would be that associated with the remote electrical power generating station as would presumably be already pollution controlled to meet applicable air quality standards.

Visual intrusion by the slender and "aesthetically clean" elevated guideway is anticipated to be minimal except perhaps when viewed from directly below or from the immediate vicinity of the elevated guideway.

Elevation of the guideway minimizes intrusion upon local land usage as is particularly important in the urban and immediately surrounding areas. Elevation of the guideway also allows for the possibility of guideway location either directly above or immediately adjacent to existing railway lines or alternatively along the median of existing divided express highways with negligible loss of land usage.

The only potentially significant environmental impact of the proposed system exterior to the vehicles is the noise generated by the air flow over the vehicle at high velocity and to a much lesser extent by the exhaust of the small on-board auxiliary power gas turbine. An estimation of the anticipated exterior noise associated with a vehicle passing at cruise velocity (483 km/hr) suggests that peak noise intensity would be about the same as that generated by diesel truck traffic on an express highway (85-95 dBA sideline noise at 15 meters). This external noise will rapidly diminish with decreasing vehicle velocity, reducing to a level about equivalent to that generated by automobile traffic on an express highway when the Maglev vehicle velocity is in the order of 300 km/hr.

The potentially adverse effects of the proposed system upon the "welfare" of the vehicle passengers and crew are anticipated to be limited to acceptably low levels by means of the following vehicle design features:

- cabin interior noise — noise generated by the air flow over the vehicle and by the on-board auxiliary power gas turbine will be attenuated to low level by the cabin wall indulation and the cabin interior wall liner which will both act as good acoustic energy absorbers.

- vehicle vibration — reduced well below standard international passenger comfort limits by the soft vertical and lateral secondary suspensions between the vehicle structure and the magnets.

- magnetic field exposure — reduced to intensities of less than the magnetic leakage fields surrounding conventional permanent magnets (i.e. less than 100 gauss at cabin floor level) by locating the cabin enclosure as remotely as practical from the on-board superconducting magnet winding and by adding some iron sheet shielding over specific areas of the cabin floor. Should the passenger cabin magnetic field levels for the proposed vehicle design be demonstrated to have any significant long term biological effects, then vehicle performance degrading design changes would be required. Such changes could be the addition of more iron sheet shielding with an attendant vehicle weight penalty and associated moderate propulsion energy increase and/or the increase of vehicle height with an attendant significant propulsion energy increase due to higher aerodynamic drag.

2.10 System Safety Considerations

The primary safety considerations for the proposed Maglev system are the avoidance of collision between vehicles plus the retention of vehicle lateral guidance and vertical support under the worst anticipated system failure conditions.

Vehicle collision avoidance can be realized by maintaining at least five unpowered guideway motor winding 5-km block lengths between any two vehicles on the guideway (equivalent to a minimum headway between vehicles of about 3 minutes at cruise velocity). This allows sufficient length of unpowered guideway for a following vehicle to stop at an acceptable deceleration of about 0.1 g's with programmed levitation magnet retraction as a result of vehicle retarding aerodynamic plus magnetic drag down to landing velocity and wheelset braking below landing velocity.

Loss of the vehicle electrodynamic guidance or levitation at high speeds could only be induced by the loss of superconductivity in either all of the on-board linear motor magnets or all of the levitation magnets. The probability of a sudden unpredictable loss of superconductivity in more than a small fraction of the on-board magnet windings during a typical route trip duration, as might be induced by a sudden magnet cryostat vacuum leak due to a structural failure or vacuum vessel puncture, a localized individual cryostat cryogenic cooling system malfunction due to helium passage contamination blockage or an isolated mechanical failure, excessive magnet vibration induced local heating, or winding exposure to very high rate of changes of external magnetic field, is effectively eliminated in the proposed vehicle design by means of:

- providing a number of separate magnet winding dewars (10 levitation magnet dewars and 7 linear motor magnet dewar pods), each having a self-contained helium reservoir capacity sufficient to provide emergency single trip duration cooling of the windings in the event of a helium liquefying refrigeration system breakdown.

- provision for a very substantial factor of safety between the maximum provided vehicle electrodynamic guidance forces and the anticipated maximum lateral disturbance force levels.

- distribution of both levitation and LSM magnet winding dewars over the length of the vehicle such that an isolated magnet failure will not induce significant transient vertical or lateral re-orientation of the vehicle relative to the guideway.

- providing a "mini-magnet" winding at the end of each pod of the linear motor magnet array to largely eliminate electromagnetic coupling between adjacent pods so as to prevent the propagation of any winding superconductivity loss from pod to pod.

The loss of superconductivity in all of the vehicle magnet windings as induced by the sudden failure of the complete as opposed to an isolated cryostat portion of the on-board cryogenic cooling system would be predictable to the extent that the heat absorption capacity of the small reservoir of helium associated with each magnet cryostat would sustain magnet superconductivity at least until the vehicle could be decelerated to a normal wheel-set landing. Such a sudden failure of the complete on-board cooling system could be induced by the breakdown of the helium compressor, by the breakdown of the single centrally located helium liquefier should the single liquefier system option be used, or by the structural failure of a system critical helium transmission line. However, such types of cryogenic cooling system failures may be effectively eliminated by incorporating a redundant back-up safety helium compressor, liquefier, and on-board distribution system with the automatic control means to switch over to the appropriate spare component in the event of a system failure.

Emergency vehicle support in the unlikely event of the simultaneous loss of most of the electrodynamic lift is provided by skids permanently located along the underside of the vehicle. Emergency vehicle guidance is provided in the proposed design by hydraulic deployment of the outrigger wheels. Should an in-depth system reliability evaluation indicate that a more rapidly deployable or a vehicle permanent emergency mechanical guidance capability be essential, then a guideway switch concept such as the previously described hydraulically actuated vertically deflecting flexible beam design would be required in being compatible with provision for continuously in-place vehicle emergency lateral guidance skids straddling the guideway beam.

Emergency vertical secondary suspension capability between the levitation magnets and the vehicle structure is provided in the proposed design by providing mechanical spring/damper sets located in parallel with the active suspension hydraulic actuator in case of a hydraulic system or a suspension feedback control failure.

It is essential that the guideway be maintained clear of debris containing any ferromagnetic material to ensure system operational safety in that magnetic attraction of such debris towards the superconducting magnets of a passing vehicle could cause serious vehicle structural impact damage.

3.0 CONCLUSIONS

The main conclusion of the conceptual design study is that the proposed electrodynamically suspended and linear synchronous motor propelled Maglev vehicle/guideway would appear design viable but not necessarily economically feasible for a Canadian corridor high speed guided ground transportation system. The study also indicates that the proposed system would be capable of providing the following potentially advantageous features as listed in estimated order of priority:

- high speed operational capability providing Toronto-Ottawa-Montreal corridor urban centre-to-centre travelling time comparable with airport-to-airport travelling time provided by current airline schedules but with less overall expenditure of energy per passenger trip and with the potential for significantly lower terminal access and processing time than is at least currently required for the air mode.

- high speed operational capability on a dedicated guideway providing the potential for a large passenger capacity per unit time while ensuring sufficient spacing between vehicles for emergency stopping by automatically maintaining an appropriate number of unpowered linear synchronous motor winding guideway block lengths between vehicles.

- the direct utilization of electrical power to operate a high capacity, high speed inter-urban transportation system which will become increasingly important as the cost and availability of petrochemical fuels for aircraft, automobiles, trucks, diesel-electric trains, etc. becomes more acute.

- all weather operational capability anticipated to be provided by the combination of a relatively large vehicle-to-guideway gap and minimal snow accumulation on the wind swept elevated flat topped guideway plus the absence of adhesion requirements for the non-contacting linear electrical motor propulsion.

- minimal maintenance of the guideway "running" surfaces in the absence of friction wear.

- very infrequent adjustment of the guideway structural alignment in the absence of pier frost heave provided that deep pile foundations as per conventional Canadian highway bridge construction practice are incorporated.

- good vehicle ride quality relative to internationally accepted ride comfort limit specifications for all vehicle operation conditions excepting very severe crosswinds with guideway construction tolerances associated with conventional low cost reinforced concrete fabrication practices.

- vehicle generated air pollution limited to that produced by the exhaust of the small on-board gas turbine auxiliary power unit.

These potentially advantageous features of the proposed system must be assessed primarily in relation to the very large capital investment which is anticipated to be required for the fixed route guideway with its associated electrical power and passenger terminal installations and in relation to the potential of the system revenue to write off such a debt load over a realistic depreciation period while providing some margin for return on the large front end investment. The listed potentially advantageous features also tend to be offset by the as yet largely unproven operational reliability and the possibly demanding preventative maintenance requirements of the vehicle magnet cryogenic cooling system and perhaps of the superconducting magnets themselves.

There is the further potentially adverse feature of the proposed high speed system associated with constraints on the choice of guideway routing. Such constraints are imposed by the very large radius of guideway curvature which must be maintained in order to meet the sustained centrifugal acceleration limits as dictated by passenger ride comfort considerations. Such constraints are anticipated to more than offset any flexibility in the choice of guideway routing as is provided by the potential for relatively steep guideway grade climbing capability of the vehicle as compared with conventional railway locomotives in the absence of any Maglev vehicle propulsion adhesion limitations.

A further important conclusion of the conceptual design study is that the proposed Maglev transportation system could be readily constructed on the basis of current state-of-the-art engineering design practice in all respects excepting possibly:

— the vehicle magnet liquid helium cryogenic cooling system in the case of the on-board closed cycle isothermal refrigeration system option.

— the advanced performance superconductor magnet winding with its associated highly-rigid lightweight cryostat in the case of the sealed cryostat isochoric cooling system option.

The conceptual design study indicated that further engineering development in these key system component areas was required in order to establish acceptable design practices with respect to revenue system operational reliability, servicing, and maintenance. This Maglev system design study as well as other available evidence would suggest that there is no apparent fundamental technical deterrent to the eventual successful practical development of these components provided that adequate economic incentives are forth-coming. On-going lightweight superconducting magnet and on-board cryogenic refrigeration system hardware development in Japan in support of their extensive domestic electrodynamic Maglev program is anticipated to establish many such design practice requirements in the fairly near future.

4.0 RECOMMENDATIONS

The NRC engineering design investigation recommended that an economic study of the high speed electrodynamic Maglev transportation alternative for the Canadian Toronto-Montreal corridor as was expressly excluded from this conceptual design study be undertaken using the present system design as a baseline reference. It was suggested that such an economic study incorporate:

- determination of the dependency of the system capital investment and operational costs upon vehicle cruise velocity wherein the electromagnetic elements of the system are re-optimized as required using the available analytical techniques derived and verified by the CIGGT research team.
- economic analysis at differing system vehicle operational cruise speeds selected so as to facilitate cost comparisons between the electrodynamic Maglev system and available alternative air plus ground transportation modes in order to assess the long term suitability of the Maglev concept as a financially viable transportation mode within the Canadian corridor on the basis of projected traffic densities.

This recommended economic study is now nearing completion at the Canadian Institute of Guided Ground Transport at Kingston under the sponsorship of the Research and Development Centre of Transport Canada.

The NRC study further recommended that technical investigations of superconducting magnets and their associated cryogenic cooling systems be pursued in parallel with the system economic study but on a relatively low priority basis pending the availability of the economic study results and their subsequent assessment by transportation policy specialists.

Such investigations were suggested to preferably be comprised of laboratory experiments devised to provide such specific design data as would be required to define full scale revenue system prototype magnet assemblies with considerable confidence. Specific areas for such investigations were identified to preferably include:

- investigation of alternative engineering design concepts for lightweight dewars with emphasis on magnet winding load transfer elements having minimal heat leak.
- establishing the dependency of the current capacity of high performance cubic structured A15 type superconductors, suitable for the isochoric sealed magnet dewar helium cooling system option, upon temperature and ambient magnetic field.
- performance degradation of magnet winding superconductor under mechanical strain as induced by the dewar winding support structure deflections as well as winding compaction during operation.

5.0 REFERENCES

The reference upon which this summary report is based is:

Hayes, W.F. — *High Speed Electrodynamic Maglev Guided Ground Transportation System Conceptual Design Study.* Laboratory Technical Report LTR-CS-176, Division of Mechanical Engineering, National Research Council Canada, Ottawa, September 1977.

Other references which are most directly relevant to the Canadian electrodynamic Maglev R&D activity on the part of the University research team are:

Eastham, A.R. (editor) — *Superconducting Magnetic Levitation and Linear Synchronous Motor Propulsion for High Speed Ground Transportation.* Phase II CIGGT Report No. 75-5, Canadian Institute of Guided Ground Transport, Queen's University, Kingston, Ont., March 1975.

Eastham, A.R. (editor) — *Electrodynamic Suspension and Linear Synchronous Motor Propulsion for High Speed Guided Ground Transportation.* Phase III Ciggt Report No. 77-13, Canadian Institute of Guided Ground Transport, Queen's University, Kingston, Ont., September 1977.

Atherton, D.L., Belanger, P.R., Burke, P.E., Dawson, G.E., Eastham, A.R., Hayes, W.F., Ooi, B.T., Silvester, P., Slemon, G.R. — *The Canadian High Speed Magnetically Levitated Vehicle System.* Canadian Electrical Engineering Journal, Vol. III, No. 2, April 1978.

Further references relevant to this conceptual design study summary as well as to the very considerable foreign electrodynamic Maglev R&D activity are listed in the extensive bibliographies of the above four reports.

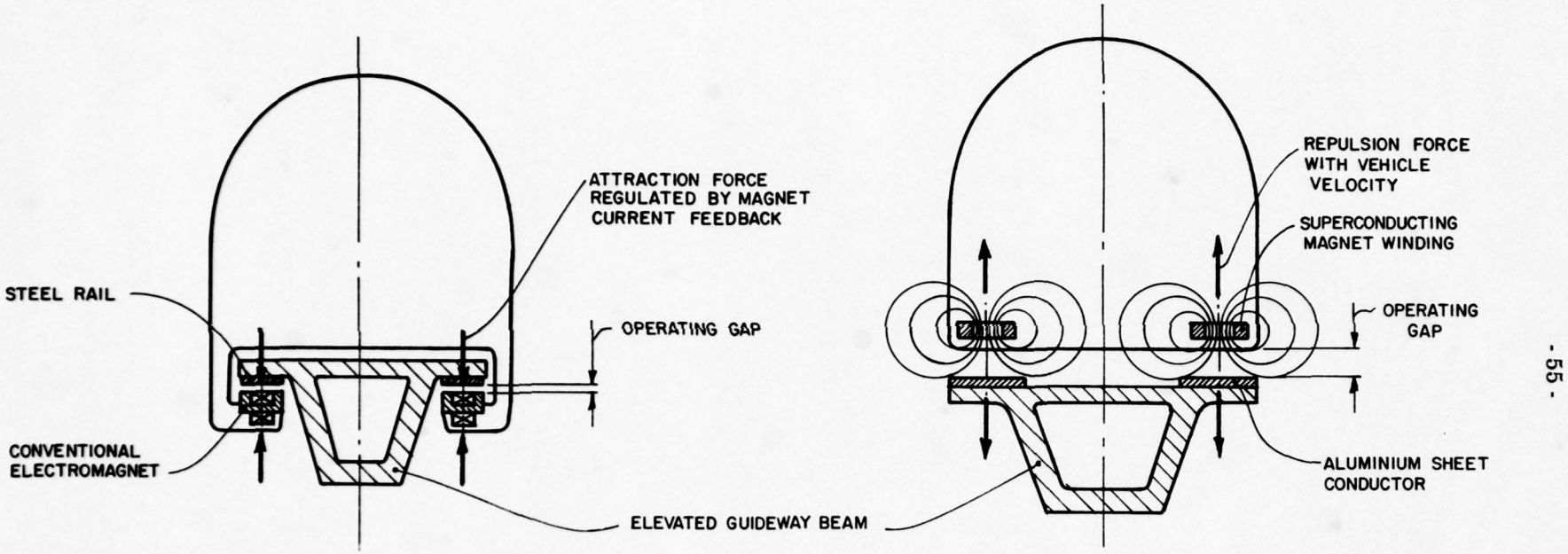

ELECTROMAGNETIC SUSPENSION SYSTEM
(ATTRACTION FORCE GENERATION)

ELECTRODYNAMIC SUSPENSION SYSTEM
(REPULSION FORCE GENERATION)

FIG. 1: MAGNETIC SUSPENSION SYSTEM OPTIONS

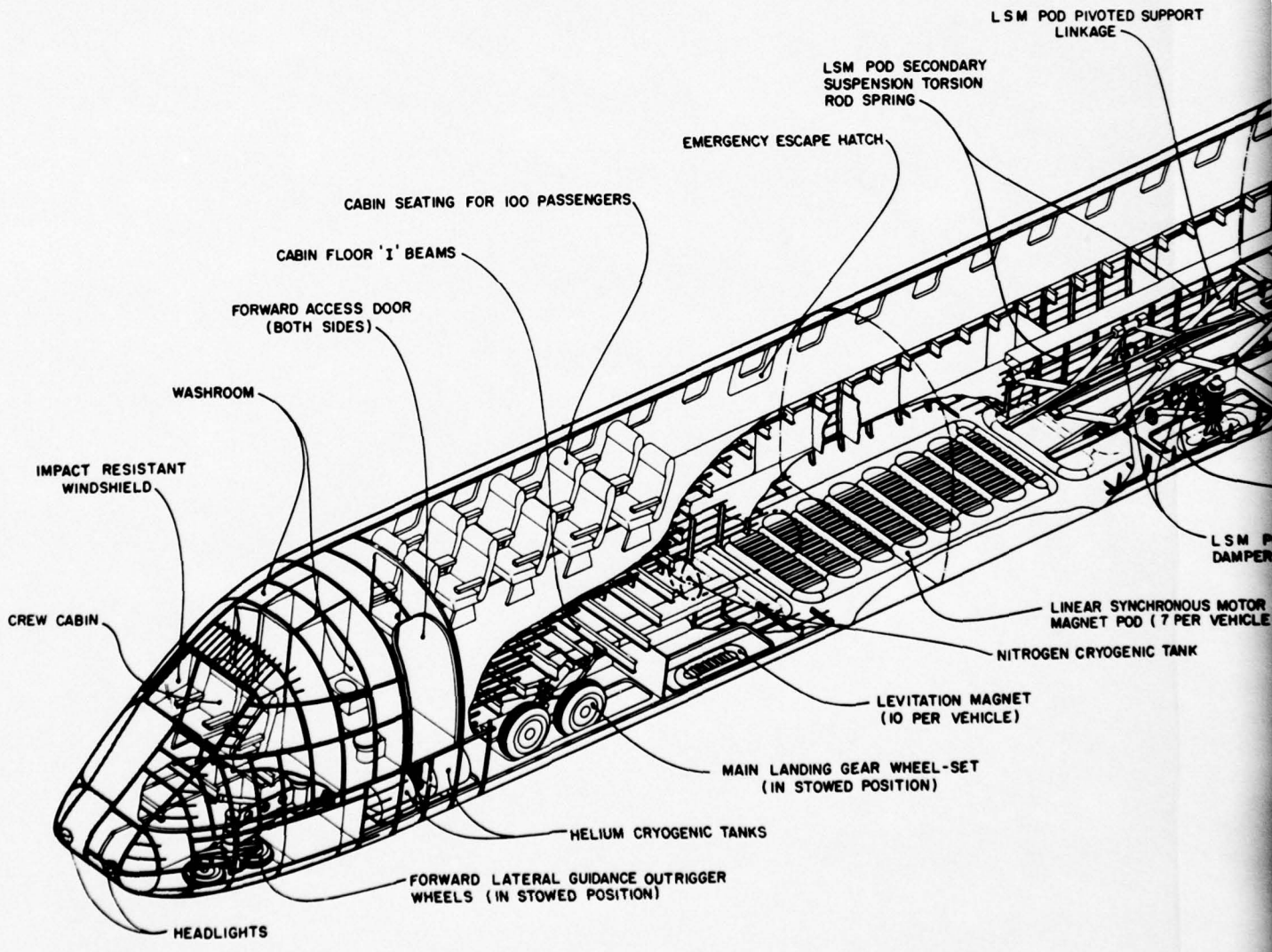
LSM POD PIVOTED SUPPORT LINKAGE
LSM POD SECONDARY SUSPENSION TORSION ROD SPRING
EMERGENCY ESCAPE HATCH
CABIN SEATING FOR 100 PASSENGERS
CABIN FLOOR 'I' BEAMS
FORWARD ACCESS DOOR (BOTH SIDES)
WASHROOM
IMPACT RESISTANT WINDSHIELD
CREW CABIN
LINEAR SYNCHRONOUS MOTOR MAGNET POD (7 PER VEHICLE
NITROGEN CRYOGENIC TANK
LEVITATION MAGNET (10 PER VEHICLE)
MAIN LANDING GEAR WHEEL-SET (IN STOWED POSITION)
HELIUM CRYOGENIC TANKS
FORWARD LATERAL GUIDANCE OUTRIGGER WHEELS (IN STOWED POSITION)
HEADLIGHTS

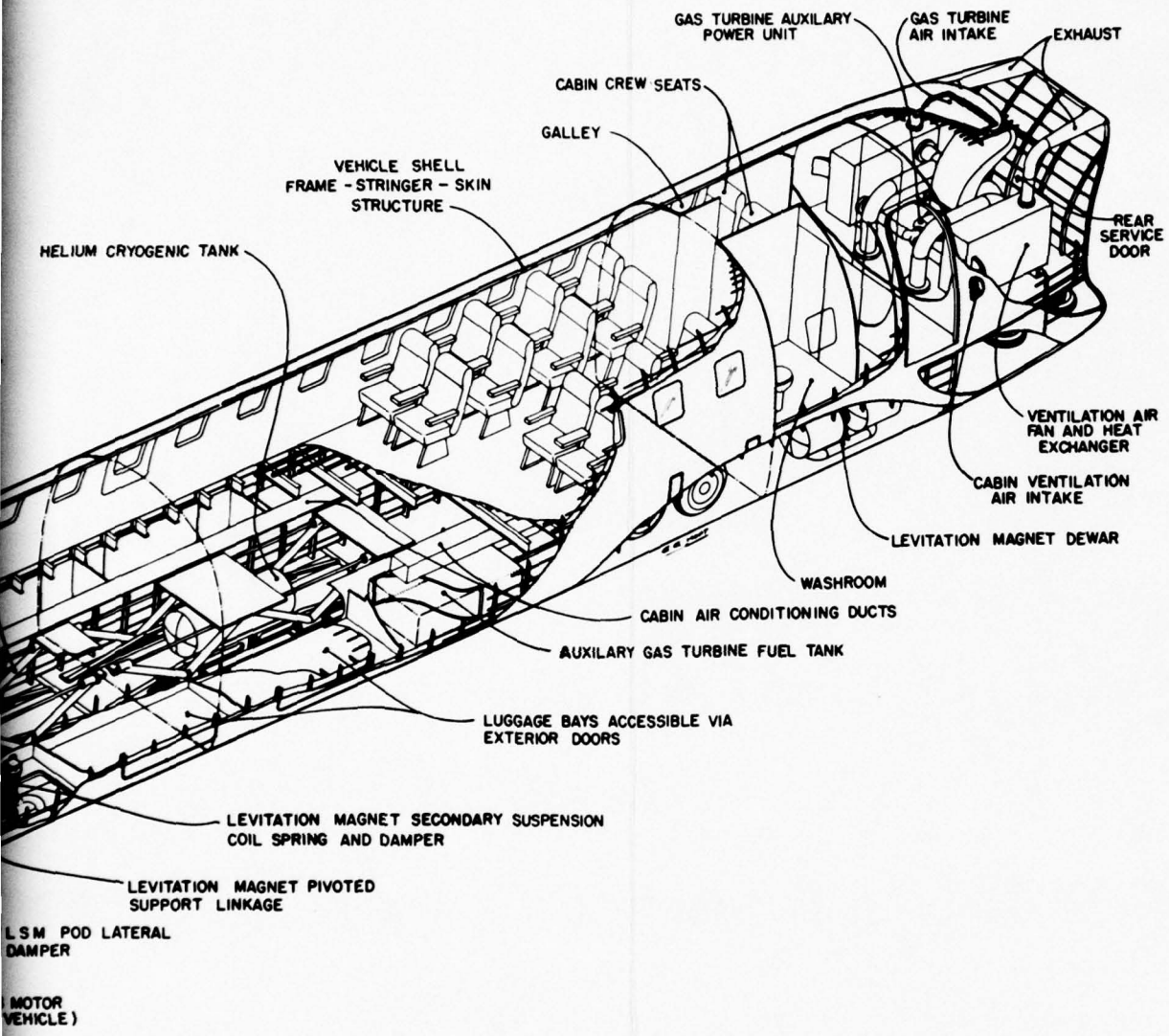

FIG. 2: CANADIAN MAGLEV REVENUE VEHICLE CONCEPTUAL DESIGN

DIVISION OF MECHANICAL ENGINEERING
NATIONAL RESEARCH COUNCIL OF CANADA

2

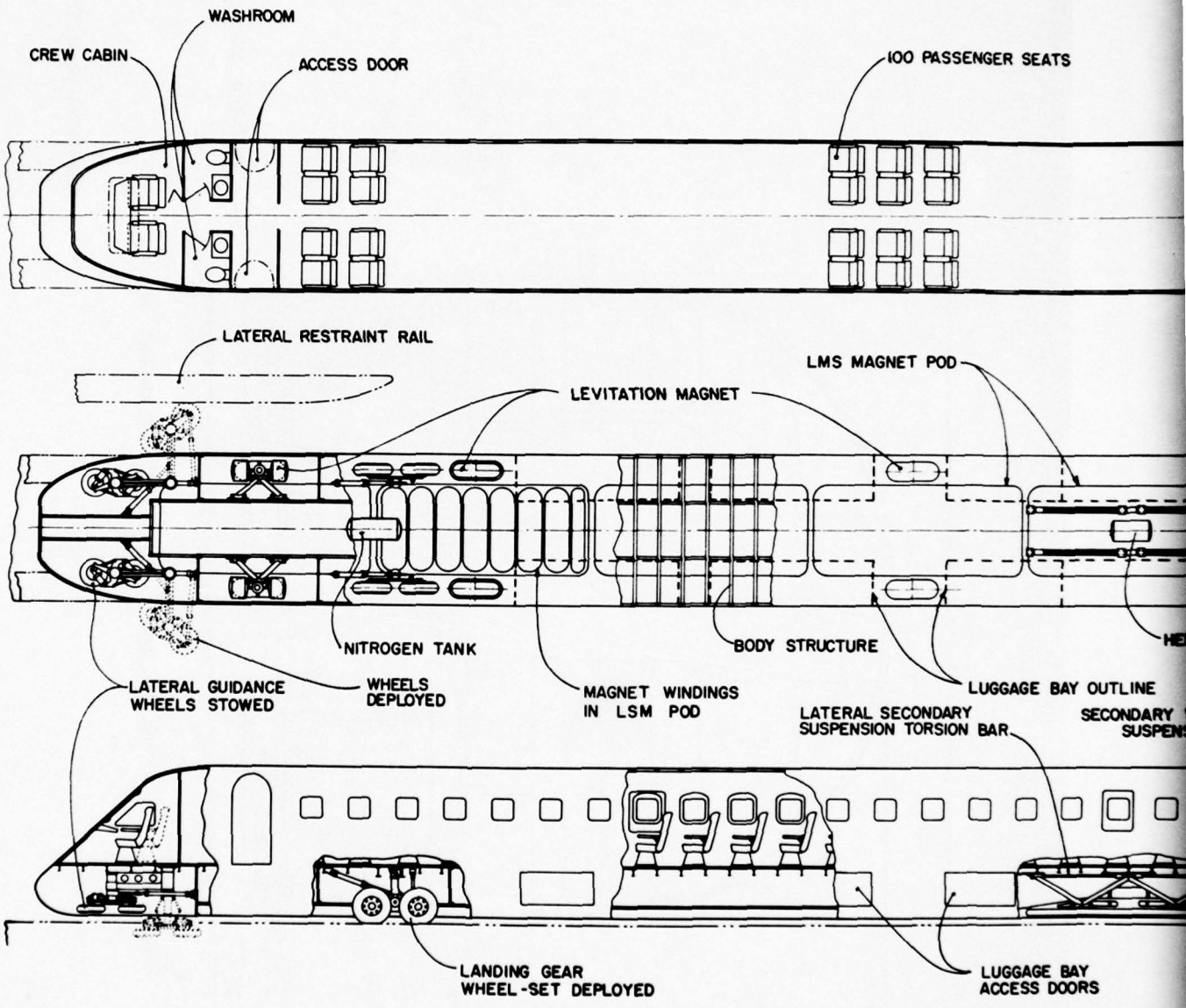

FIG. 3: PROPOSED MAGLEV VEHICLE LAYOUT

DIVISION OF MECHANICAL ENGINEERING
NATIONAL RESEARCH COUNCIL OF CANADA

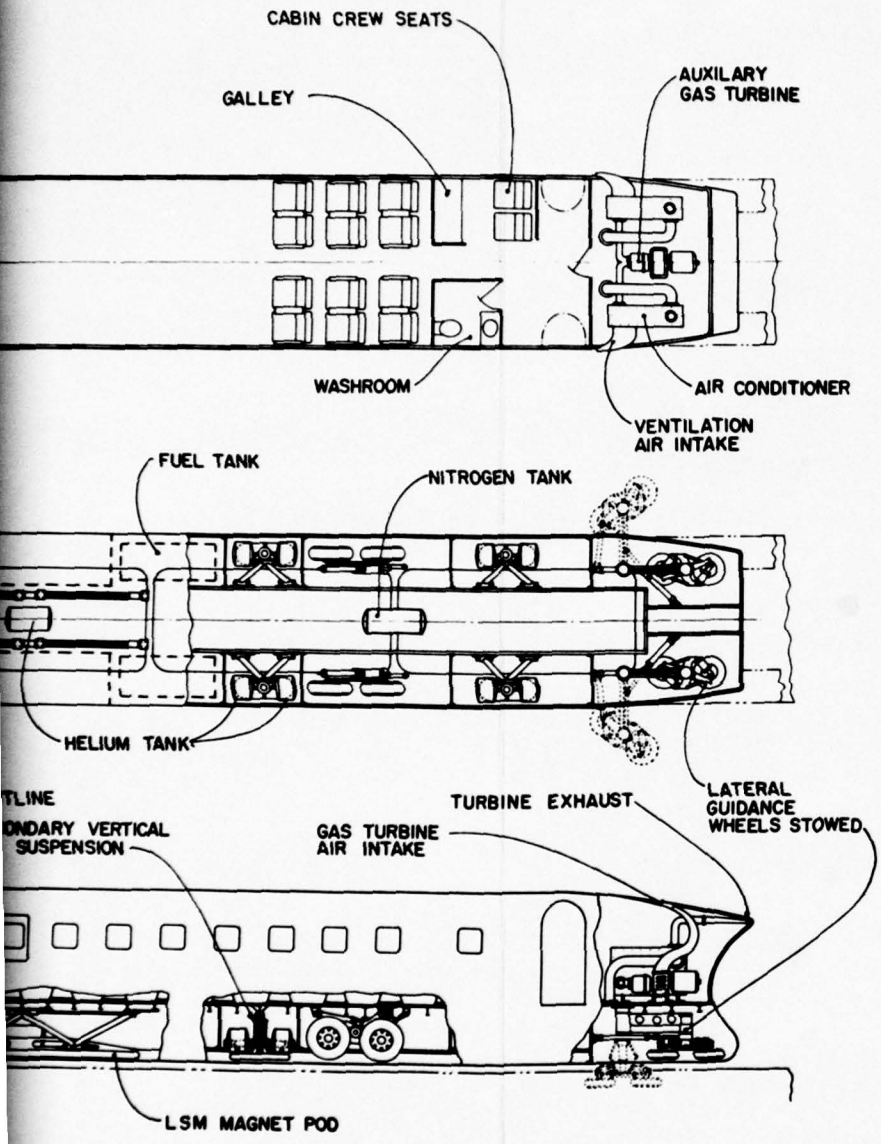
CABIN CREW SEATS
GALLEY
AUXILARY GAS TURBINE
WASHROOM
AIR CONDITIONER
VENTILATION AIR INTAKE
FUEL TANK
NITROGEN TANK
HELIUM TANK
TLINE
ONDARY VERTICAL SUSPENSION
GAS TURBINE AIR INTAKE
TURBINE EXHAUST
LATERAL GUIDANCE WHEELS STOWED
LSM MAGNET POD
0 1 2 3 4 5
SCALE (METERS)

UT

1

2

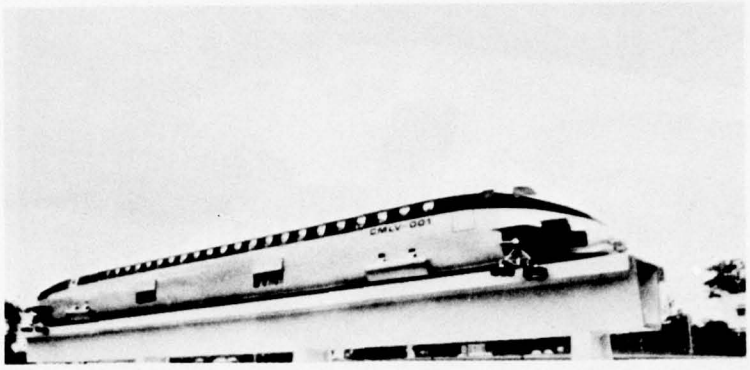

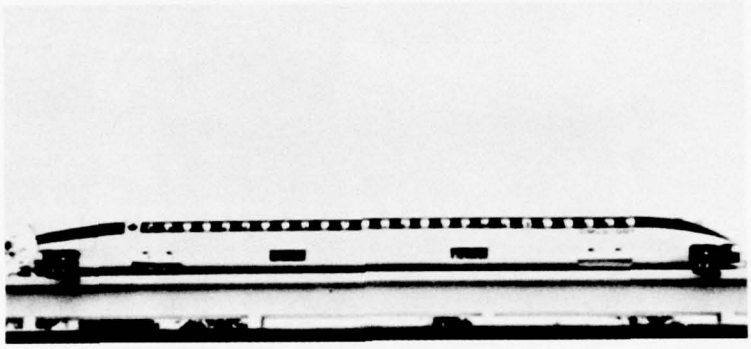

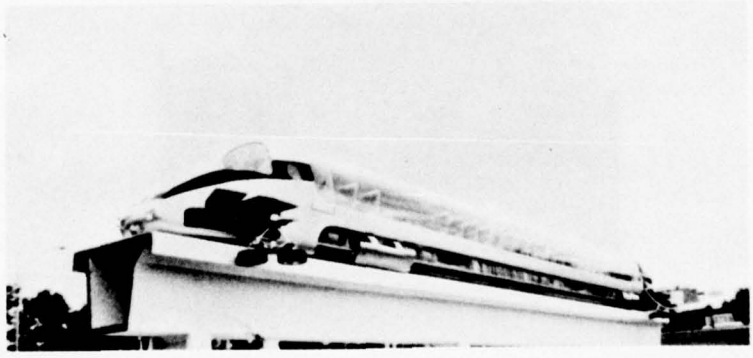

PHOTO A: SIDE EXTERIOR VIEWS OF PROPOSED MAGLEV VEHICLE
(MODEL SHOWN ON PROPOSED GUIDEWAY WITH LOW SPEED WHEELS DEPLOYED)

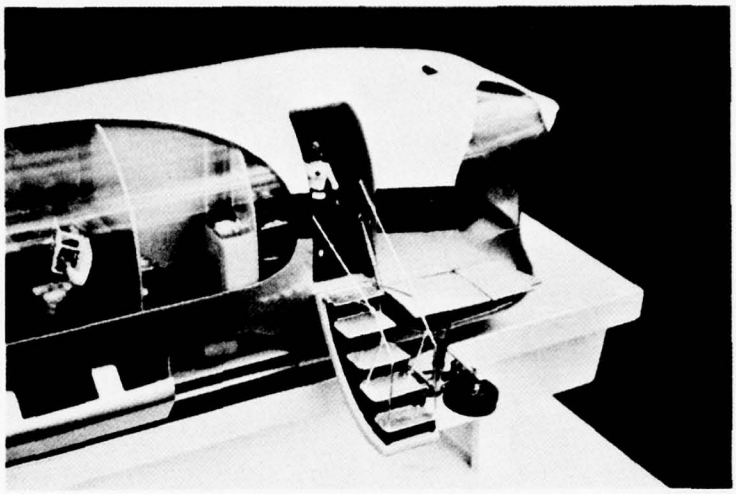

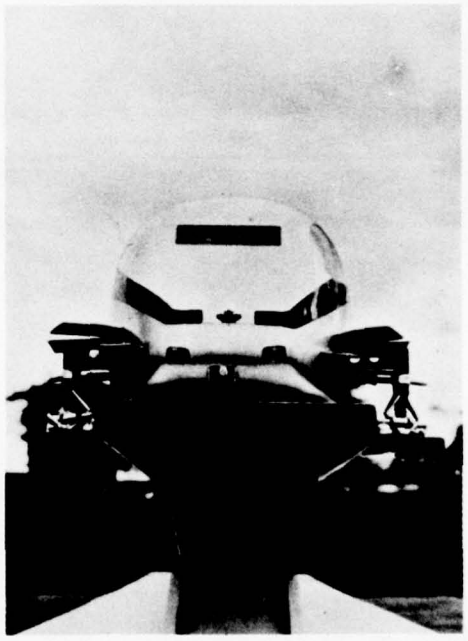

PHOTO B: END AND FRONT VIEWS OF PROPOSED MAGLEV VEHICLE
(MODEL SHOWN ON PROPOSED GUIDEWAY WITH LOW SPEED WHEELS DEPLOYED AND ACCESS DOOR OPEN)

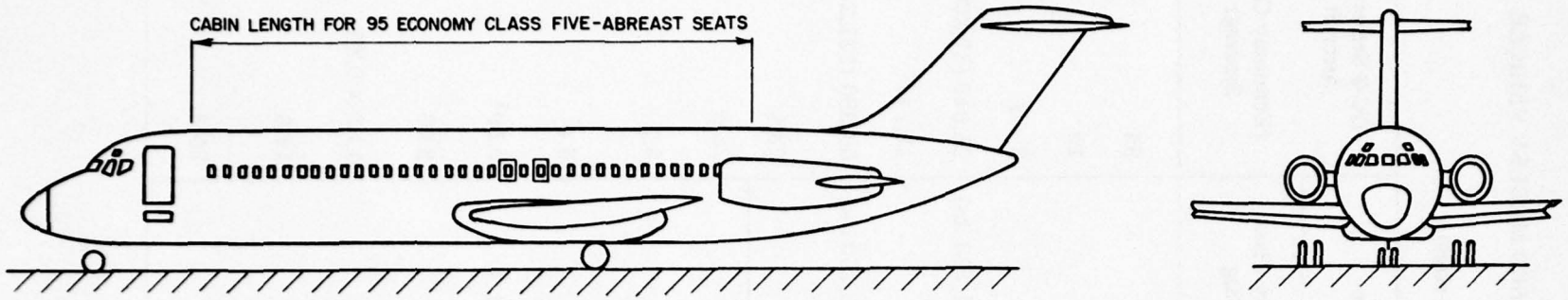

McDONNELL DOUGLAS DC-9 SERIES 30

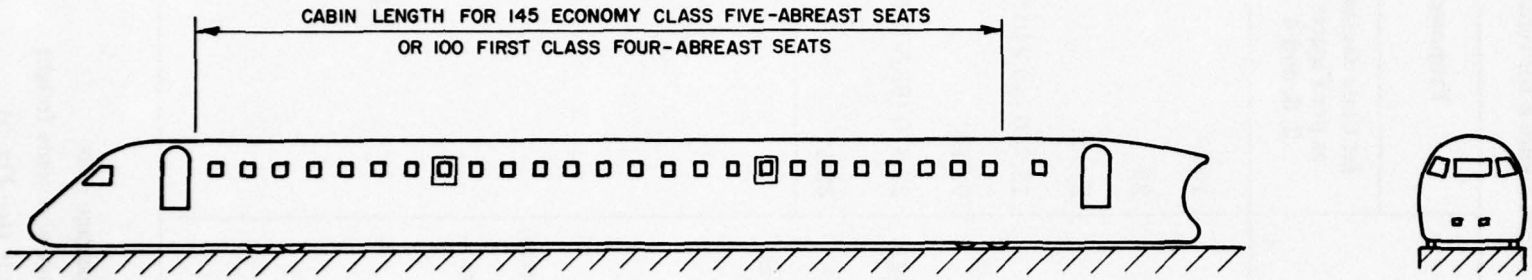

PROPOSED MAGLEV VEHICLE

FIG. 5: COMPARISON OF PROPOSED MAGLEV VEHICLE WITH A SIMILAR SIZED COMMERCIAL AIRCRAFT

TABLE I

COMPARATIVE DESIGN PARAMETERS FOR PROPOSED MAGLEV VEHICLE AND THE DC-9 AIRCRAFT

(see Figure 5 for vehicle comparative sizes)

Item	Proposed Maglev Vehicle Design		DC-9 Series 30 Aircraft
	1st Class Seating as per Figures 2, 3, and 4	Economy Class Seating	(Economy Class Seating)
passenger seats	100	145	95
seat rows	25	29	19
seats per row	2 + 2	2 + 3	2 + 3
empty weight (kg)	18,260 (40,240 lbs)	18,930 (41,720 lbs)	25,940 (57,200 lbs)
payload weight (kg)	9,320[1]	13,520[1]	12,743[2]
maximum gross weight (kg)	28,810 (63,500 lbs)	33,000 (72,760 lbs)	54,980 (121,230 lbs)
payload as percentage of gross weight	32%	41%	23%
overall body length (meters)	36.5		36.4
maximum body height (meters)	3.2		3.7
maximum body width (meters)	3.2		3.4
body frontal area (sq. meters)	9.39 (see Fig. 4)		9.59[3]
maximum cabin headroom (meters)	2.05		2.06
access door (meters)	1.80 X 0.80		1.83 X 0.85
passenger cabin length (meters)	25.5		17.0
under floor baggage hold capacity (cu. meters)	19.5		25.3

[1] includes passengers plus baggage only

[2] includes passengers, baggage and some freight

[3] elliptic fuselage section only (see Fig. 5)

TABLE II

ESTIMATED WEIGHT BREAKDOWN FOR PROPOSED MAGLEV VEHICLE DESIGN

Item	Weight (kg)	Percentage of Gross Weight
Ten levitation magnet assemblies	1,050	3.6
Seven LSM magnet pod assemblies	5,130	17.8
Secondary vertical plus lateral suspensions	1,460	5.1
Landing plus lateral guidance wheel-sets	1,280	4.4
Body shell structure	4,020	14.0
Internal furnishings (seats, floor cover, etc.)	3,130	10.8
Auxiliary power systems	600	2.1
Passive magnetic field shielding	1,590	5.5
• Vehicle Net Weight: (without on-board helium refrigeration)	18,260 kg	63.3%
104 passengers plus crew	7,960	27.6
Luggage	1,360	4.8
Supplies plus gas turbine fuel	1,230	4.3
• Vehicle Gross Weight: (without on-board helium refrigeration)	28,810 kg	100%
(With on-board refrigeration)		
Rough estimate of on-board refrigeration system:	1,400 kg	
Resultant vehicle net weight:	19,660 kg	
Resultant vehicle gross weight:	30,210 kg	

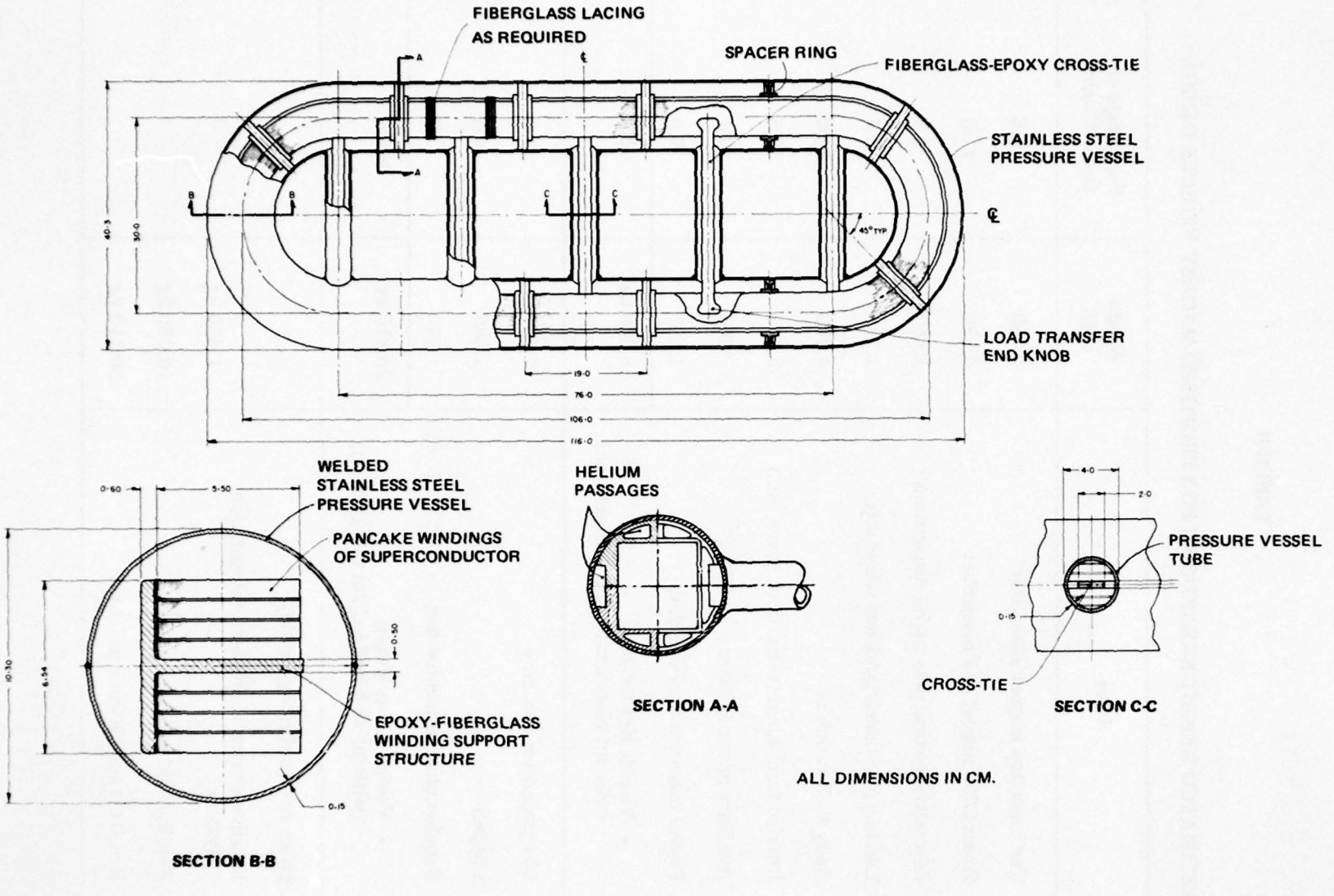

FIG. 6: SUPERCONDUCTING LEVITATION MAGNET WINDING AND PRESSURE VESSEL

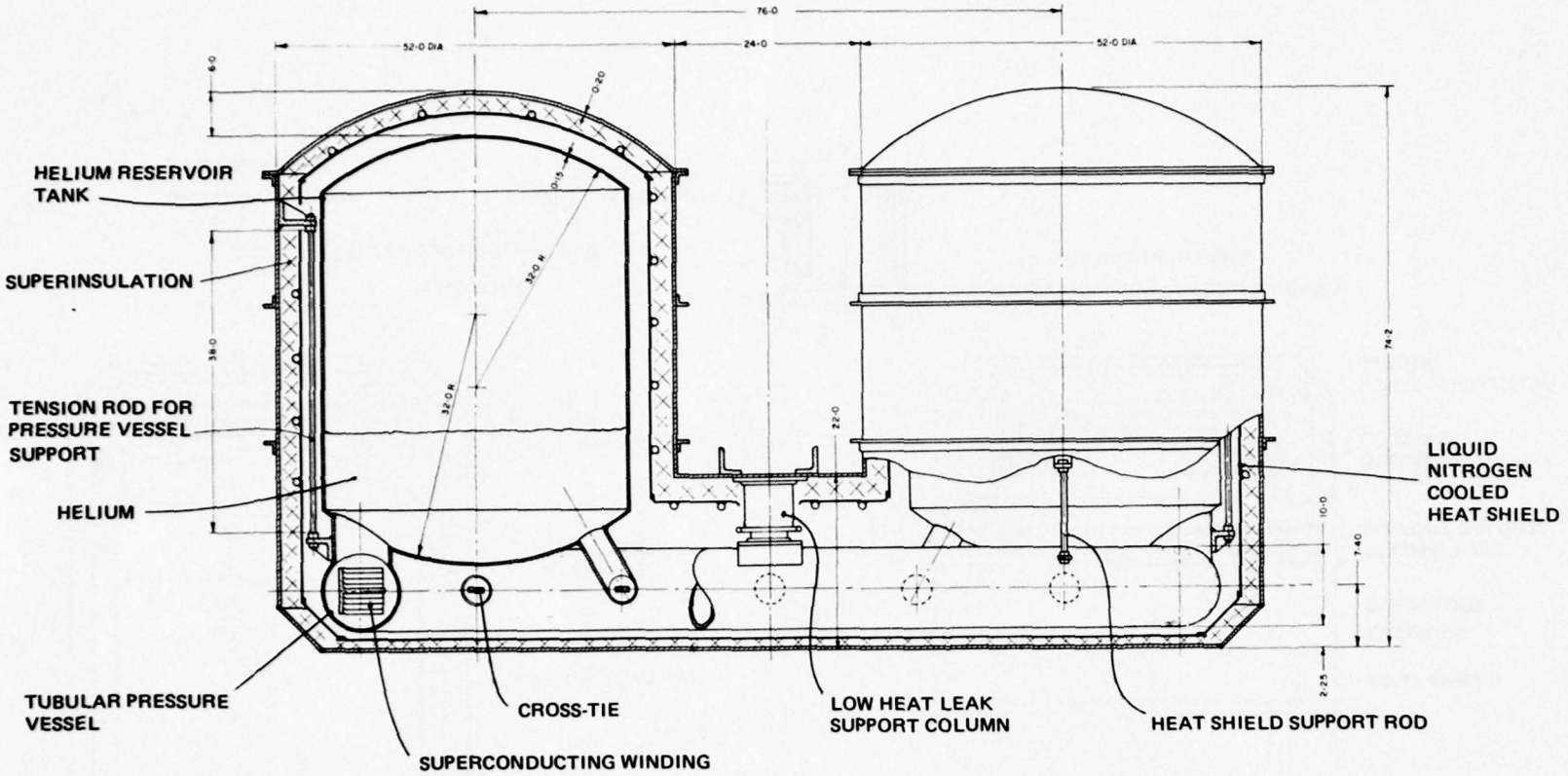

ALL DIMENSIONS IN CM.

FIG. 7: LONGITUDINAL CROSS-SECTION OF SUPERCONDUCTING LEVITATION MAGNET ASSEMBLY

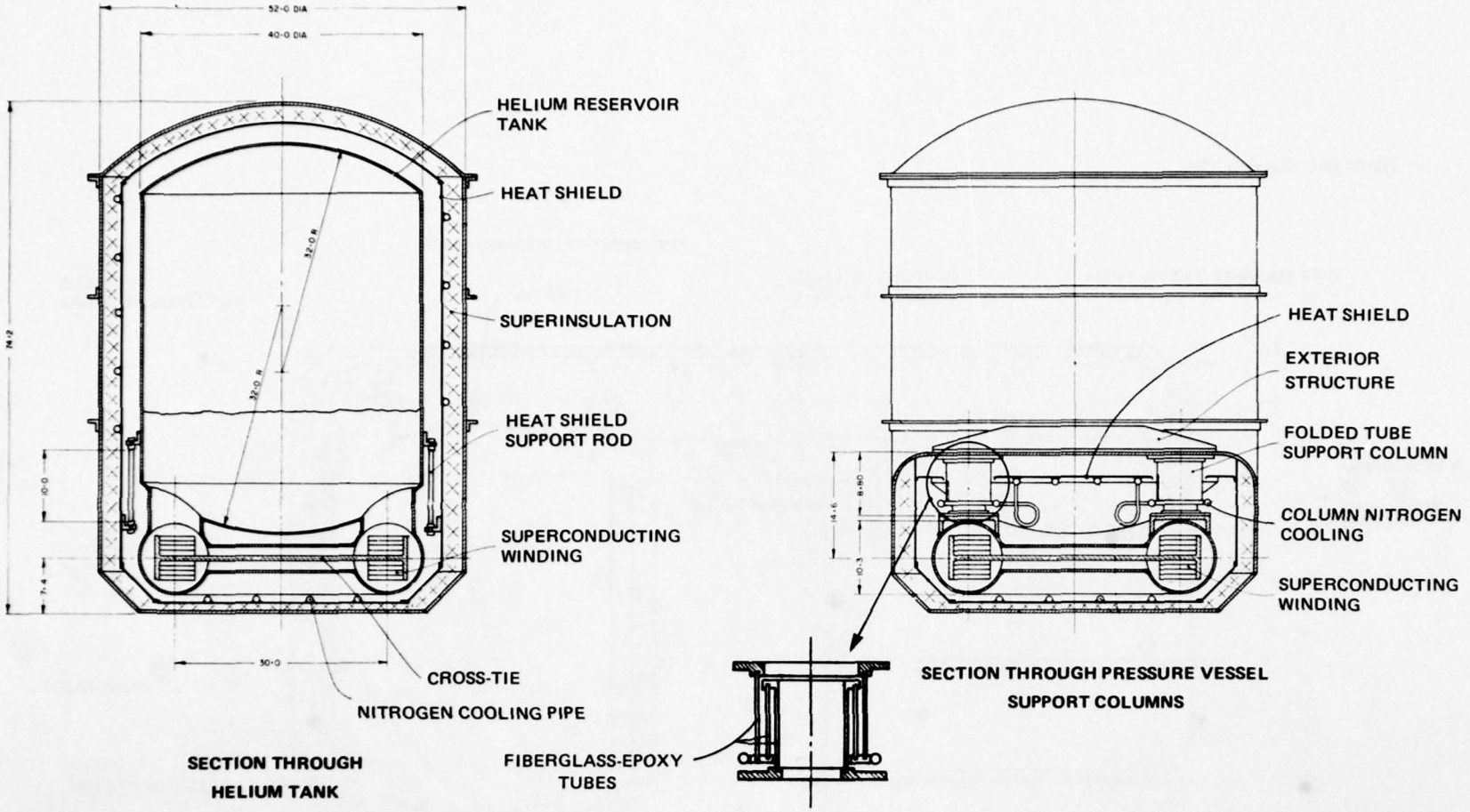

ALL DIMENSIONS IN CM.

FIG. 8: TRANSVERSE CROSS-SECTIONS OF SUPERCONDUCTING LEVITATION MAGNET ASSEMBLY

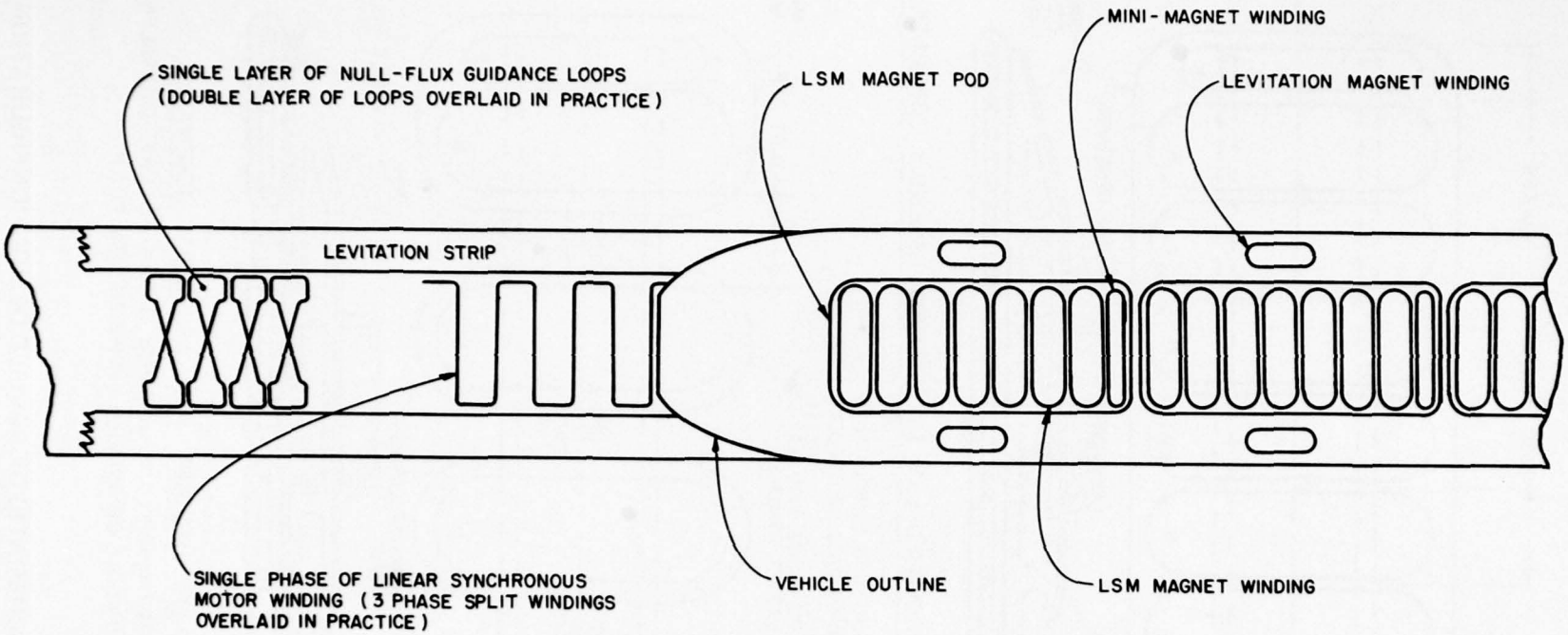

FIG. 9: SCHEMATIC OF GUIDEWAY AND VEHICLE MAGNET WINDINGS

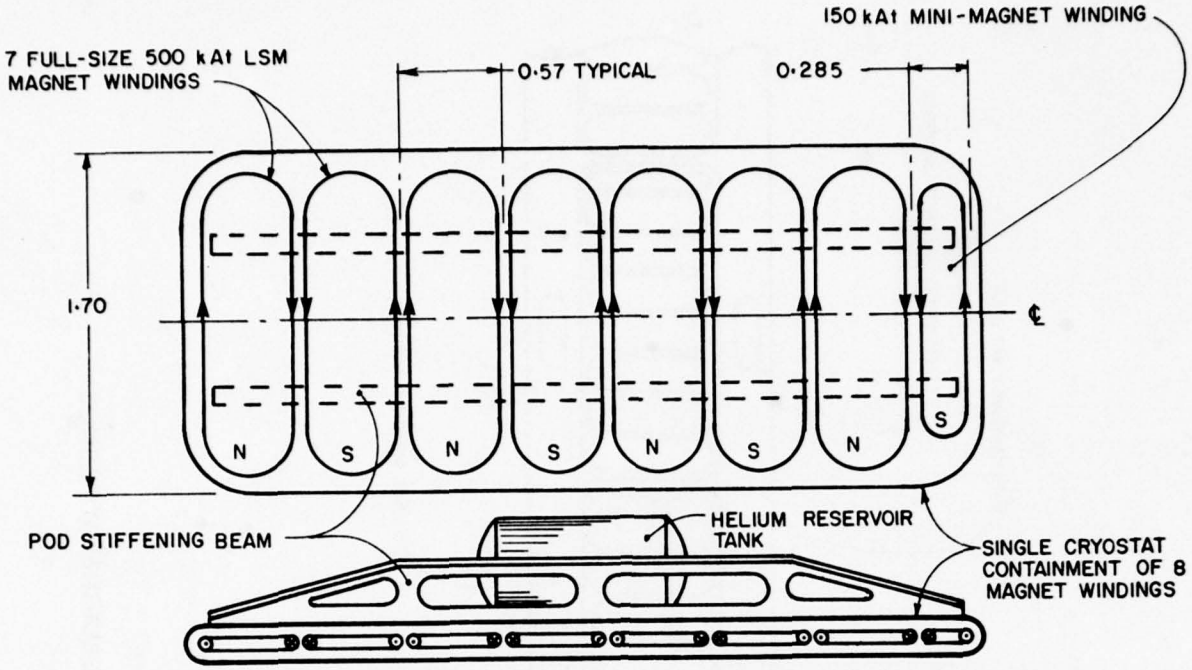

ORIGINALLY PROPOSED LSM MAGNET POD ASSEMBLY SCHEMATIC

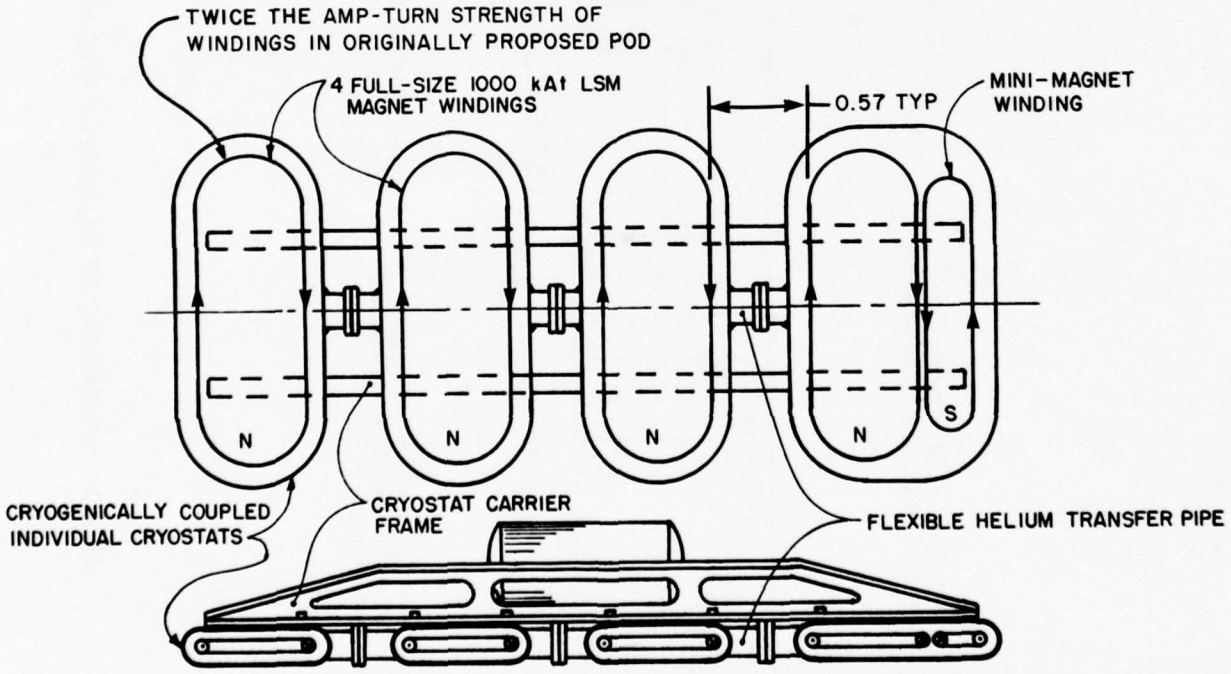

REVISED LSM MAGNET POD ASSEMBLY SCHEMATIC

(GENERATES MOTOR THRUST AND GUIDANCE FORCES AT LEAST EQUIVALENT TO ABOVE ORIGINALLY PROPOSED LSM POD)

(DIMENSIONS IN METERS)

FIG. 10: SCHEMATIC OF REVISED DESIGN CONFIGURATION FOR VEHICLE LSM POD ASSEMBLY

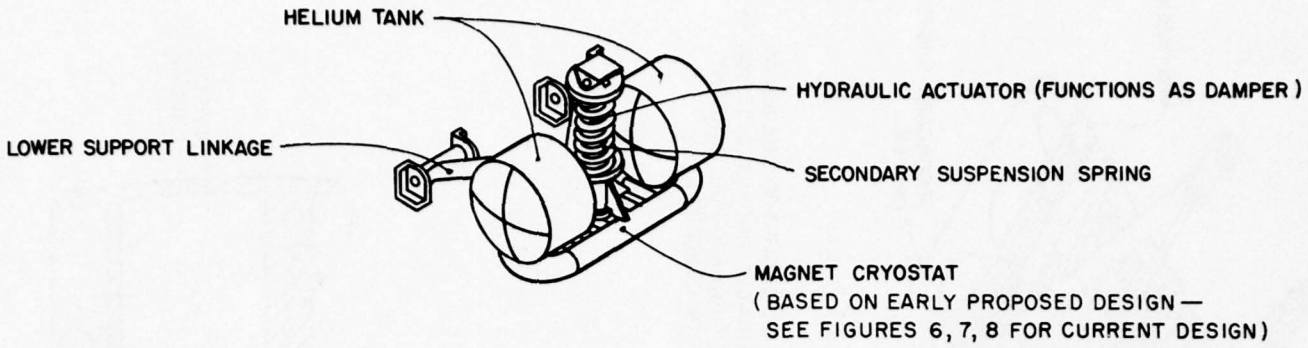

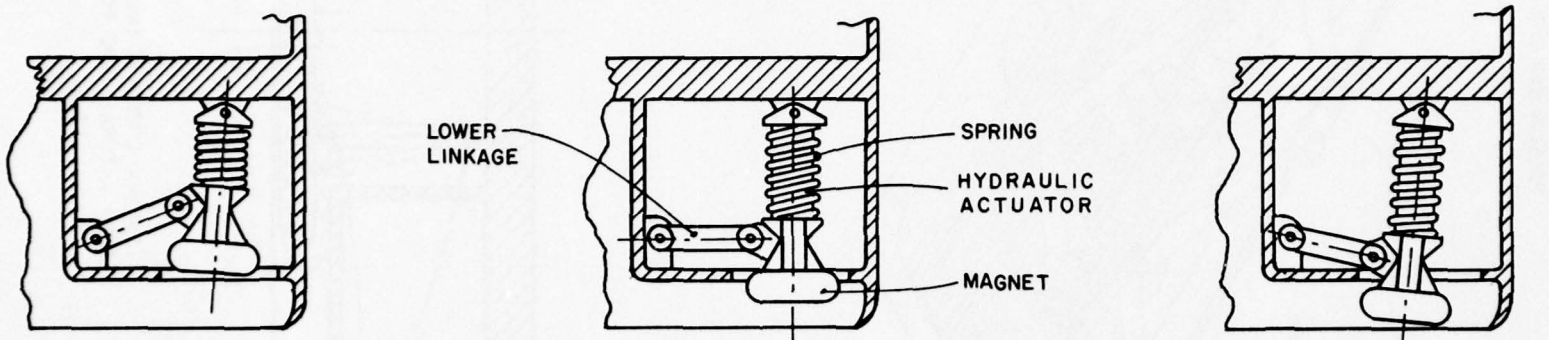

FIG. 11: LEVITATION MAGNET ASSEMBLY VEHICLE SECONDARY VERTICAL SUSPENSION SYSTEM

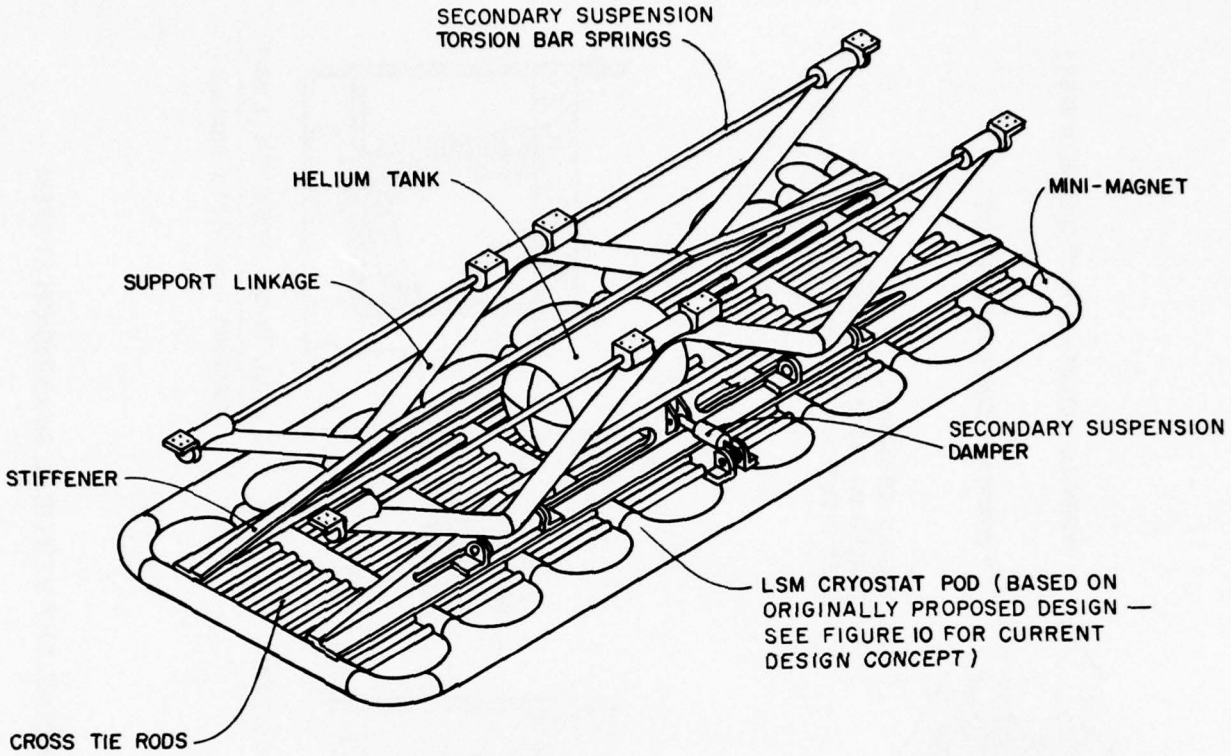

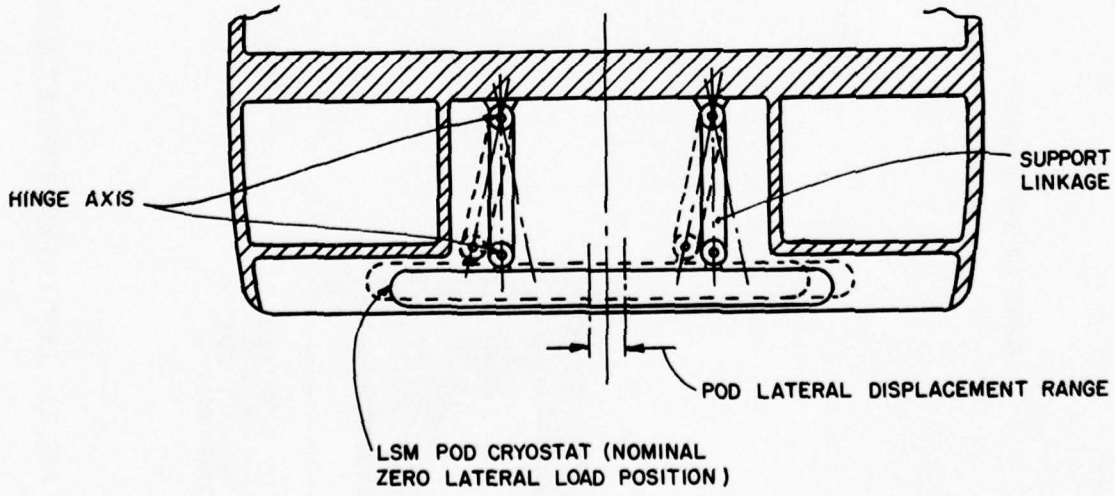

FIG. 12: LSM MAGNET POD ASSEMBLY VEHICLE SECONDARY LATERAL SUSPENSION SYSTEM

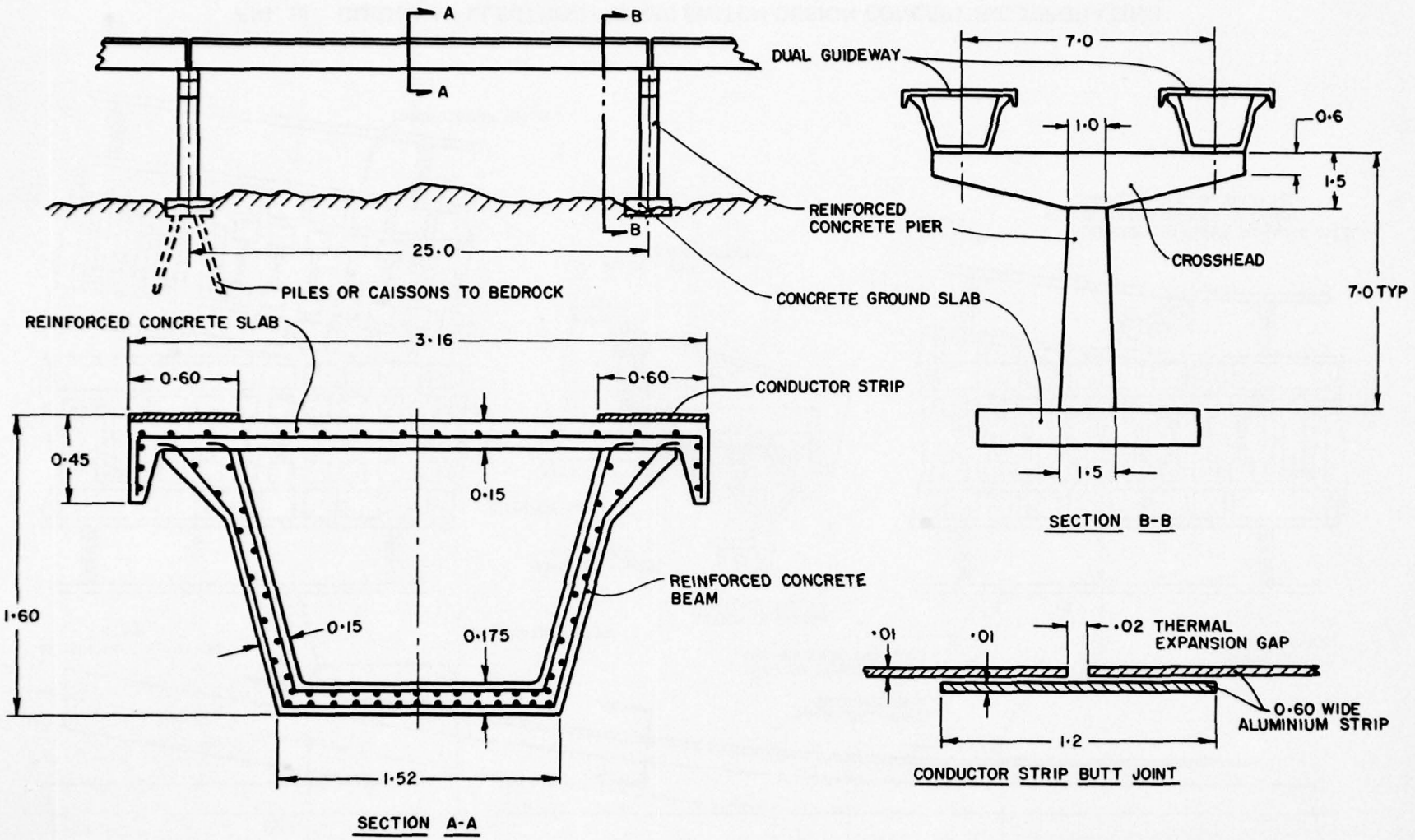

FIG. 13: PROPOSED ELEVATED GUIDEWAY CONFIGURATION

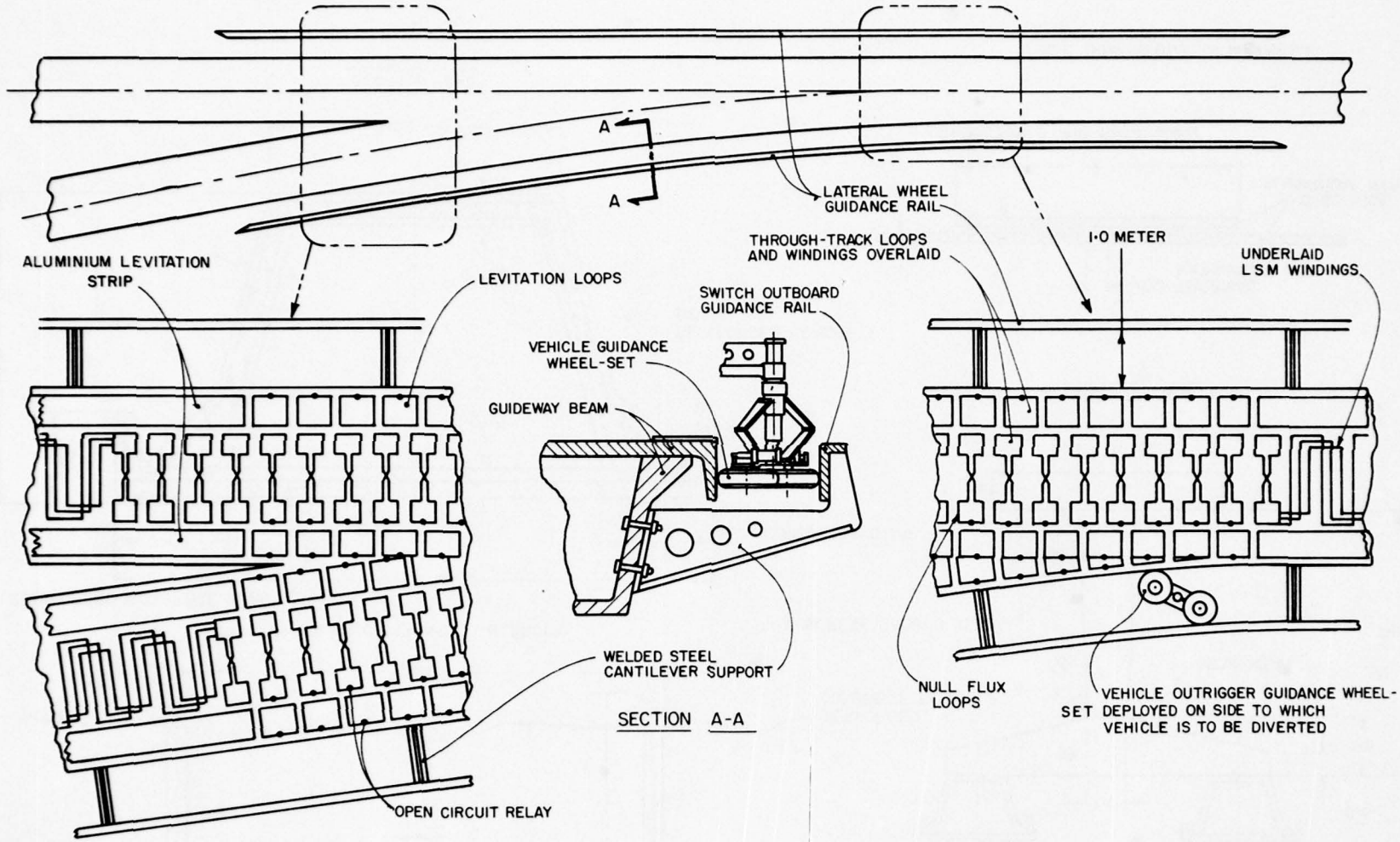

FIG. 14: GUIDEWAY ELECTRODYNAMIC SWITCH DESIGN CONCEPT INCORPORATING LOW SPEED MECHANICAL GUIDANCE MEANS

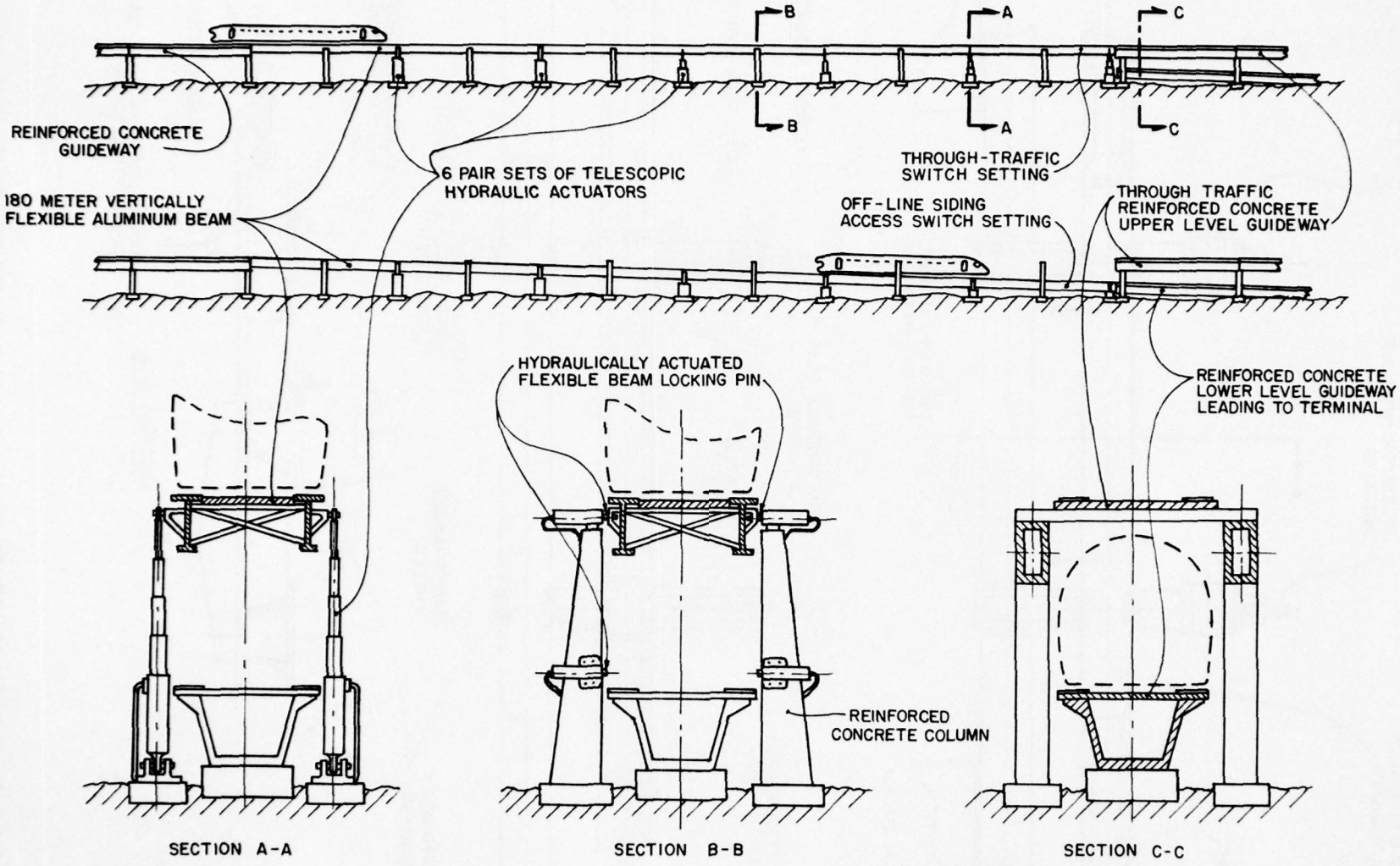

FIG. 15: PROPOSED INCLINE RAMP TYPE ACTIVE SWITCH DESIGN CONCEPT

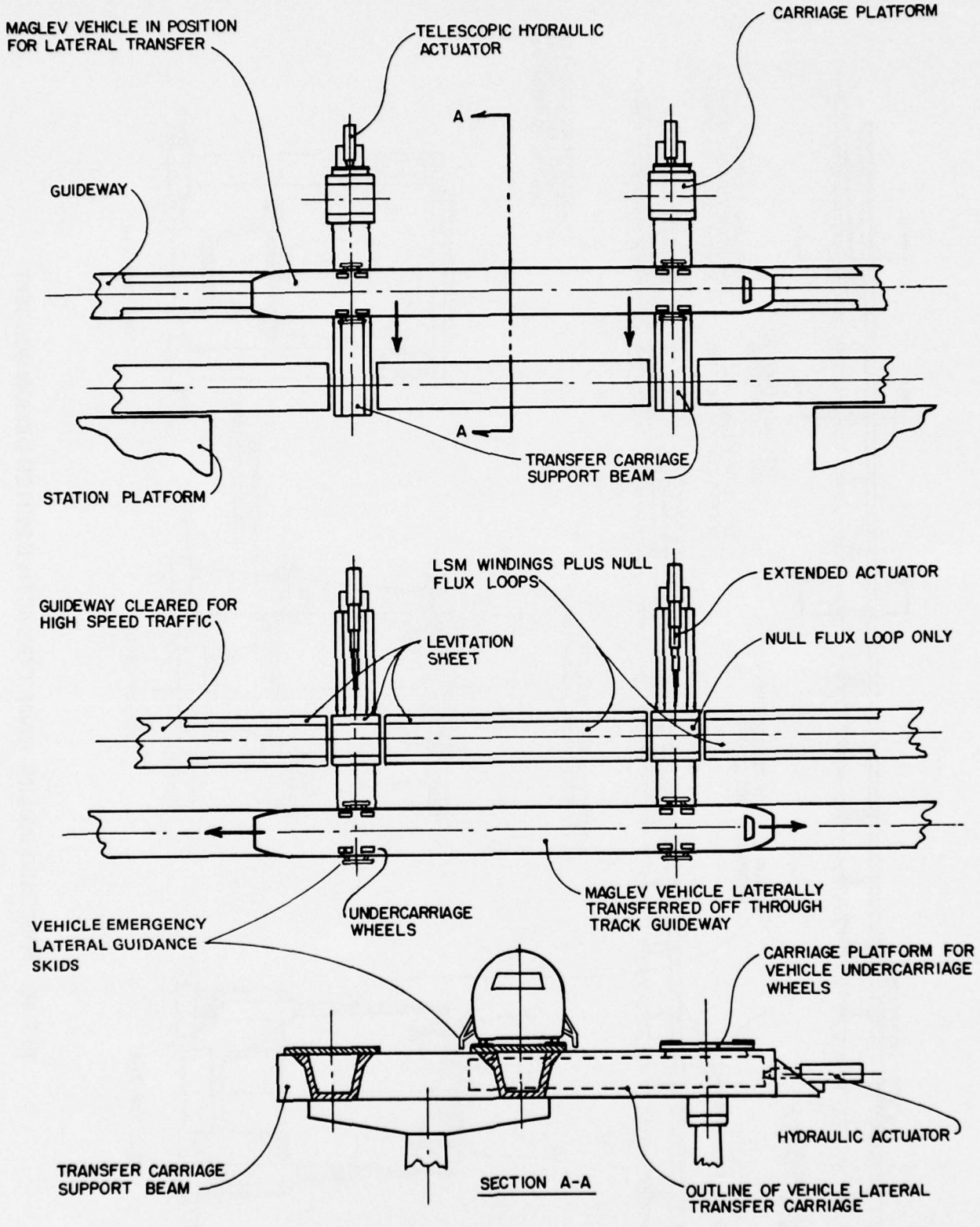

FIG. 16: MAGLEV SYSTEM PROPOSED VEHICLE LATERAL TRANSFER SWITCH DESIGN

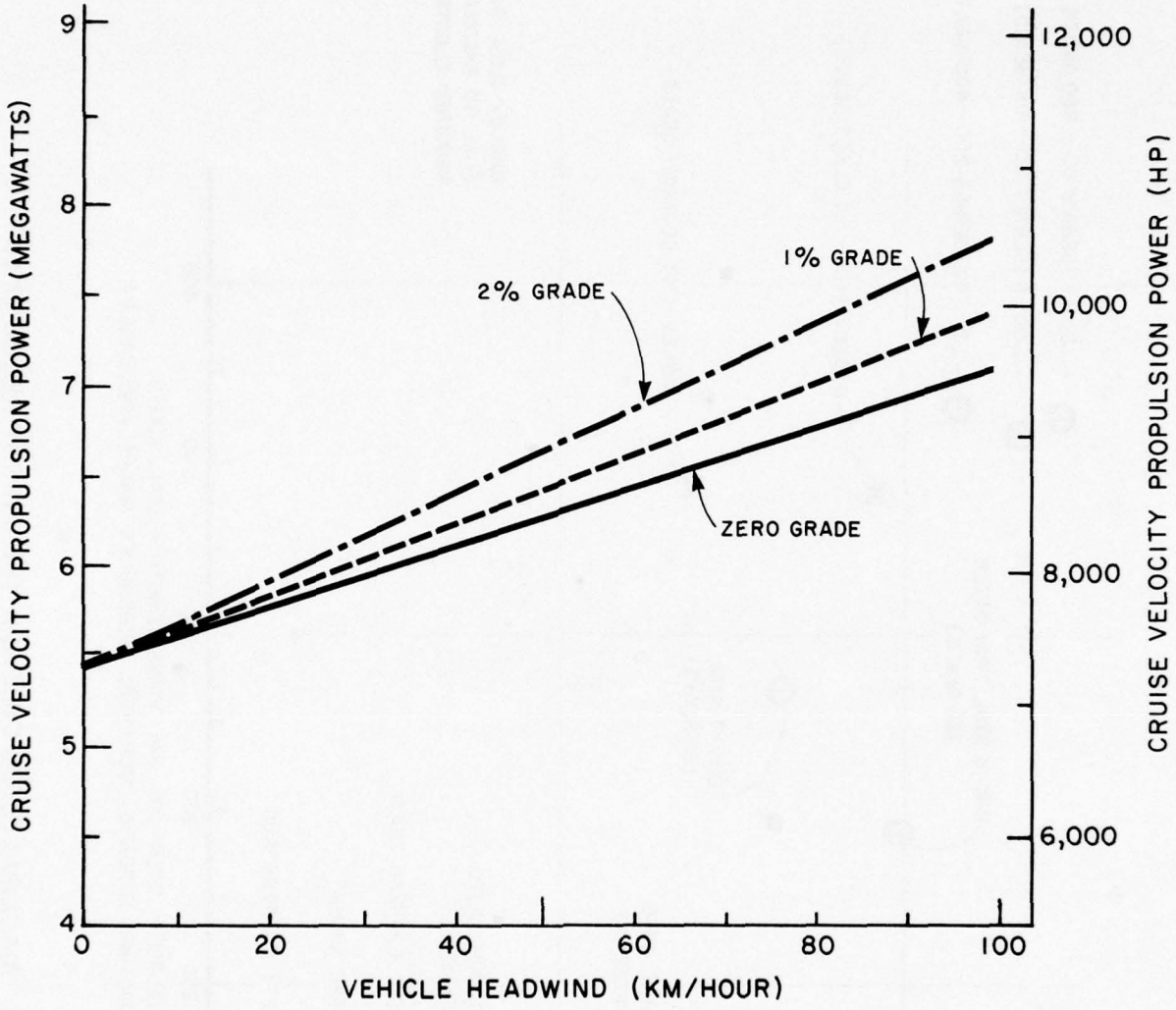

FIG. 17: ESTIMATED PROPULSION POWER REQUIREMENTS FOR PROPOSED MAGLEV VEHICLE
(SYSTEM OPTIMIZATION BIASED TOWARDS REDUCING PROPULSION MOTOR CAPITAL COSTS RATHER THAN MINIMIZING PROPULSION POWER)

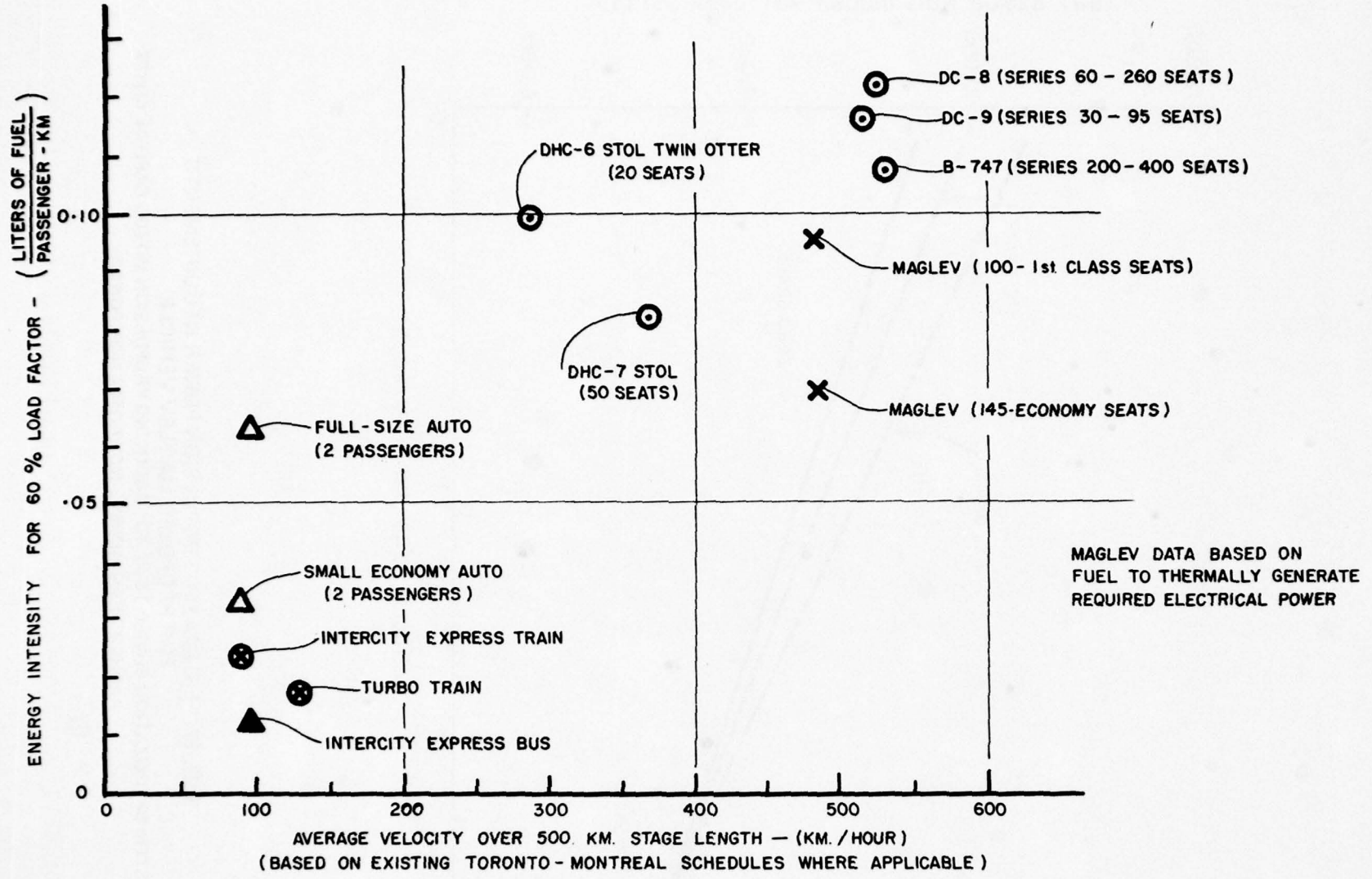

FIG. 18: MAGLEV SYSTEM COMPARATIVE ENERGY REQUIREMENT

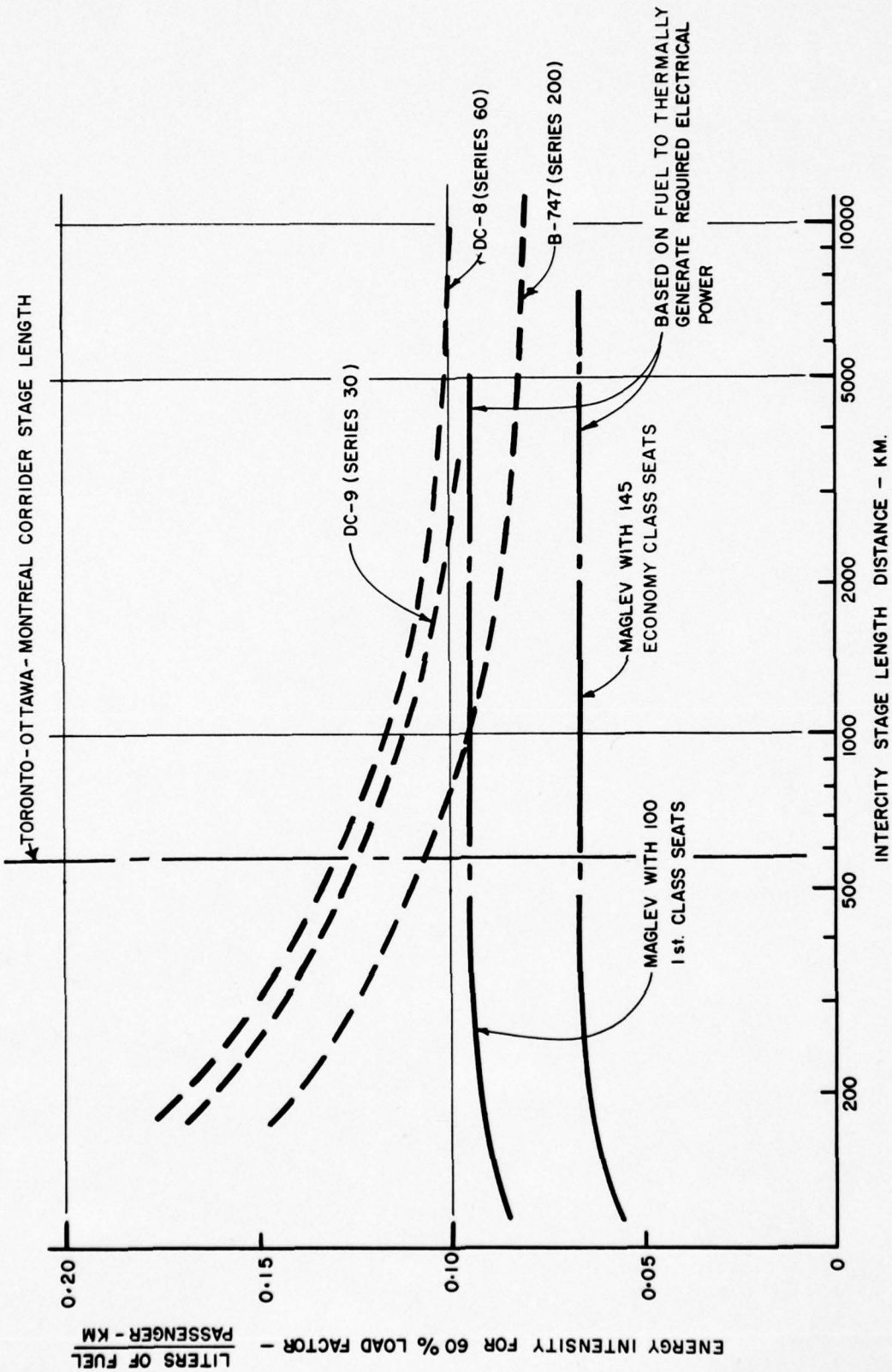

FIG. 19: TRANSPORTATION SYSTEM COMPARATIVE ENERGY REQUIREMENT DEPENDENCY UPON TRIP STAGE LENGTH

CURRENT PROJECTS

Much of the work in progress in the laboratories of the National Aeronautical Establishment and the Division of Mechanical Engineering includes calibrations, routine analyses and the testing of proprietary products; in addition, a substantial volume of the work is devoted to applied research or investigations carried out under contract and on behalf of private industrial companies.

None of this work is reported in the following pages.

ANALYSIS LABORATORY

AVAILABLE FACILITIES

This laboratory has analysis and simulation facilities available on an open-shop basis. Enquiries are especially encouraged from industry for projects that may utilize the facilities in a novel and/or particularly effective manner. Such projects are given priority and are fully supported with assistance from laboratory personnel. The facilities are especially suited to system design studies and scientific data processing. Information is available upon request.

EQUIPMENT

An Electronic Associates 690 HYBRID COMPUTER consisting of the following:

(a) PACER 100 digital computer

- 32K memory
- card reader
- high speed printer
- disc
- digital plotter
- Lektromedia interactive terminal

(b) Two EAI 680 analogue computer consoles

- 200 amplifiers including 60 integrators
- 100 digitally set attenuators
- non-linear elements
- x-y pen recorders
- strip chart recorders
- large screen oscilloscope

(c) EAI 693 interface

- 24 digital-to-analogue converters
- 48 analogue-to-digital converters
- interrupts, sense lines, control lines

Dual channel real time portable spectrum analyser, Hewlett Packard Model 3582A. Bandwidth 0.02 to 25.5 Hz. Built-in periodic and random sources for transfer function and transient signal analysis.

GENERAL STUDIES

A microprocessor-based function generator for the hybrid computer is being designed. A TI 9900 development system has been obtained to be used for the project.

A study is being made on the use of topological methods to describe and analyze complex systems.

APPLICATION STUDIES

Aviation Electric Ltd. hybrid computer modeling work is continuing in support of their advanced control concepts for both the small business jet engine and the helicopter engine. GasTOPS Ltd. are collaborating with AEL.

Canadian Westinghouse Ltd. are continuing a study of fuel controller requirements for a new family of industrial gas turbines. A hybrid computer model is being used to evaluate control system hardware.

In collaboration with Kendall Consultants Ltd., and SPAR Aerospace Products Ltd., a hybrid computer model of the remote manipulator arm for the space shuttle is being assembled. The model includes all allowable motions in three dimensions as well as arm flexibility effects. The three dimensional model is complete and arm control algorithms are being evaluated.

In collaboration with the Railway Laboratory, a pilot hybrid computer model of the NRC roller rig for railway vehicle testing is being used as an aid in the design of the roller rig and its controls.

In collaboration with the Control Systems and Human Engineering Laboratory and the International Nickel Co., Ontario Division, an interactive computer model of a copper-nickel smelter is being developed to study material handling and scheduling in the plant.

In collaboration with DME Engine Laboratory a hybrid computer model of an air cushion vehicle is being assembled.

In collaboration with DME Engine Laboratory analysis of fuel consumption and travel time of test cars with two computer controlled traffic light sequencing plans.

In collaboration with Glenayre Electronics Ltd. and Lornex Mines a computer model of open pit mining operations is being developed for use in the design and evaluation of a truck dispatching system.

Carleton University and Engine Laboratory are collaborating on a study of a heavy equipment propulsion system using a co-rotating compressor.

In collaboration with Stephens-Adamson of Belleville a hybrid computer model of long conveyor belts is being assembled.

In collaboration with Davis Eryou and Associates a hybrid computer model of an automobile is being assembled.

Davis Eryou and Associates are assembling a computer aided design package for Solar Heating Systems under contract to the NRC Energy Project.

Two PILP contracts are under way to conduct a market survey and feasibility study for a commercial hybrid computer simulation facility.

Kendall Consultants Ltd. are carrying out a preliminary study for Guildline Instruments Ltd. on their Batfish cable-towed oceanographic survey system.

SYSTEM SOFTWARE STUDIES

A preprocessor for hybrid computer model digital programs.

Character string manipulation routines to be used in a Fortran environment.

CONTROL SYSTEMS AND HUMAN ENGINEERING LABORATORY

INDUSTRIAL CONTROL PROBLEMS

In collaboration with the Analysis Laboratory interactive computer models are being developed and applied to a variety of scheduling and materials handling projects in the mining and metal processing industries.

Application of microprocessors to improve quality, performance and efficiency in the metal forming industry is currently being undertaken in collaboration with a Canadian company.

To study distributed process control a network software system (DECNET) is being installed to connect together the PDP-11/45 and PDP-11/60 computers in the Laboratory. Also, a serial communication system based on the HDLC line protocol is being implemented with microprocessors. This activity is proceeding in parallel with the development of an international standard for industrial intersubsystem communication.

A flowmeter, viscometer, consistency sensor and control valve utilizing radial laminar flow have been developed and patented. The devices, currently under test for industrial application, are mechanically simple and have a minimum of machining tolerances. They offer significant advantages over those currently available in that the maintenance of laminar flow provides quiet operation while allowing accurate performance production.

ADVANCED TRANSPORTATION CONCEPTS

The conceptual design for a high speed intercity magnetically levitated and linear synchronous motor propelled vehicle plus elevated guideway system as based on the results of a basic Maglev research program jointly conducted by Queen's University, University of Toronto and McGill University has been carried out in collaboration with Transport Canada. Ongoing study includes computer modeling for ride quality assessment, vehicle dynamic behaviour prediction and engineering design consideration of the magnets.

HUMAN ENGINEERING -- BEHAVIOURAL STUDIES

The investigation of the effect of internal and external environments on human psychomotor performance has been extended to Ministry of Transport radio communications staff operating in the high Arctic under conditions of continuous darkness. A study is also being conducted in collaboration with Indian Air Force on the psychomotor performance of aircrew on long range flights.

Tracking experiments have been designed and initiated in the series dealing with precision of movement to a target. These are further tests of the hypothesis that subjects move in a frame of reference based on proprioceptive rather than visual information.

HUMAN ENGINEERING -- MEDICAL AND SURGICAL

A production model portable thermoelectric cooling system is being developed in collaboration with the Montreal Neurological Institute for controlled cooling of the exposed spinal cord at operation.

A prototype model miniature instrument for measuring the viscoelastic properties of skin is being developed.

ENGINE LABORATORY

ACOUSTICS

Computational methods are being developed for propagating modes in ducts based on sound pressure level around the circumference of the duct using cross spectral density and phase-locked methods. A series of experiments were completed in support of the analytical instruments.

An improved technique for noise source identification in small reciprocating engines is being developed. Experimental measurements have been completed and analysis is proceeding.

AIR CUSHION VEHICLES

A study on the drag and stability of low speed AC rafts over water is in progress. Model experiments in a flume have been completed, and further tests will be carried out in the open on a 4 X 3 m model now under construction.

GAS TURBINE OPERATIONS

Studies of J85-CAN-15 gas turbine operation and performance were conducted. An assessment of deliberate downtrimming of the gas turbine as anti-compressor stall and peak temperature reduction measures was made. A number of T5 amplifiers of the fuel control system were tested for their proper and repeatable functioning. The evaluation of test data is in progress.

AUTOMOTIVE FUEL ECONOMY

The report on the effect of traffic signal control strategy on automotive fuel consumption is in its final draft. The TRANSYT-5 traffic light control program saves time, a small amount of fuel and has fewer stops than the EXISTING control program. Further regression analysis is being done on test data to determine the effect of delay time. The original study considered number of stops, total time and calculated fuel consumption.

FUEL CONTROL SYSTEMS

A major Canadian manufacturer of fuel control systems for gas turbines in the general aviation market is developing an advanced concept digital fuel control system that was verified on a computer model of a gas turbine at the NRC. To prove the hardware of the system on a real engine, a co-operative program with the manufacturer will use a Twin-Pac helicopter engine on a dynamometer to enable a steady-state and transient performance assessment to be made. The Twin-Pac is in an advanced state of installation with all major facilities connected.

NRC-PRATT & WHITNEY HIGHLY LOADED TURBINE

Preliminary tests have been conducted at rotor speeds up to 2000 rpm to examine the controllability of the dynamometer loading system. Higher speeds were not attempted as a solid shaft was used temporarily to couple the turbine to the dynamometer.

ROTOR DYNAMICS

Construction and equipment acquisition has begun on a large rotor dynamics and balancing facility. This facility will accommodate rotors of diameters up to 6 m in length and approximately 2 m in diameter. Installed drive motors have a capacity of 1200 HP. Eventually, the test chamber will be capable of operating at reduced pressures allowing bladed rotors to be tested without serious power dissipation.

In co-operation with a Canadian manufacturer, a calibration rotor for industrial balancing machines has been precision balanced using air bearing supports for the rotor. These bearings allowed a more rapid balance and a more accurate determination of the residual unbalance in the test rotor.

HYDROSTATIC BEARINGS

This laboratory continues to provide assistance and design service to other potential gas and fluid film bearing users both within NRC and in other government laboratories. In co-operation with three Canadian industrial firms a study to compare the predicted results of computer programs designed to calculate the dynamic performance of self-acting bearings with incompressible lubricants has been completed. Comparison was also made with a broad cross-section of example bearings from the literature.

VIBRATION MONITORING

An experimental rig has been assembled to allow the testing of rolling element bearings to failure. This rig is now being used to compare current methods of vibration detection and their ability to discover incipient faults in rolling element bearings. Because of the nature of fault generation in rolling element bearings the result gathering process is of a rather long-term nature.

A co-operative program with the Defence Research Establishment (Pacific) in Victoria is underway to investigate the combined merits of oil analysis and vibration monitoring as tools for helicopter transmission gear box monitoring.

AUTOMOTIVE ENGINE COOLING SYSTEM PERFORMANCE

In collaboration with Canadian automotive industry and with financial support by Transport Canada the Division of Mechanical Engineering is doing research to try to improve fuel economy through better use of cooling fans. The specific objective will be to reduce the total power draw by controlling the interaction between the cooling fan and the external vehicle aerodynamics.

A suitable test vehicle has been provided by industry and this car is being instrumented for road and wind tunnel test work.

HOSPITAL AIR BED

Evaluation and use of the NRC Mark I Cairbed is continuing in the Burns Unit of the Hotel Dieu Hospital in Kingston, Ontario. The latest trials have involved the bed continuously for over one year.

A great many advantages over standard support methods have been demonstrated, most notably a better rate of epithelial repair. The chief drawback of the experimental unit placed in Kingston has been its noise.

At present plans are being made to modify the Mark I bed to increase its life and to reduce noise. Negotiations for commercial fabrication of four advanced air bed versions for future clinical assessments are proceeding.

FLIGHT RESEARCH LABORATORY

AIRBORNE MAGNETICS PROGRAM

Experimental and theoretical studies relating to the further development of airborne magnetometer and gradiometer equipment and the application of same to submarine detection and geological survey, are currently in progress. The final report on methods of magnetic aircraft compensation, based on data collected with the North Star aircraft, has been published. A Convair 580 aircraft has been equipped as a multi-purpose flying laboratory for research in aeromagmetic detection and for development of radio and inertial navigation methods. Further modifications may be done to provide a capability for evaluating advanced synthetic aperture radar techniques.

INVESTIGATION OF PROBLEMS ASSOCIATED WITH STOL AND V/STOL AIRCRAFT OPERATIONS

The Laboratory's Airborne V/STOL Simulator is being employed in programs to investigate STOL and V/STOL aircraft flying qualities and terminal area operational problems. Areas of research include a general investigation of flight path control and stability characteristics required to compensate for single engine failure in twin or multi-engine powered-lift aircraft, and the identification of minimum acceptable flying qualities for civil helicopters operating under instrument flight rules.

INVESTIGATION OF ATMOSPHERIC TURBULENCE

A T-33 aircraft, equipped to measure wind gust velocities, air temperature, wind speed, and other parameters of interest in turbulence research, is used for measurements at very low altitude, in clear air above the tropopause, in the neighbourhood of mountain wave activity, and near storms. Records are obtained on magnetic tape to facilitate data analysis. The aircraft also participates in co-operative experiments with other research agencies, in particular, the Summer Cumulus Investigation (see below). A second T-33 aircraft is used in a supporting role for these and other projects.

AIRCRAFT OPERATIONS

The Flight Recorder Playback Centre is engaged in the recovery and analysis of information from the various flight data recorders and cockpit voice recorders used on Canadian military and civil transport aircraft. The military systems are being monitored on a routine basis. Civil aircraft recorders are being replayed to investigate incidents or accidents at the request of the Ministry of Transport. Technical assistance is being provided during incident and accident investigations and relevant aircraft operational problems studied.

INDUSTRIAL ASSISTANCE

Assistance is given to aircraft manufacturers and other companies requiring the use of specialized flight test equipment or techniques.

INVESTIGATION OF SPRAY DROPLET RELEASE FROM AIRCRAFT

Theoretical and experimental studies on spray droplet formation and distribution are carried out. Flight experiments utilize a Harvard aircraft modified to carry external spray tanks. Automatic flying spot droplet and particle analysis equipment is in operation for processing samples obtained in the laboratory and in the field by various agencies. The equipment has potentialities for the analysis of many unusual configurations provided that these may be photographed with sufficient contrast.

AUTOMOBILE CRASH DETECTOR

There is a need for a sensing device to activate automobile passenger restraint systems in incipient crash situations. Investigations are in progress to determine the applicability of C.P.I. technology to this problem.

SUMMER CUMULUS INVESTIGATION

At the request of the Department of the Environment flight studies of Cumulus cloud formations over Quebec and Ontario were instituted during the Summer of 1974. Instrumented T-33 and Twin Otter aircraft with a Beech 18 are being used to determine the properties of Cumulus clouds which extend appreciably above the freezing level. The measurements are being made to assess the feasibility of inducing precipitation over forest fire areas by seeding large cumulus formations. During 1975 a variety of cloud physics instruments were added to the Twin Otter, and special pods for burning silver iodide flares were attached beneath the wing of the T-33 turbulence research aircraft. The effects of seeding on the microstructure of individual cumulus clouds were studied in the Yellowknife area during the summers of 1975 and 1976 and in Thunder Bay in 1977 and 1987. During the summer of 1979 the Twin Otter participated in similar flight experiments in Montana, jointly arranged by U.S. and Canadian government agencies.

FUELS AND LUBRICANTS LABORATORY

COMBUSTION RESEARCH

Investigation of handling and combustion problems involved in using hydrogen as a fuel for mobile prime movers.

Co-operative studies with Advisory Group for Aerospace Research and Development (AGARD) Working Group 11 to produce a report on aircraft fire safety.

Biogas as an alternate fuel in engine operation.

EXTENSION AND DEVELOPMENT OF LABORATORY EVALUATION

Development of new laboratory procedures for the determination of the load carrying capacity of hypoid gear oils under high speed conditions and under low speed high torque conditions.

Water separation characteristics of aviation turbine fuels.

PERFORMANCE ASPECTS OF FUELS, OILS, GREASES, AND BRAKE FLUID

Investigation of laboratory methods for predicting flow properties of engine and gear oils under low temperature operating conditions.

Evaluation of static dissipator additives for distillate fuels.

Evaluation of Properties of re-refined base oils and recycled industrial oils.

Properties of summer and winter unleaded motor gasolines.

Properties of Canadian, USA and USSR car journal box oils.

Road test of re-refined automotive oils (co-operation with Environment Canada).

Investigation of the use of anti-icing additive in aviation gasoline.

Investigation of hydrogen content as a means of estimating the combustion characteristics of aviation turbine fuels.

MISCELLANEOUS STUDIES

Investigation of the stability of highly compressed fuel gases.

Analytical techniques for analysis of engine exhaust emissions.

Participation in the Canadian (CGSB), American (ASTM) and International (ISO) bodies to develop standards for petroleum products and lubricants.

The design and development of an internal combustion engine/hydraulic transmission hybrid power plant for the energy conserving car.

Further developments of specialized pressure transducers for engine health diagnosis and the development of diagnostic techniques and consultation with licencee in developing production methods for patented transducers.

Evaluation of various products, fuels, lubricants and hardware in respect of their effects upon overall vehicle fuel economy and energy conservation properties.

GAS DYNAMICS LABORATORY

V/STOL PROPULSION SYSTEMS

A general study of V/STOL propulsion system methods with particular reference to requirements of economy and safety.

INTERNAL AERODYNAMICS OF DUCTS, DIFFUSERS AND NOZZLES

An experimental study of the internal aerodynamics of ducts, bends, diffusers and nozzles with particular reference to the effect of entry flow distortion is geometries involving changes of cross-sectional area, shape, and axial direction.

SHOCK PRODUCED PLASMA STUDIES

A general theoretical and experimental investigation of the production of high temperature plasma by means of shock waves generated by electromagnetic and gas dynamic means, and the development of diagnostic techniques suitable for a variety of shock geometries and the study of physical properties of such plasmas.

NON-DESTRUCTIVE SURFACE FLAW DETECTION IN HOT STEEL BILLETS

A flaw detection system for metal bars is being tested. Eight inductive bridge circuits, spaced around the bar and sequentially sampled, detect the flaw through a change in coil inductance. The system lends itself to easy elimination of stand-off and eccentricity errors and is currently being adapted to industrial use. Interpretation of test results via microprocessors is in hand. A rugged, heat-resistant circuit is being designed for in-plant application.

HARD SURFACE PLATING

The high temperature, high speed plasma flow generated by a high voltage, capacitive discharge in a pulsed plasma gun is used to melt and propel various powders in thermal spraying applications. Coatings obtained to date are similar to those applied with conventional means. The powder acceleration in the gun and impact on the substrate is presently being studied using a laser, with the aim of improving the process.

HIGH PRESSURE LIQUID JETS

High speed water jets generated by pressures in the range of 1000 to 60,000 psi can be used for cutting a wide variety of materials, e.g. paper, lumber, plastics, meat, leather, rock, etc., and for cleaning surfaces such as masonry, tubular heat exchangers, etc. Nozzle sizes, depending on the application, are in the range from 0.002 to 0.15 in. diameter. A technique for manufacturing small nozzles in the range 0.002 to 0.015 has been developed using standard sapphire jewels available from industry. Larger orifices are manufactured and polished using standard shop procedures.

At present, the following investigations are active in the laboratory:

1. Drilling of rocks of various types, including granite, using a high pressure rotating seal and single and dual orifice nozzles specially developed for this purpose.

2. Study of the effects produced by cavitating jets, how best to produce them and where they may be usefully applied.

3. Collaborative experimental work, in collaboration with the Low Temperature Laboratory, on the breaking and cutting of ice.

HEAT TRANSFER STUDIES

An investigation of methods of increasing boiling and condensing heat transfer coefficients by treatment of the heat transfer surface is in progress.

A co-operative project with the Division of Building Research will determine the usefulness of the thermosiphon as a ground heat source for a heat pump.

An inexpensive, leakproof heat exchanger has been developed for use in solar energy and heat pump systems. Fabrication is simple and it is suitable for production in small batches.

Work has started on a new type of temperature control thermosiphon. Previous types have been designed to control the temperature of a heat source; this design controls the temperature of a heat sink.

COMPUTATIONAL FLUID DYNAMICS

Numerical simulations are carried out in connection with projects initiated internally or as collaborations with outside organizations. Present studies involve problems of the absorption of laser energy by plasmas and the dynamics of plasmas under three dimensional magnetic compression. The main topics pursued currently are:

1. A study of the mechanism of re-entry waves occurring when beam intensity is reduced below the level at which laser-supported detonation can exist.

2. Absorption of laser energy by hydrogen plasma confined by a magnetic field (laser heated solenoid).

3. A study of the fluid mechanics accompanying continuous discharge of laser energy into a spot fixed in space.

4. Laser-initiation of a high-density Z-pinch.

5. Static and dynamic equillibria of plasma in a spherical θ-pinch device.

GAS TURBINE BLADING STUDIES

A theoretical and experimental study of the performance of highly loaded gas turbine blading has been undertaken as a collaborative program with industry and universities.

INDUSTRIAL PROCESS, APPARATUS, AND INSTRUMENTATION

There is an appreciable effort, on a continuing basis, directed towards industrial assistance. This work is of an extremely varied nature and, in general, requires the special facilities and capabilities available in the laboratory.

Current and recent co-operative projects with manufacturers and users include:

(a) Flow problems associated with industrial gas turbine exhaust systems (Foster Wheeler).
(b) *Combustion studies for industrial gas turbine applications (Westinghouse and Rolls-Royce).*
(c) Application of thermosiphon as an energy conserving device in industrial applications (Dept. of Agriculture, Ministry of Transport, Farinon Electric, Chromalox Canada Ltd).
(d) Scaled model studies on steel and copper converters to establish relative performance and ceramic liner deterioration rates (Canadian Liquid Air and Noranda).
(e) High pressure water jet applications in industry (High Pressure Systems Ltd.).
(f) Scaled model studies to establish the performance of complex industrial flue systems with a view to establishing specific design and performance criteria. (Noranda and Inco Canada Ltd.).
(g) Model studies of internal flows in reactor hood and waste heat boiler (Noranda and Kennecott Copper Corp.).
(h) *Altitude test chamber for small gas turbines (Pratt & Whitney Aircraft of Canada Ltd.).*
(i) Experimental study of a novel fan design (Rolls-Royce).

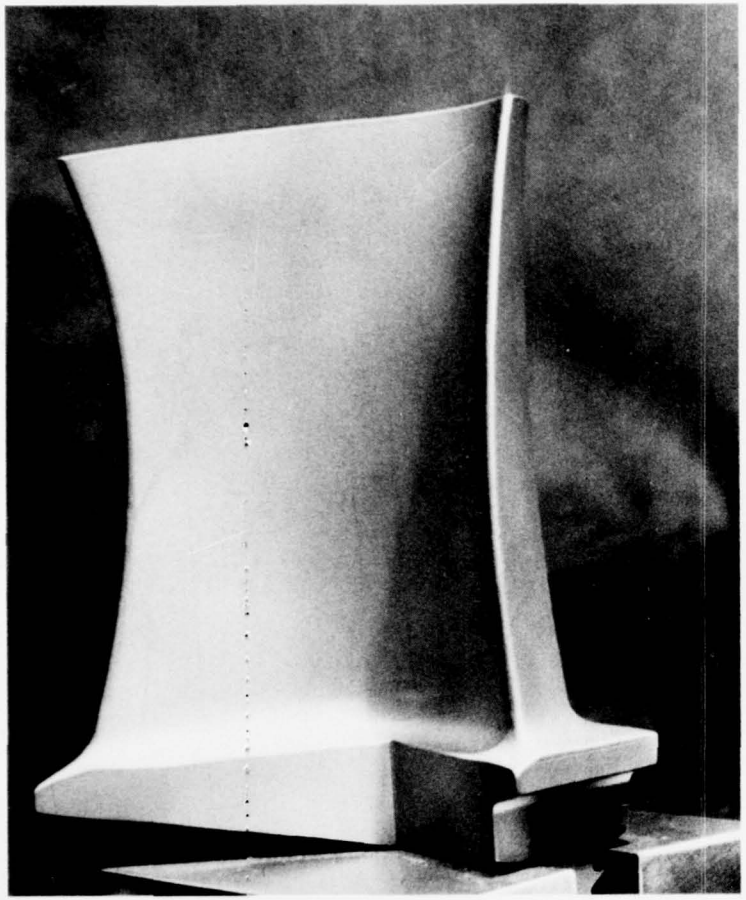

TURBINE BLADING ASSOCIATED WITH JOINT NRC/PRATT AND WHITNEY AIRCRAFT OF CANADA
HIGHLY LOADED TURBINE INVESTIGATION

GAS DYNAMICS LABORATORY AND ENGINE LABORATORY

DIVISION OF MECHANICAL ENGINEERING

HIGH SPEED AERODYNAMICS LABORATORY

DATA SYSTEM IMPROVEMENTS ON 5-FT. X 5-FT. WIND TUNNEL

Installation of the new PDP 11/t55 based data acquisition system is now nearing completion and the first live test using the system will be done early this autumn. All components are in place and interconnected, and simulation testing with hardware is well advanced. Replacement software for various 'quick-look' programs has been written, with improved flexibility. An automatic amplifier calibration process is installed and tested.

A total of up to 96 analog channels (48 high quality and 48 lower quality) will be available, with switch selected gains of 1 to 5000 and front end filters of 3 Hz to 10 kHz. "Status" channels will be digitized at source and packed to minimize data volumes.

Data conversion throughputs have been demonstrated at 40 kHz average, with bursts of 100 kHz rates through 2 15-bit A/D converters simultaneously.

Real-time tunnel control, model attitude and data acquisition tasks will be performed in the same processor through software, utilizing tables prepared in advance to define the various operations required.

Progress toward on-line data reduction is proceeding.

CALIBRATION OF THE SUBSONIC AND TRANSONIC TEST SECTIONS OF THE 5-FT. X 5-FT. BLOWDOWN WIND TUNNEL

In addition to the calibration measurements and results reported in QB 1979(1), further measurements have been made in the transonic and subsonic test sections to assess the flow quality.

These were effected with an instrumented cone, loaned by N.L.R., Amsterdam. The cone was equipped with 14 responsive Kulite pressure transducers mounted at intervals of 15 and 25 mm along 340 mm of the cone surface. One side of each transducer was closely connected to the surface and able to respond to pressure fluctuations in the boundary layer up to nearly 10 kHz.

Discrete high frequency peaks which varied almost linearly with Mach number (5.75 kHz at M = 0.6, 7.8 kHz at M = 1.2) were noticed in transonic test section runs. These are believed to be the 'edge tones' as generated by the porous walls.

For the transonic test section, in the range $0.5 \leq M \leq 1.2$, the foremost transducer indicated a noise level that, in terms of C_p rms, varied with M from about 0.75% at M = 0.5, rising to 1.3% at M = 0.7 and falling to 0.6% at M = 1.2. A slight Reynolds number effect was noted, the tendency being for C_p rms to increase by 0.1 to 0.2% as the unit Reynolds number increased from 16×10^6 to 26×10^6 per metre. While the edge tones were responsible for the largest contribution to the overall noise level (about 50%) a significant content, up to 38% of the total, is due to frequencies below 1 kHz.

The subsonic test section exhibited the highest noise at M = 0.3 (1.2%) but increasing Mach numbers reduced the value to little more than 0.5% for $0.5 \leq M \leq 0.8$. Low frequency contents (below 1 kHz) contributed to the majority of the overall noise level (62%–79%). The Reynolds number influence was very small for this test section.

CALIBRATION OF TRANSONIC SECTION IN HALF-MODEL GEOMETRY

Calibration of the empty transonic 5-ft X 5-ft. section in half-model geometry is completed. Static pressure measurements along the ceiling, floor and reflection plate were made at three stagnation pressures in the Mach number range $0.3 < M < 0.99$. Preliminary results indicate that in the region extending 10 inches forward and aft of the balance centre there is little or no Mach number gradient and little or no difference between the static pressures measured in the plenum chamber and in the working section.

TRANSONIC EQUIVALENCE RULE INVOLVING LIFT

The classical area rule is well known and its application to wing-body design and drag reduction is demonstrated on many existing aircraft. Recent advances in transonic aerodynamic theory show that the classical area rule requires a modification to account for lift. A series of experiments is being prepared in order to investigate these new concepts. The results of these experimental studies will provide criteria for wing-body design with emphasis on drag reduction for aircraft cruising at transonic speeds. In conjunction with the experimental studies, computational methods are being developed to calculate the flow field around slender aircraft with lift at transonic speeds.

TWO-DIMENSIONAL TRANSONIC FLOW STUDIES

The small disturbance transonic computer program, developed for free air isolated airfoils, has been extended to include porous wall effects in the wind tunnel.

STUDIES OF WING BUFFETING

A theoretical study of the transient response of a wing to non-stationary buffet loads is in progress. Various forms of the power spectral density of the aerodynamic loading on the wing have been considered for a number of load versus time history during buffet manoeuvres. A wind tunnel investigation of the surface pressure and normal force fluctuations associated with buffeting has been carried out on the BGK No. 1 airfoil.

REYNOLDS NUMBER EFFECTS ON TWO-DIMENSIONAL AEROFOILS WITH MECHANICAL HIGH LIFT DEVICES

Under a joint NRC/de Havilland enterprise administered under the PILP program an extensive set of low speed aerodynamic measurements were made in the 2-D insert in the period September 26 – November 30, 1978, on a multi-component aerofoil model.

During the first phase of the work several trailing-edge flap geometries (with and without a leading-edge slat) were optimized at a chord Reynolds number of 6×10^6; subsequently their performance at lower and high Reynolds numbers were checked.

In a second phase of tests with this aerofoil some boundary layer measurements were made near the trailing-edge of the main element, utilizing a new boundary-layer traversing rig. These latter measurements were primarily directed at checkout of the traversing rig in its simplest form, with the objective of developing reliable gear for more extensive boundary layer measurements on high lift multi-component aerofoils in the near future.

Since these measurements were taken, the traversing rig has been modified to allow measurements to be made at more chordwise stations. A test program is planned for late 1979 involving the above-mentioned multi-component aerofoil.

HOLE ERROR INVESTIGATION

An experimental study has been completed, in collaboration with Professor J.C. Menneron, of the University of Sherbrooke, of the effect of orifice size on the measurement of pressure on the surface of an aerofoil at subsonic free-stream velocities. Speeds up to $M = 0.7$ and chord Reynolds number from 6×10^6 to 33×10^6 were used. Orifice diameters range from 0.006 in. to 0.016 in. Analysis of the data clearly indicates that the value of the chordwise force coefficient, obtained by integration of the surface pressure, consistently increases with the size of the orifice. The effect is rather more pronounced at $M = 0.5$ and 0.7 than at $M = 0.3$.

HYDRAULICS LABORATORY

ST. LAWRENCE SHIP CHANNEL

Under the sponsorship of the Ministry of Transport, a study to improve navigation along the St. Lawrence River, using hydraulic and numerical modeling techniques.

NUMERICAL SIMULATION OF RIVER AND ESTUARY SYSTEMS

Mathematical models have been developed to simulate tidal propagation in estuaries, wave refraction in shallow water and littoral drift processes. The feasibility of using array processors to solve the hydrodynamic equations is presently under study.

WAVE FORCES ON OFF-SHORE STRUCTURES

Wave flume study to determine design criteria for off-shore structures, such as cooling water intakes or outfalls, mooring dolphins, drilling rigs, etc.

RANDOM WAVE GENERATION

A study of random waves generated in a laboratory wave flume by signals from a computer. Special attention is paid to the simulation of wave groups.

STABILITY OF RUBBLE MOUND BREAKWATERS

A flume study for the Department of Public Works to determine stability coefficients of armour units and the effect of a number of wave parameters on the stability of rubble mound breakwaters, including the effect of wave grouping.

WAVE LOADS ON CAISSON TYPE BREAKWATERS

A flume study for the Department of Public Works to determine the overall loading, as well as the pressure distribution on various Caisson-type breakwaters.

WAVE POWER AS AN ENERGY SOURCE

A general study to assess the wave power available around Canada's coast and to evaluate various proposed schemes to extract this energy. International co-operation is taking place through the International Energy Agency of OECD.

MOTIONS OF LARGE FLOATING STRUCTURES, MOORED IN SHALLOW WATER

A mathematical and hydraulic modeling program will be carried out to develop techniques and methods to forecast motions of, and mooring forces on large structures moored in shallow water.

CALIBRATION OF FLOW MEASURING DEVICES

Facilities to calibrate various types of low meters up to a maximum capacity of 5,000 gpm are regularly used for/or by private industry and other government departments.

FIFTY MILE POINT MODEL STUDY

A hydraulic model study for Public Works, Canada of the Fifty Mile Point Marina on Lake Ontario, to investigate various layouts of breakwaters to minimize the level of wave agitation inside the basin.

TRANSPORT OF SAND ON BEACHES

A method has been developed for calculating rates of sand transport in the presence of waves, a modification of the Ackers and White method for river flows. A new flume was recently constructed in which the method can be tested.

LOW HEAD WATER TURBINES

A research program has been started to investigate the feasibility of extracting power from water currents, by using low head turbines.

HYBRID MODELING TECHNIQUES USING ARRAY PROCESSORS

Estuaries where tidal power can be developed require the use of large physical models of the area. The laboratory has demonstrated that a "hybrid model" can dynamically couple together a mathematical model to the physical model at the boundaries, therefore the physical model need not be very large in extent. An array processor will be used to realize the mathematical portion of the hybrid model.

LOW SPEED AERODYNAMICS LABORATORY

WIND TUNNEL OPERATIONS

The three major wind tunnels of the laboratory are the 15-ft. diameter open jet vertical tunnel, the 6-ft. X 9-ft. closed jet horizontal tunnel and the 30-ft. X 30-ft. V/STOL tunnel. During the quarter, a number of test programs were carried out for groups both within and outside the government. Within the government, test programs included studies on building aerodynamics and transport trucks. Studies for non-government groups included the aerodynamics of road vehicles, two aircraft models, a horizontal axis and a vertical axis windmill and an aircraft insecticide spray-boom system.

Software development is continuing for the new data acquisition, reduction and control system for the 6-ft. X 9-ft. wind tunnel.

WIND ENGINEERING

In collaboration with the Division of Building Research, an aerodynamic investigation of Commerce Court, Toronto is being undertaken. The purpose is to obtain wind tunnel comparisons with full-scale measurements of surface pressures and building movements. Motion response measurements on a 1:200 scale aeroelastic model have now been completed in the 9 m X 9 m wind tunnel. Surface pressure measurements were completed earlier. A series of six 1:10 scale truck models designed and constructed to continue NRC's program in truck energy conservation through aerodynamic drag reduction and in support of a joint NRC/ Transport Canada – DOT/SAE (U.S.A.) wind tunnel testing program. Comparative testing has been completed in the NAE 2 m X 3 m wind tunnel and at the University of Maryland and the California Institute of Technology. In the next quarter the program will be completed with testing in the General Motors Research wind tunnel and at Purdue University.

Measurements of wind properties are being continued on the Lions Gate Bridge, Vancouver as part of an aerodynamic investigation of the bridge. Outputs from five anemometers and two accelerometers that measure bridge motion are recorded by an automated system. Site assistance is being provided by Buckland and Taylor Limited, Vancouver.

Wind measurements are continuing at the site of an ore conveyer bridge crossing the Similkameen river valley in British Columbia. The proposed conveyer bridge was wind tunnel tested at NAE in Dec. 1978 and Jan. 1979 for Buckland and Taylor Ltd.

A study of street level winds in the downtown core of the City of Ottawa is underway. The first phase will establish a probability distribution of the existing wind climate and the second phase will be the simulation of the wind conditions using a 1:400 scale model in the NAE 30-ft. X 30-ft. wind tunnel. The study is jointly sponsored by the City of Ottawa, the Department of Public Works, the National Capital Commission and the National Aeronautical Establishment. A contract for the construction of remote wind sensing units has been let and a PDP 11/03 micro system has been received. Construction of the wind tunnel model has been completed and the first series of wind tunnel tests was begun.

Development work on a novel surface mounted device for measuring street level winds on city model was carried out in the 3-ft. X 3-ft. wind tunnel. The device connects to a pressure transducer and scanivalve and allows street level winds to be measured rapidly at a large number of locations.

Experimental work on the effect of turbulence on the flutter instability of a 1:110 scale bridge sectional model was completed in the 3-ft. X 3-ft. wind tunnel.

FLUIDICS

Co-operative studies with D.G. Instruments of a 3-axis velocity sensor are continuing using both NRC and industry developed concepts. Studies of vortex excitation of velocity sensor probes have been carried out in co-operation with Fluidynamics Devices Ltd. A program of applications of laminar flow in thin passages is being carried out in co-operation with the Control Systems and Human Engineering Laboratory of DME.

VERTICAL AXIS WIND TURBINE

In July 78, the rotor of the 230-kW demonstrations wind turbine on the Magdalen Islands collapsed while the drive train was undergoing maintenance. An investigation of the causes of the accident uncovered no basic flaw in its design or construction. Therefore, it was decided to rebuild it. A new rotor has been installed and the turbine is expected to be in operation by end of October. Two 50 kW wind turbines were installed (in 1978) and connected to local power networks in Newfoundland and Saskatchewan. The Newfoundland turbine has been in operation for over a year. The turbine in Saskatchewan suffered a bearing failure last summer and is being repaired.

Two more 50 kW turbines are on order for delivery early 1980. One of these will be operated in Churchill, Manitoba and the other near Victoria, British Columbia.

Twenty wind speed measurement and recording systems have been ordered. These systems will be installed at possible future sites for wind turbines identified by utility companies – to better assess the wind power potential of these sites.

LOW TEMPERATURE LABORATORY

THERMAL PROTECTION OF TRACK SWITCHES

The use of heat to eliminate switch failures from snow and ice is a standard approach to this problem. Work has been carried out on improving the efficiency of forced convection combustion heaters and the means of distributing heat to the critical areas of a switch.

HORIZONTAL AIR CURTAIN SWITCH PROTECTOR

A non-thermal method of protecting a switch from failure due to snow has been undergoing development and evaluation. This method consists of high velocity horizontal air curtains designed to prevent the deposit of snow in critical areas of a switch. The tests conducted to date are especially encouraging with respect to yards and terminals. Additional evaluation is required for the line service application.

NEW RAILWAY SWITCH DEVELOPMENT

The ultimate solution to the existing problem of snow and ice failure of the point switch would appear to be replacement by a new design that is not subject to failure in this way. A switch has been designed, fabricated, laboratory tested and has now completed one winter season of field trials. The design involves only shear loading from snow and ice.

MISCELLANEOUS ICING INVESTIGATIONS

Analytical and experimental investigations of a non-routine nature, and the investigation of certain aspects of icing simulation and measurement.

TRAWLER ICING

In collaboration with Department of Transport, an investigation of the icing of fishing trawlers and other vessels under conditions of freezing sea spray, and of methods of combatting the problem.

AIRBORNE SNOW CONCENTRATION

To provide statistical data on the airborne mass concentration of falling snow in order to define suitable design and qualification criteria for flight through snow, measurements of concentration and related meteorological parameters are being made.

SEA ICE DYNAMICS

Analytical and experimental work on the techniques of forming low-strength ice from saline solutions is being carried out in connection with proposed modeling studies of icebreaking ships and arctic port facilities.

An investigation is being made into the modeling of sea ice based on the freezing of aqueous solutions. The objective of the investigation is to improve the dynamic similarity in model testing in simulated sea ice.

LOCOMOTIVE TRACTION MOTORS

An investigation into the failure of locomotive traction motor support bearings due to winter service has been undertaken. The presence of moisture either as water or ice in the oil reservoirs is suspected to be a contributing cause of the failures.

HIGH PRESSURE CUTTING OF ICE

Experimental work is being carried out in collaboration with Gas Dynamics personnel on the cutting of ice with high pressure water jets. One phase of this work has been concerned with the removal of ice from a substrate such as concrete. The other work on ice cutting has been for possible application to ice breaking ships.

MARINE DYNAMICS AND SHIP LABORATORY

HULL FORM SERIES FOR FAST SURFACE SHIPS

A series of 24 designs has been developed to enable the effects of changing beam, draught, and block and waterplane area coefficients to be determined for hull forms of frigates and for fast patrol vessels. Models have been made of 10 of these designs and are split amidships which enables the effect of changing the bow to be investigated on each of the sterns and vice versa.

Resistance, propulsion and seakeeping tests have been carried out with 10 models from the series, and the results analyzed to determine trends of performance with variation in hull form parameters.

An additional model, made by combining the bow of one, with good seakeeping characteristics, with the stern of one with good calm water performance, was tested. This proved to have good overall performance and the combined hull was selected as the basis of a practical frigate design.

LOCK MODEL STUDY – EXTENSION

The second series of model tests for the St. Lawrence Seaway Authority into the effect of vessel size and lock geometry on lock transit times in the Welland Canal has been analyzed and reported. These studies are in direct support of a prototype marine shunter trials program currently being carried out by the Seaway Authority.

COMBINATION FISHING VESSEL

Model tests carried out last year on a new design of 70 ft. West Coast combination salmon and herring fishing vessel have been extended in order to define more comprehensively its safety against capsize in waves. Parameters investigated were ship displacement, initial stability condition, wave height, wave length, ship speed and relative wave direction.

These additional experiments, carried out in the 130 m X 65 m X 3.5 m seakeeping and manoeuvring basin using a radio-controlled free-running model, are in support of a current move internationally to place the subject of vessel capsize on a more scientific footing.

65 FT. EAST COAST FISHING VESSEL

The laboratory is currently investigating whether increase in the beam of small fishing vessels, which has advantages for deck working, leads to any deterioration in seakeeping qualities.

Beam wave rolling experiments have indicated that the use of passive anti-rolling tank stabilization is not altogether suitable for this class of vessel. Conventional bilge keels suffer from ice damage so the possible use and effectiveness of bottom keels is being investigated.

SWATH MANOEUVRING INVESTIGATION

A model of a Small Waterplane Area Twin Hull (SWATH) vessel has been constructed in the laboratory. An investigation into the effect of rudder position on its manoeuvrability is to be carried out using this radio-controlled free-running model in the laboratory's large manoeuvring basin.

AIRCRAFT DITCHING CHARACTERISTICS

In order to comply with Federal Air Regulations, it is necessary to carry out model ditching tests for the aircraft considered.

The work entails launching a dynamically scaled model of the aircraft into free flight over water and recording its behaviour, including structural factors, as it lands on the water surface. Ditching tests are required for a range of glide approach path angles, flap settings and aircraft altitudes, the object being to determine the optimum approach conditions for safe ditching. To this end the laboratory is making the necessary final preparations for a series of experiments for a particular aircraft design.

RUDDER-FORCED ROLLING

Model studies are being carried out to determine the frequency response in roll and yaw motion to sinusoidal oscillation of the rudder of a self-propelled radio-controlled model of an existing frigate form. The object of this work is twofold:

AD-A082 059 NATIONAL RESEARCH COUNCIL OF CANADA OTTAWA (ONTARIO) --ETC F/G 13/6
QUARTERLY BULLETIN OF THE DIVISION OF MECHANICAL ENGINEERING AN--ETC(U)
SEP 79

UNCLASSIFIED DME/NAE-1979(3) NL

2 OF 2
AD
A082059

END
DATE
FILMED
4-80
DTIC

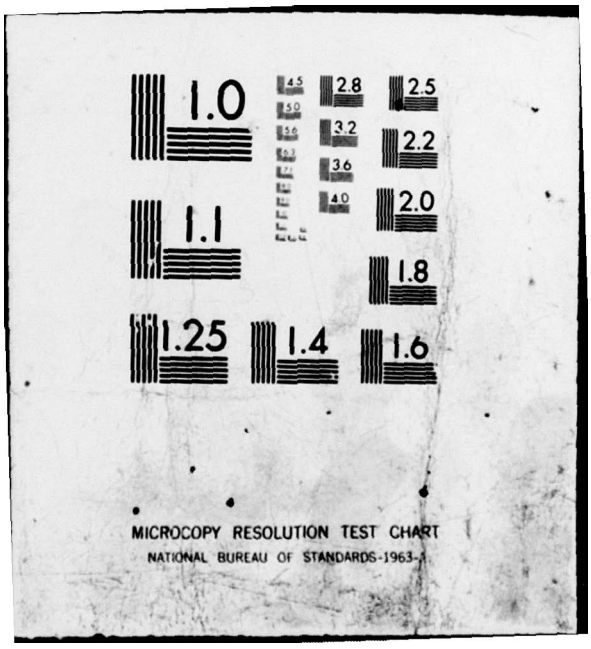
1.0
1.1
1.25
1.4
1.6
1.8
2.0
2.2
2.5
2.8
3.2
3.6
4.0
4.5
5.0
5.6
6.3
7.1
MICROCOPY RESOLUTION TEST CHART
NATIONAL BUREAU OF STANDARDS-1963-A

(i) Data on the roll and yaw motions induced by rudder movement in calm water may be used to determine the effectiveness of the rudder as a roll stabilizing device in rough water, in addition to its normal role as the primary steering device.

(ii) By carrying out experiments both with and without the controlled U-tube type roll stabilizer in operation, the effectiveness of this installation, which was previously investigated at zero ship speed, may be determined over a range of ship speeds.

The results of these studies are to be compared with some equivalent full scale data.

LNG CARRIER

The overall economic performance of a proposal to carry LNG from the Arctic to the Eastern Seaboard depends, among many other factors, on having ships which are as cheap to operate as possible. The hull form must offer a minimum of resistance, and the flow to the propeller be as uniform as possible.

To achieve these goals, experiments with a model of a proposed LNG ship are being made in the laboratory. The program includes resistance, self-propulsion, wake survey and overload experiments.

RAILWAY LABORATORY

YARD EXPERIMENTS

At the request of the Department of National Defence, impact tests to simulate classification yard conditions are being conducted to evaluate methods of securing heavy military vehicles to a flat car. Results are being analyzed and a report will be prepared.

FIELD EXPERIMENTS

Two bridges are being strain gauged in the Roger's Pass at the request of CP Rail.

Assistance and equipment have been loaned to CP Rail for the purpose of pinpointing where automobiles become damaged in transit on a tri-level car.

Assistance and equipment have been loaned to CP Rail for printing out the angle each axle in a train makes with the normal to a curve, as the train passes a point.

LABORATORY FACILITIES FOR RAILWAY RESEARCH

High pressure oil lines for the rail car shaker, track support and actuator attachment system for lateral vibration have been designed and installation has commenced. Instrument Rail Car 62 is now ready for single shift field trips. Sleeping and eating facilities will be added as time permits.

Work on the NRC curved track simulator continues in the Manufacturing Technology Centre with the testing of the differential drive gear units and the design of the curve control position levers.

In collaboration with the Analysis Laboratory, work continues on a mathematical model of the curved track simulator. In particular, the wheel-roller interaction phenomenon is being studied.

Studies are being conducted on a rail axle set having independently rotating wheels with regard to stability and curving.

The Laboratory is co-operating with VIA Rail to carry out the quality test program associated with the rail diesel car modernization scheme.

GENERAL INSTRUMENTATION

The Laboratory, in co-operation with the Marine Dynamics and Ship Laboratory, has built a micro-processor based ship's motion analyzer. An assessment of the analyzer on board an ocean ship will be made in the Spring of 1981.

A non-contacting transducer is being developed to measure speed and displacement of ferro-magnetic surfaces by correlating two magnetic noise signals.

An instrumented locomotive wheelset for measuring vertical and lateral rail/wheel forces in service is being developed for Transport Canada Research and Development Centre. Strain gauging, wiring, and calibration of the vertical and lateral force bridges on each wheel have been completed. Spin tests and check out of the telemetry is under way.

A commercial desktop calculator-computer with CRT display, high speed printer, and plotter have been added to our fast fourier transform set up to further enhance our data processing capabilities.

Mechanical gauging tools have been built to measure wheel and centre plate wear for CP Rail.

TECHNICAL PHOTOGRAPHY

Besides services to the Mechanical Engineering Division Laboratories, assistance was given to the Division of Physics using stills and high speed movies.

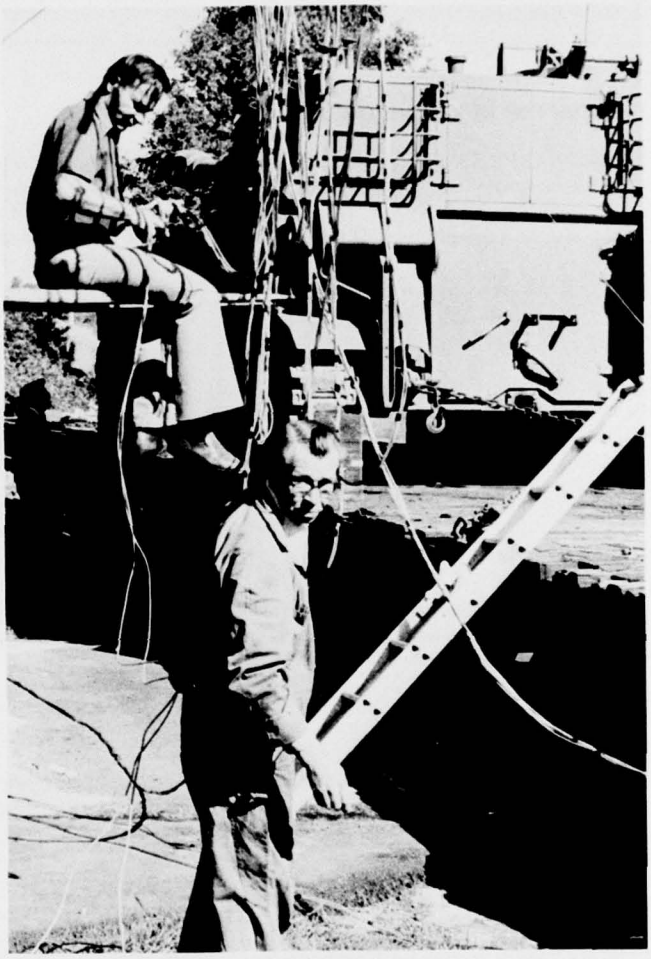

MESSRS. WATSON AND WEATHERSTON PREPARING LOAD CELL INSTRUMENTATION FOR VEHICLE TIE DOWN ASSESSMENT FOR THE CANADIAN ARMED FORCES AND THE CANADIAN RAILROADS

STRUCTURES AND MATERIALS LABORATORY

MOTOR VEHICLE SAFETY

In collaboration with the Road and Motor Vehicle Traffic Safety Branch of Transport Canada the second phase of the studies evaluating headlamp performance is underway. Attention is focussed on the determination of population characteristics of headlamps presently in use. Mean illuminance and glare quandrant values together with data describing the influence of dirt, aim and voltage for a large sample of vehicles are being analyzed within the previously defined system's concept.

VIDEO PHOTOGRAMMETRY SYSTEM FOR REAL TIME THREE-DIMENSIONAL CONTROL

Potential applications for an NRC/NAE 30 Hz Video Photogrammetry System developed for three-dimensional machine control tasks are being examined. The system is based on the principle that knowledge of the centroid data for four targets on a rigid body permits the single camera photogrammetric solution to be solved for each video frame to determine the position and orientation of the body, in real time, for three-dimensional machine control. Initial applications will focus on remote manipulator systems.

METALLIC MATERIALS

Structure-property relationships in aerospace alloys, including cast or wrought nickel and cobalt-base superalloys, high strength titanium and aluminum alloys. Studies on the consolidation and TMT processing of titanium and superalloy compacts by hot isostatic pressing, isothermal and superplastic forging, and extrusion. Studies on the mechanical properties of these materials. The mechanics of cold isostatic compaction of metal powders, and properties of hydrostatically extruded materials. Studies of the oxidation/hot corrosion behaviour of coated and uncoated refractory metals and superalloys.

FRACTOGRAPHY AND FAILURE ANALYSIS

Utilization of transmission and scanning electron microscopes in the study of fracture surfaces, leading to the identification of *the micromechanisms of fracture involved in the failure of structural components.* From such information it is frequently possible to determine the causes of failures and to suggest remedial action.

FATIGUE OF METALS

Studies of the basic fatigue characteristics of materials under constant and variable amplitude loading; fatigue tests on components to obtain basic design data; fatigue tests on components for validation of design; studies of the statistics of fatigue failures; development of techniques to simulate service fatigue loading.

OPERATIONAL LOADS AND LIFE OF AIRCRAFT STRUCTURES

Instrumentation of aircraft for the measurement of flight loads and accelerations; fatigue life monitoring and analysis of load and acceleration spectra; full-scale fatigue testing of airframes and components. Non-destructive testing and damage tolerance evaluation.

THEORY OF STRUCTURES

Studies of the application of finite element methods to structural problems. Assessment of commercially available computer programs for structural analysis. Calculation of stress-intensity factors for cracked three-dimensional bodies. Damage tolerance analysis.

AEROACOUSTICS

Studies of aerospace-related acoustical problems with special reference to intense noise and its effect on structures. Evaluation of aerospace hardware in intense noise. Studies of jet exhaust noise, wind-tunnel noise, techniques for digital signal processing, enhancement of signals obscured by noise.

FLIGHT IMPACT SIMULATOR

Simulator developed and calibrated to capability of accelerating a 4-lb. mass to a velocity of 1000 ft./sec., and an 8-lb. mass to a velocity of 760 ft./sec. Available to Canadian and Foreign manufacturers for certification of aircraft components and structures. Also used for fundamental studies of the impact process and evaluation of transparencies.

CALIBRATION OF FORCE AND VIBRATION MEASURING DEVICES

Facilities available for the calibration of government, university, and industrial equipment include deadweight force standards up to 100,000 lb., dynamic calibration of vibration pick-ups in the frequency range 10 Hz to 2000 Hz.

NON-METALLIC COMPOSITE MATERIALS

Studies of non-metallic composites including resins, cross-linking compounds, polymerization initiators, selection of matrices and reinforcements, application and fabrication procedures, material properties, and structural design.

POLICE EQUIPMENT STANDARDS

The NRC/CACP Technical Liaison Committee on Police Equipment is a bilateral arrangement for bringing together police and government personnel to review police equipment requirements, equipment performance specifications, and conformance testing procedures. Work of the Committee is expedited by a permanent Secretariat which has a primary responsibility for continuity in the activities of a number of Sections, each dealing with a particular area of expertise, and for co-ordinating work and specialist contributions from various participating Departments and organizations.

UNSTEADY AERODYNAMICS LABORATORY

DYNAMIC STABILITY OF AIRCRAFT

Measurement of direct, cross and cross-coupling stability derivatives due to roll oscillation.

Development of a translational-oscillation apparatus.

Vertical acceleration experiments.

Measurements of cross-coupling derivatives at high angles of attack.

Development of hydraulic drive systems for high-load oscillatory apparatuses.

Development and construction of new, fully-digital instrumentation system for dynamic experiments.

ATMOSPHERIC DISTRIBUTION OF POLLUTANTS

Instrumentation of a small mobile laboratory to measure airborne particulates and of an aircraft to detect atmospheric tracers.

Analysis of the downwind vertical spread and turbulent deposition of gaseous and aerosol pollutants from sources near the ground, with special emphasis on the effect of droplet evaporation.

Determination of long-distance drift of tracer chemical from a discrete spray, in New Brunswick.

TRACE VAPOUR DETECTION

Development of highly sensitive gas chromatographic techniques for detection of trace quantities of vapours of pesticides, explosives and fluorocarbons.

Sensitivity evaluation of commercially available explosive detectors.

Development of stopped-flow and continuous-flow vapour concentrators.

Testing of biosensors.

Development and construction of a portable explosives vapour detector.

WORK FOR OUTSIDE ORGANIZATIONS

Damping and cross-coupling experiments for NASA.

Feasibility and design studies for NASA.

Aircraft-security feasiblity studies and development projects for Transport Canada.

Feasibility studies for DSMA, Toronto.

Experimental assistance to RCMP.

Field experiments in New Brunswick for Forest Protection Ltd., Fredericton.

WESTERN LABORATORY (VANCOUVER)

PRACTICAL FRICTION AND WEAR STUDIES

Laboratory simulations of practical tribological systems to study friction, wear and lubrication behaviour of lubricants and bearing materials in response to specific external requests. For example a study of the galling resistance of unlubricated metal–metal pairs under high load, low speed sliding conditions has just been completed.

FUNDAMENTAL STUDIES IN TRIBOLOGY

Assembly of the laboratory rail-wheel wear simulator has been completed and calibration procedures and preliminary test runs are now being carried out. Initially the emphasis of the work will be on establishing correlations with field results and then studies of material and lubricant effects will be undertaken.

LUBRICANTS

Mechanical testing of both solid and liquid lubricants has been carried out at the request of local industry and utility organizations.

BEARINGS

The laboratory study of the wick lubrication of locomotive traction motor bearings has been continued. It has been shown that the wick not only supplies oil to these bearings, but also recirculates the oil already in the bearings. This fact explains the low oil consumption of these bearings as well as their capability to operate at temperatures below the pour point of the oil.

Investigations have been made of the surface characteristics of fibre composite bridge bearing pads removed from service because of severe stick-slip friction problems.

INSTRUMENTATION

Calibration of load cells has been completed for the rail/wheel wear test rig. While assembly is still under way for many of the computer control system interfaces to be incorporated later, the instrumentation system is nearing readiness for the first set of tests on the apparatus.

NUMERICALLY CONTROLLED MACHINING

Technical assistance on this subject is being provided to firms and other institutions in Western Canada which are considering the purchase of numerically controlled machines to improve their production efficiency. Seminars are held to explain the fundamentals of numerical control and programming.

Use is being made of computer-assisted programming and punched-tape preparation as a means of reducing manual programming time for items requiring a large number of geometrical statements. Seminars are held to demonstrate the principles and features of this method of NC part programming. This technique is being used to assist new users of NC equipment to get their equipment quickly into production.

APPROPRIATE TECHNOLOGY

The laboratory has recently been monitoring the progress of this new technological movement towards smaller scale, environmentally and socially appropriate decentralized industrial development. The laboratory has been examining the technical aspects of a number of possible small scale processes, e.g. the operation of gas or diesel generators on wood-gas on which research work might be undertaken.

LOW TEMPERATURE TEST FACILITY

The low temperature (–45°C) test chamber has been used by a manufacturer of cable TV equipment to test line amplifiers at low temperatures and for the low temperature lubrication tests on traction motor bearings.

PUBLICATIONS

LABORATORY TECHNICAL REPORTS

National Aeronautical Establishment

LTR-HA-38 Lee, B.H.K.

A Theoretical Study of the Response of a Wing to Quasi-Stationary Correlated Noise Inputs.
May 1979.

LTR-HA-41 Lee, B.H.K.

Multi-Modal Response of a Wing to Non-Stationary Loads Using a Time Segmentation Technique.
June 1979.

LTR-UA-51 Orlik-Rückemann, K., Hanff, E.S., Anstey, C.R., Kapoor, K.B.

Conceptual Design Study of Equipment for Dynamic Stability Testing in a Large "Trisonic" Wind Tunnel.
June 1979.

Division of Mechanical Engineering

LTR-AN-37 Costandi, D.

A Set of FORTRAN Function Generation Subroutines.
July 1979.

LTR-AN-38 Amyot, J.R., Costandi, D.

FORTRAN Subroutines for the Computation of Steady Flow Fluid Resistance in Pipes, Valves and Fittings.
September 1979.

LTR-GD-56 Williamson, R.G., MacDonald, C.

Calibration of the Effect of Reversed Installation on a Series of Flow Measuring Orifices.
July 1979.

LTR-HY-66 Funke, E.R., Mansard, E.P.D.

Synthesis of Realistic Sea States in a Laboratory Flume.
August 1979.

LTR-LT-99 Coveney, D.B.

Cutting Cold River Ice with Water Jets During the Winter 1977-78.
June 1979.

LTR-LT-100 Lane, J.F., Morris, D.E.

Traction Motor Suspension Bearing Leakage Tests – Phases I and II.
July 1979.

LTR-LT-101 Coveney, D.B.

Water Jet Cutting of Cold Fresh Water Ice in a Laboratory Ice Tank.
August 1979.

LTR-LT-102 Coveney, D.B.

Cutting Simulated Sea Ice with Water Jets in the Laboratory.
August 1979.

LABORATORY TECHNICAL REPORTS (Cont'd)

Division of Mechanical Engineering (Cont'd)

LTR-LT-103 Timco, G.W.

Mechanical Strength of Ice Grown from an Impure Melt.
August 1979.

LTR-LT-104 Lane, J.F.

On the Strengths of Sea Ice and a Correlation Between the Various Strength Tests.
September 1979.

LTR-WE-17 Hawthorne, H.M., Lau, R.

The Comparative Galling Resistance of Various Metal Couples.
September 1979.

MISCELLANEOUS PAPERS

Dalgliesh, W.A.*, Templin, J.T.*, Cooper, K.R. Comparisons of Wind Tunnel and Full-Scale Building Surface Pressures with Emphasis on Peaks. Proceedings Fifth International Conference on Wind Engineering, Colorado State University, Fort Collins, Colorado, 8-14 July 1979.

Deneeve, P.F.W.**, Dukkipati, R.V. A Procedure for Axial Blade Optimization. Transactions of the ASME, Journal of Engineering for Power, Vol. 101, No. 3, pp. 315-320, July 1979.

Dukkipati, R.V., Sankar, S.***, Osman, M.O.M.*** On the Use of Complex Method of Constrained Optimization in Linkage Synthesis. Presented at the Fifth World Congress on the Theory of Machines and Mechanisms, July 8-13, 1979, Montreal, Québec. Published in Proceedings Vol. 1, pp. 382-388.

Foster, L.R., Hanff, E.S. A Second Generation Instrumentation System for Measuring Cross-Coupling Derivatives. ICIASF-79 Record, pp. 251-256, Sept. 1979.

Fowler, H.S. Hoverferry Drag and Stability at Low Speed Over Water. Presented at the 13th Canadian Symposium on Air Cushion Technology, arranged by the Canadian A.C. Technology Society of the CASI, Montréal, Québec, 17-19 September 1979.

Gupta, R.P., Panarella, E., Bhakar, B.S.**** Uncertainty Principle and Photon-Photon Scattering. Bull. Am. Phys. Soc. 24, 682 (1979).

Hanff, E.S., Kapoor, K.B. Measurement of Dynamic Direct and Cross-Coupling Derivatives Due to Oscillatory Roll. ICIASF-79 Record, pp. 186-193, Sept. 1979.

Irwin, H.P.A.H., Wardlaw, R.L. A Wind Tunnel Investigation of a Retractable Fabric Roof for the Montreal Olympic Stadium. Proceedings Fifth International Conference on Wind Engineering, Colorado State University, Fort Collins, Colorado, 8-14 July 1979.

Irwin, H.P.A.H. Cross-Spectra of Turbulence Velocities in Isotropic Turbulence. Research Note, Boundary Layer Meteorology, Vol. 16, 1979, pp. 237-243.

Krishnappa, G. Effects of Blade Shapes and Casing Geometry on Noise Generation from an Experimental Centrifugal Fan. Proceedings of the 5th World Congress on the Theory of Machines and Mechanisms, ASME, Vol. 2, July 1979.

Laneville, A.*****, Williams, C.D. The Effect of Intensity and Large Scale Turbulence on the Mean Pressure and Drag Coefficients of 20 Rectangular Cylinders. Proceedings Fifth International Conference on Wind Engineering, Colorado State University, Fort Collins, Colorado, 8-14 July 1979.

---

* Division of Building Research
** Pratt & Whitney Aircraft of Canada Ltd., Montreal, Quebec
*** Concordia University, Montreal, Quebec
**** University of Manitoba
***** University of Sherbrooke

MISCELLANEOUS PAPERS (Cont'd)

Larkin, B.S., Ramsden, J.* A Simple Leak-Proof Heat Exchanger for Use in Solar Energy Systems. 14th Intersociety Energy Conversion Engineering Conference, Boston, Mass., Aug. 1979.

Larkin, B.S. Electricity Rate Systems and Energy Conservation. 14th Intersociety Energy Conversion Engineering Conference, Boston, Mass., Aug. 1979.

Lau, J.J., Lougheed, G.D. Numerical Calculations of Micro-Particle Acceleration by Spherical Shocks. Canadian Association of Physicists Annual Congress 1979, Vancouver, B.C., June 21, 1979.

Panarella, E., Gupta, R.P. The Reximplo Experiment: Conversion from Cylindrical to Quasi-Spherical Plasma Compression. 9th European Conference on Controlled Fusion and Plasma Physics, Oxford, England, 17-21 Sept. 1979, p. 52.

Savic, P., Kekez, M.M. Shock Waves in Spark Discharges, Part 1. XIVth International Conference on Phenomena in Ionized Gases, Grenoble, France, 9-14 July 1979.

Savic, P., Kekez, M.M., Lougheed, G.D. Shock Waves in Spark Channels, Part 2. XIVth International Conference on Phenomena in Ionized Gases, Grenoble, France, 9-14 July 1979.

Savic, P., Kekez, M.M. Derivation of the Breakdown Characteristics of a Positive Rod-Plane Gap Over a Three-Decade Range. Third International Symposium on High Voltage Engineering, Milan, Italy, 28-31 Aug. 1979.

Savic, P., Lau, J.H., Kekez, M.M., Lougheed, G.D. Spherically Converging Shock Waves in Dense Plasma Research. 12th International Symposium on Shock Tubes & Waves, Jerusalem, July 16-19, 1979.

Thamburaj, R.**, Golak, J.A.**, Wallace, W. The Influence of Chemical Composition on Post-Weld Heat Treatment Cracking in Rene 41. SAMPE Quarterly, July 1979, pp. 6-12.

Timco, G.W. The Mechanical and Morphological Properties of Doped Ice: A Search for a Better Structurally Simulated Ice for Model Test Basins. Paper presented at the Fifth International Conference on Ports and Ocean Engineering under Arctic Conditions, Trondheim, Norway, Aug. 13-17, 1979. Published in POAC 79 Proceedings, Vol. I, pp. 719-739, 1979.

Wardlaw, R.L. Approaches to the Suppression of Wind-Induced Vibrations of Structures. Proceedings IAHR/IUTAM Symposium on Practical Experiences With Flow-Induced Vibrations, Karlsruhe, Germany, 3-6 September 1979.

Wardlaw, R.L. Unresolved Problems – Bridge Decks, Beams and Cables. Proceedings IAHR/IUTAM Symposium on Practical Experiences With Flow-Induced Vibrations, Karlsruhe, Germany, 3-6 September 1979.

Whyte, R.B. Future Availability of Fuels. Presented at ACOP 3rd Symposium on Gas Turbine Operations and Maintenance, Halifax, N.S., 17 and 18 Sept. 1979.

UNPUBLISHED PAPERS

Buck, Leslie The Role of Proprioceptive Information in Establishing a Frame of Reference. Paper read at International Conference in Physical Education, Trois-Rivières, Québec, June 1979.

Irwin, H.P.A.H. Wind Tunnel Testing of Membrane Structures. Department of Architecture and Building Engineering, University of Bath and Bureau Huppold, Bath, England, 10 Sept. 1979.

Kapoor, K. A Simple One-Piece Five-Component Balance for Dynamic Experiments. Presented at the 52nd Meeting of the Supersonic Tunnel Association, Notre Dame, Indiana, Sept. 1979.

Mokry, M., Öhman, L.H. Comparison of Methods for Two-Dimensional Wind Tunnel Interference Corrections from Wall Pressure Measurements. Presented by M. Mokry at the 52nd Meeting of the Supersonic Tunnel Association in Notre Dame, Indiana, on September 13-14, 1979.

Wardlaw, R.L. Tutorial on Wake-Induced Oscillations of Bundled Power Conductors. IEEE Power Engineering Society, 1979 Summer Meeting, Vancouver, B.C., 15-20 July 1979.

---

* Nortec Air Conditioning Industries Ltd.

** Graduate Student, Department of Mechanical and Aeronautical Engineering at Carleton University, Ottawa, Ont.

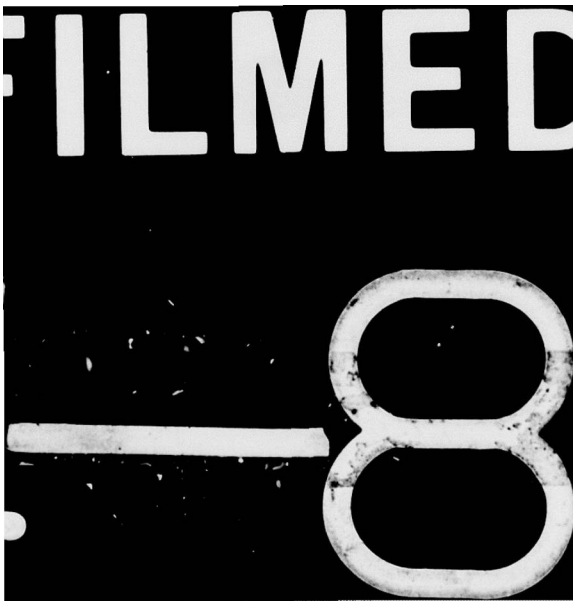
FILMED
8